

**Experimental Crack Length Measurement Under  
Variable Temperature using a Thin Film AC  
Potential Difference Technique**

by

**Douglas M. Roberge**

A thesis  
presented to the University of Manitoba  
in fulfilment of the  
thesis requirement for the degree of  
Master of Science  
in  
Mechanical Engineering

Winnipeg, Manitoba, Canada 1997

©Douglas M. Roberge 1997



National Library  
of Canada

Acquisitions and  
Bibliographic Services

395 Wellington Street  
Ottawa ON K1A 0N4  
Canada

Bibliothèque nationale  
du Canada

Acquisitions et  
services bibliographiques

395, rue Wellington  
Ottawa ON K1A 0N4  
Canada

*Your file* *Votre référence*

*Our file* *Notre référence*

The author has granted a non-exclusive licence allowing the National Library of Canada to reproduce, loan, distribute or sell copies of this thesis in microform, paper or electronic formats.

The author retains ownership of the copyright in this thesis. Neither the thesis nor substantial extracts from it may be printed or otherwise reproduced without the author's permission.

L'auteur a accordé une licence non exclusive permettant à la Bibliothèque nationale du Canada de reproduire, prêter, distribuer ou vendre des copies de cette thèse sous la forme de microfiche/film, de reproduction sur papier ou sur format électronique.

L'auteur conserve la propriété du droit d'auteur qui protège cette thèse. Ni la thèse ni des extraits substantiels de celle-ci ne doivent être imprimés ou autrement reproduits sans son autorisation.

0-612-23477-0

**THE UNIVERSITY OF MANITOBA  
FACULTY OF GRADUATE STUDIES  
\*\*\*\*\*  
COPYRIGHT PERMISSION PAGE**

**EXPERIMENTAL CRACK LENGTH MEASUREMENT UNDER VARIABLE  
TEMPERATURE USING A THIN FILM AC POTENTIAL DIFFERENCE TECHNIQUE**

**BY**

**DOUGLAS M. ROBERGE**

**A Thesis/Practicum submitted to the Faculty of Graduate Studies of The University  
of Manitoba in partial fulfillment of the requirements of the degree  
of  
MASTER OF SCIENCE**

**Douglas M. Roberge 1997 (c)**

**Permission has been granted to the Library of The University of Manitoba to lend or sell  
copies of this thesis/practicum, to the National Library of Canada to microfilm this thesis  
and to lend or sell copies of the film, and to Dissertations Abstracts International to publish  
an abstract of this thesis/practicum.**

**The author reserves other publication rights, and neither this thesis/practicum nor  
extensive extracts from it may be printed or otherwise reproduced without the author's  
written permission.**

**I hereby declare that I am the sole author of this thesis.**

**I authorize the University of Manitoba to lend  
this thesis to other institutions or individuals  
for the purpose of scholarly research.**

**I further authorize the University of Manitoba  
to reproduce this thesis by photocopying or by  
other means, in total or in part, at the request  
of other institutions or individuals for the  
purpose of scholarly research.**

The University of Manitoba requires the signatures of all persons using or photocopying this thesis. Please sign below, and give address and date.

## Abstract

An alternating current (AC) potential drop (PD) method is developed for measuring crack length under combined thermal and mechanical loading. An insulated aluminum film deposited on the surface of center cracked 6061-T6 aluminum alloy test specimens provides a medium for the measurement of PD data used in calculating crack length. Experimental PD data is collected over a range of crack lengths and temperatures and compared against theoretical and numerical models. Potential difference data is found to be linear over a wide range of crack lengths. An analytical relationship is derived based on a theoretical model to provide a predicted crack length given potential difference and specimen temperature. Calculated crack lengths are compared to optically measured crack lengths for cracks 0 to 30 mm in length at temperatures up to 300 °C. Calculated values were found to be within  $\pm 0.3$  mm of measurement results over nearly all temperatures and crack lengths. Improvement of the accuracy of calibration equations and the sensitivity of the foil deposit is achieved through a numerical study of the film potential field in various configurations. Application of the technique to studies of creep and fatigue induced crack growth under varied thermomechanical loading suggested a resolution of 0.02 mm and accuracy within  $\pm 0.09$  mm using an excitation current of only 1.98 mA.

## **Acknowledgements**

I would like to thank my advisor and friend Dr. M.L. Ayari for all the guidance and support that he provided throughout my program of study at the University of Manitoba. I would also like to extend my thanks to Dr. G.E. Sims, Mr. V. Burachynsky, and Mr. P. Zhang for their interest and useful discussions regarding my research.

Thanks also to Mr. B. Bourbonnais and Mr. I. Penner for their assistance in the preparation of test specimens and Mr. K. Majury for troubleshooting and providing advice on problems electrical in nature.

Finally, I would like to sincerely thank my parents and Heather Pitcher for their interest and support through all the ups and downs of my graduate work.

# Contents

<b>List of Figures</b>	<b>x</b>
<b>List of Tables</b>	<b>xiii</b>
<b>1 Introduction</b>	<b>1</b>
1.1 Background . . . . .	1
1.2 Research Objective . . . . .	4
1.3 Scope of Thesis . . . . .	5
<b>2 The Potential Difference Method of Crack Length Measurement</b>	<b>8</b>
2.1 Calibration Methods . . . . .	9
2.1.1 Theoretical Methods of Calibration . . . . .	10
2.1.2 Experimental Methods of Calibration . . . . .	14
2.2 Optimization of Lead Positions . . . . .	16
2.3 AC and DC Potential Difference Methods . . . . .	17
2.3.1 The DC Potential Difference Method . . . . .	17
2.3.2 The AC Potential Difference Method . . . . .	20

2.3.3	Comparison of AC and DC methods . . . . .	24
2.4	Problems and Limitations of Potential Difference Methods . . . . .	25
2.4.1	Problems Associated with the Shape of the Crack Front . . . . .	25
2.4.2	Problems Associated with Fracture Surface Touching . . . . .	26
2.4.3	Problems Associated with the Nature of Crack Extension . . . . .	27
2.4.4	Limitations of the Potential Difference Method . . . . .	28
<b>3</b>	<b>The 'Thin Film' AC Potential Difference System</b>	<b>30</b>
3.1	Crack Length Measurement Using a Thin Conducting Film . . . . .	31
3.1.1	Producing the Crack Measuring Deposit . . . . .	32
3.1.2	The Influence of Insulating Barrier Properties on Surface Crack Transference . . . . .	35
3.2	The Test Specimen . . . . .	39
3.3	AC Potential Difference Measurement Circuit . . . . .	41
<b>4</b>	<b>Experimental Calibration of the Thin Film AC Potential Difference System</b>	<b>44</b>
4.1	Test Apparatus . . . . .	45
4.1.1	Automated Control of Testing Apparatus . . . . .	48
4.2	Experimental Calibration . . . . .	51
4.3	Analysis of Calibration Data . . . . .	53
4.3.1	Calibration Relationship Based on a Simplified Model . . . . .	54
4.4	Accuracy and Resolution of the Crack Length Measurement System . . . . .	58

<b>5</b>	<b>Numerical Analysis of the Film Potential Field</b>	<b>61</b>
5.1	Numerical Simulation of the Voltage Field . . . . .	62
5.2	The Effect of Crack Length . . . . .	67
5.2.1	Deviation at Short Crack Lengths . . . . .	68
5.2.2	Deviation at Long Crack Lengths . . . . .	69
5.3	The Effect of Film Aspect Ratio on Calibration Curves . . . . .	70
5.4	The Effect of Current and Potential Lead Location on Calibration Curves	72
5.4.1	The Effect of Current Lead Location . . . . .	72
5.4.2	The Effect of Potential Lead Location . . . . .	74
5.5	Summary of Numerical Findings . . . . .	74
<b>6</b>	<b>Application of the Crack Measurement System to Fatigue and Creep Induced Crack Growth</b>	<b>77</b>
6.1	The Fatigue and Creep Testing Program 'Creep.c' . . . . .	78
6.2	Potential Difference System Configuration . . . . .	80
6.3	Fatigue and Creep Testing Results . . . . .	82
6.3.1	Fatigue Induced Crack Growth under Constant Temperature .	82
6.3.2	Creep Induced Crack Growth . . . . .	84
6.3.3	Summary of Creep Test Findings . . . . .	94
6.4	Performance of the Crack Measurement System during Testing . . . .	95
<b>7</b>	<b>Summary, Conclusions, Contributions and Recommendations</b>	<b>97</b>
7.1	Summary . . . . .	97

7.2	Conclusions . . . . .	98
7.3	Original Contributions . . . . .	101
7.4	Recommendations for Further Research . . . . .	102
<b>A</b>	<b>The Skin Effect Phenomenon</b>	<b>107</b>
A.1	Evaluation of Skin Effect in an Aluminum Film . . . . .	108
<b>B</b>	<b>Photos of Experimental Apparatus</b>	<b>110</b>
<b>C</b>	<b>Program Listings</b>	<b>117</b>
C.1	Program Listing For 'calib.c' . . . . .	118
C.2	Program Listing for 'aspect.f' . . . . .	124
C.3	Program Listing for 'creep.c' . . . . .	131

# List of Figures

1.1	Thermomechanical Loading Schedule for a Turbine Blade . . . . .	2
2.1	Potential Measurement Points For Compact Test Specimen . . . . .	9
2.2	Geometry for Johnson's Solution . . . . .	11
2.3	Potential Field Distributions in Single Edge Notch Specimens . . . . .	12
2.4	Typical Through-Thickness Crack Front Profile . . . . .	15
2.5	DC Potential Difference System Layout . . . . .	18
2.6	AC Potential Difference System Layout . . . . .	20
2.7	Normalized Potential vs. Normalized Thickness [5] . . . . .	23
2.8	Fracture Surface Touching . . . . .	27
3.1	Crack Measurement Deposit On Specimen . . . . .	31
3.2	Potential Difference Circuit Through Conducting Film . . . . .	34
3.3	Vapor Deposition Apparatus . . . . .	35
3.4	Behavior of Insulating Barrier Cross Section Near Crack Tip . . . . .	36
3.5	Aluminum Test Specimen . . . . .	40
3.6	Potential Difference Measurement Circuit . . . . .	42

4.1	Cross Section of Specimen Test Enclosure . . . . .	46
4.2	Control Pathways for Test Station . . . . .	50
4.3	Flowchart for Calibration of Thin Film Technique . . . . .	51
4.4	Representation of Simplified Model . . . . .	56
4.5	Accuracy of Crack Length Predictions . . . . .	59
5.1	Conservation of Charge in the Control Volume . . . . .	63
5.2	Boundary Conditions of Potential Field Problem . . . . .	64
5.3	Half Potential Field for 32mm Crack . . . . .	66
5.4	Potential Drop in Foil at 200 ° C . . . . .	67
5.5	Predicted Potential at 30 ° C - Short Crack . . . . .	68
5.6	Predicted Potential at 30 ° C - Long Crack . . . . .	70
5.7	Effect of Film Aspect Ratio on Calibration Curves . . . . .	71
5.8	Effect of Current Lead Location on Calibration Curves . . . . .	73
5.9	Effect of Potential Lead Location on Calibration Curves . . . . .	75
6.1	Program Flowchart for 'creep.c' . . . . .	79
6.2	Creep Testing under Variable Temperature . . . . .	81
6.3	Potential Change with Fatigue Crack Growth . . . . .	84
6.4	Fatigue Crack Growth at 21 ° C . . . . .	85
6.5	Strain-Time Curves for Logarithmic ( $T < 0.4T_m$ ) and Normal Creep ( $T > 0.4T_m$ ) Response [8] . . . . .	87
6.6	Specimen Response During Constant Temperature Creep Test . . . . .	89

6.7	Crack Growth During Constant Temperature Creep Test . . . . .	90
6.8	Specimen Response During Variable Load Creep Test . . . . .	91
6.9	Crack Growth During Variable Load Creep Test . . . . .	92
6.10	Potential Difference During In-Phase Thermomechanical Loading . . . . .	93
6.11	Crack Growth During In-Phase Thermomechanical Loading . . . . .	94
B.1	Finished Test Specimen . . . . .	111
B.2	Installed Specimen . . . . .	112
B.3	Specimen Insulation . . . . .	113
B.4	Test Configuration . . . . .	114
B.5	Control and Measurement Apparatus . . . . .	115
B.6	Testing Station . . . . .	116

# List of Tables

4.1	Calibration Parameters . . . . .	52
4.2	Actual and Calculated Electrical Constants for Aluminum . . . . .	58
5.1	Optimal Film Parameters . . . . .	76
6.1	User Specified Test Parameters . . . . .	78
6.2	Fatigue Test Parameters . . . . .	83
6.3	Creep Test Parameters . . . . .	88
7.1	Optimal Film Configuration . . . . .	100

## Nomenclature and Abbreviations

$a$	crack length
$a_o$	reference crack length
$a_{corr}$	corrected crack length
$\Delta a$	incremental crack length
$A$	current carrying cross section of conductor
AC	alternating current
$B$	conductor thickness
COD	crack opening displacement
DC	direct current
EMF	electromotive force or potential
$i$	electrical current
$K_I$	stress intensity factor (mode I loading)
$K_1, K_2$	curve fit constants
$K_{Ic}$	fracture toughness
$L$	foil deposit length
PD	potential difference
RF	radio frequency
rms	root mean square
$r_p$	plastic zone radius
$T$	temperature
$T_o$	reference temperature
$T_m$	melting point of material
$\Delta T$	incremental temperature
$t$	foil deposit thickness
$V$	measured potential

$V_o$	reference potential
$\Delta V$	incremental potential
$W$	foil deposit width
$\alpha$	temperature coefficient of resistivity
$\delta$	skin effect depth
$\varepsilon$	electric field strength
$\theta_d$	debye temperature
$\mu_o$	magnetic permeability of free space
$\mu$	absolute magnetic permeability
$\rho$	electrical resistivity of conductor
$\rho_o$	reference resistivity
$\sigma_y$	stress in y-direction
$\sigma_{yld}$	yield stress of material
$\sigma_{min}$	relaxation or minimum specimen stress
$\sigma_{max}$	maximum specimen stress
$\chi$	magnetic susceptibility
$\omega$	reference frequency
$\ell$	model Conductor length

Other symbols and abbreviations used are defined in the text.

# Chapter 1

## Introduction

### 1.1 Background

The growth of cracks under elevated or rapidly varying thermomechanical loads is recognized as a key issue in the structural integrity assessment of many structures. The most notable examples are those components found in the aerospace and nuclear power industries. Modern machinery such as steam and gas turbine engines, nuclear reactors and high performance automobile engines undergo large thermomechanical transient loading during service. Voids, inclusions and microcracks within components can coalesce during service to form macroscopic cracks. Creep and fatigue growth of these macroscopic cracks during service is controlled not only by the level of thermomechanical loads, but also by the schedule of thermomechanical loading they are subjected to [23] (Fig. 1.1). These macroscopic cracks can reduce the load-carrying capacity and the lifetime of a component considerably.

For machine components operating under extreme thermomechanical loads, the prediction of service life is an important part of the design process. Failure of critical machine components during service can produce catastrophic results. Knowledge of

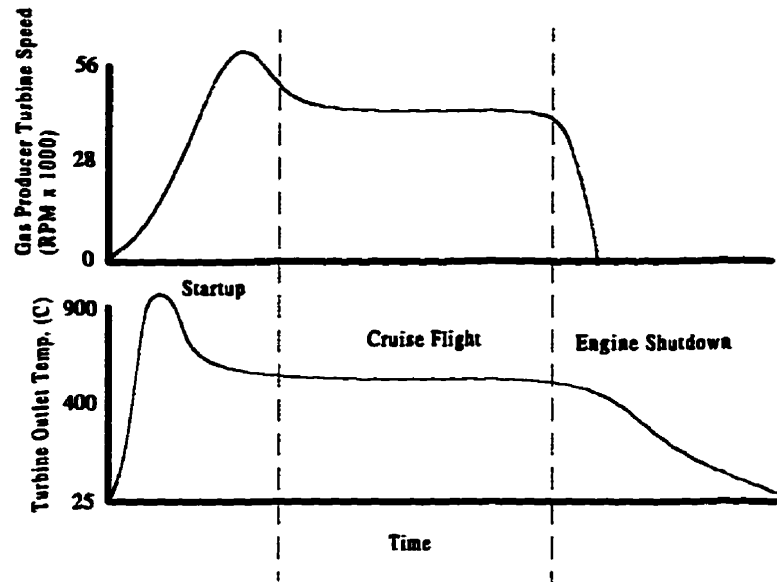


Figure 1.1: Thermomechanical Loading Schedule for a Turbine Blade

the service life for a design serves to give a replacement time for such components. Understanding the life-limiting aspects of a design during the evaluation of service life also aids in producing a longer lasting product. Evaluation of service life for many aerospace components is ongoing even after the initial numerical and experimental analyses during the design stage. In-service component removal and inspection data is continually used to re-evaluate currently used component life limits.

Since the service lives of machine components can be lengthy, obtaining enough data for statistical confidence in new service life estimates can take years. To avoid component failure during operation, initial service life estimates are commonly extremely conservative resulting in the 'scrapping' of many serviceable components [23]. Many design codes stipulate that high temperature components cannot have any crack-like defects at all [10]. Better understanding of material degradation and crack growth under varying thermomechanical loading will lead to more accurate design service life estimates. This can be achieved through conducting numerical and

experimental analyses which simulate operating conditions as nearly as possible.

Stresses based upon traditional creep data alone are inadequate for the design of a high temperature engine required to start up and shut down frequently. For components operating under these conditions, the combination of creep and fatigue reduces cyclic life far more than the contribution of fatigue or creep alone [9]. To arrive at an accurate prediction of service life, the cyclicity of thermal and mechanical loading as well as the schedule of thermal and mechanical loading during a cycle must be considered. Through suitable numerical and experimental analysis of the problem, expected times of crack initiation and failure of the component must be determined.

Unfortunately, the mechanisms of slow crack growth through creep and fatigue under transient thermal and mechanical stresses are not well understood. Numerical techniques for simulating material fracture under complex loadings predict areas of material 'damage' but are unable to accurately relate these results in terms of crack position, length and rate of advance. Methods are needed which more accurately relate operating conditions to crack initiation and growth, which are the ultimate cause for component failure. Experiments relating crack growth response to transient thermomechanical loads will help to validate new predictive models for crack growth under these conditions.

The ability to measure crack response to a complex thermomechanical loading pattern is also important to the development of high temperature technology. Understanding the response of new materials such as ceramics and fiber composites to complex loading patterns is important in many high temperature applications. Higher efficiencies are realized at higher operating temperatures for internal combustion engines. Trends towards the application of refractory materials to realize higher efficiencies in engines will increase the need for test facilities capable of evaluating fracture properties of these materials at high temperature.

In studying crack propagation due to thermomechanical transient loading, many methods of crack length measurement cannot be used or are not sensitive or accurate enough for such testing. Although both optical and potential difference methods of crack length measurement are considered sensitive enough for slow crack growth studies, optical methods cannot be used when the specimen cannot be viewed directly. This problem arises when dealing with specimens contained within a furnace or another enclosure [4]. Current potential difference methods are highly sensitive to specimen temperature change. As a result, measurement accuracy decreases rapidly with any temperature change beyond a steady value.

In order to perform studies of creep and fatigue crack growth under complex thermal and mechanical loading, a sensitive method of crack length measurement is needed which provides continuous length monitoring. The resolution of crack length measurement must be sufficient to detect the small changes of the crack tip position which occur during creep crack growth. Facilities must be developed which can provide tight control over the thermal and mechanical loading of a specimen and record the material response to these conditions. The system should demonstrate a high level of sensitivity and accuracy of measurements throughout a wide range of temperature and mechanical loading over long periods of time.

## **1.2 Research Objective**

The objective of this research is to develop a test station capable of subjecting cracked specimens to a controlled schedule of thermal and mechanical loading and record the time-dependent crack response to the applied loading. For simplicity and ease of implementation in other systems, it is desired to have a crack length feedback signal which is linear with actual crack length. In addition, it is desired that this system be capable of performing automated mechanical and thermal transient loading,

measurement of crack length and measurement of specimen temperature, load and strain.

The application of this system to fatigue and creep crack growth study of cracked panels under time dependent thermomechanical loading will be investigated. As well, ability of the system to indicate crack growth under creep and fatigue mechanisms will be assessed. In particular, the ability of the system to record the response of creep crack growth to a load change or relaxation period is to be evaluated.

### **1.3 Scope of Thesis**

This thesis is divided into the following chapters:

**Chapter 1** provides an introduction to the thesis work. This includes a discussion of the need for specialized crack length measurement techniques in the design and evaluation of components subjected to complex thermomechanical loading schedules. A statement of the objective of the research details the goals set for the design and testing of the crack length measurement system. The scope of the thesis provides an outline of the topics covered in this document.

**Chapter 2** contains a review of the development and operation of the AC and DC potential difference crack length measurement techniques. Methods of calibration and differences between the AC and DC systems are compared. Problems and limitations of current AC and DC systems are also examined.

**Chapter 3** covers the design and operation of the 'thin film' AC potential difference system. Production of test specimens incorporating the crack measurement film is detailed along with important design considerations. A discussion of the advantages of the thin film method over conventional PD systems is also included.

**Chapter 4** discusses the development of a simplified model and equations for predicting potential change in the conducting film based on experimental data. The method of data collection is discussed along with the apparatus used. Accuracy of the calibration equations in calculating crack length is investigated by comparing results with optical crack length measurements.

**Chapter 5** describes numerical studies of the film potential field to study the effects of crack length and film configuration on the accuracy and sensitivity of the system. Results of these studies are used to provide improved calibration relations and indicate the optimal configuration of the film deposit. This involves a systematic study of the calibration curves associated with various electrical lead locations and film aspect ratios.

**Chapter 6** discusses the application of the PD system to the study of fatigue and creep induced crack growth under various thermomechanical loading schedules. Experimental results are used to investigate the performance of the system under various test situations in light of expected crack growth trends.

**Chapter 7** presents the summary, conclusions, and contributions of this thesis study. Recommendations for further research are also included.

**Appendix A** contains a discussion of the 'skin effect' phenomenon in AC current flow through conducting material. An investigation of the influence of the skin effect on the film potential field of the proposed crack length measurement system is also included.

**Appendix B** contains various photos of the experimental apparatus used in testing and data collection for the thesis work.

**Appendix C** contains short descriptions and program listings for the calibration and creep/fatigue testing control programs 'calib.c' and 'creep.c'. A program listing is also included for the fortran program 'aspect.f' used in solving the film potential field.

## Chapter 2

# The Potential Difference Method of Crack Length Measurement

The potential difference method of crack length measurement relies on correlating potential differences in the potential field of a current carrying cracked conductor with a change in crack length. A typical specimen setup for PD crack measurement is shown in Figure 2.1. Potential changes occur only in the plane of crack extension and are assumed constant through the specimen thickness. Increments in crack length will cause the potential field in the conductor to adjust to a new geometry, and point voltages throughout this field will change. By measuring potential difference between two points in this field, correlations between crack length and PD can be formed. The location of these potential measurement points are selected to provide maximum sensitivity to crack length change and linearity of potential difference with crack extension.

The PD technique was first used by Barnett and Troiano in studying hydrogen embrittlement of steel in 1957 [11]. The resistance change of notched specimens was measured by using a double Kelvin bridge. Steigerwald and Hanna [12] used a similar

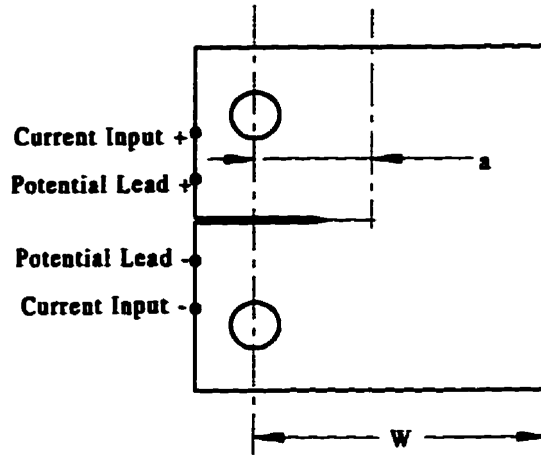


Figure 2.1: Potential Measurement Points For Compact Test Specimen

procedure in 1962 to study rising load tests on fatigue pre-cracked steel specimens. Correlation between crack length and voltage change was established by experimentation, which required discrete crack length measurements by the operator and new calibrations for each material tested. Thermal effects on results were documented as major sources of error, since the electrical resistivity  $\rho$ , of the material tested varies with temperature. Temperature controlled rooms were used in order to minimize the effects of temperature variation on readings.

## 2.1 Calibration Methods

To relate potential difference measurements to crack length, a means of calibrating results is needed. For simple specimen geometries, the potential field can be solved analytically for various crack lengths. An expression relating potential difference between two points in the potential field as a function of crack length can then be developed. Calibration relations are independent of specimen thickness, electrical properties and current level when presented in a normalized form [1]. The following

equation has been suggested.

$$\frac{V}{V_0} = f\left(\frac{a}{W}\right), \quad (2.1)$$

where  $\frac{V}{V_0}$  is the ratio of current and initial potential and  $\frac{a}{W}$  is the ratio of crack length to specimen width. For more complex specimen geometries in which the potential field cannot be solved analytically, crack length measurements must be taken over a range of crack lengths and compared to measured voltages. This data provides an empirical relationship between crack length and potential drop for the measured range of crack lengths. Once again data is presented in a normalized form  $\frac{V}{V_0}$  vs.  $\frac{a}{W}$  to produce results independent of specimen thickness, electrical properties and current level. It is important to note that normalized test data does not produce results which are independent of the location of potential measurement points.

### 2.1.1 Theoretical Methods of Calibration

To avoid time consuming experimental calibrations, the potential field produced under simple geometrical arrangements can be solved as a function of crack length and probe position. These expressions provide a theoretical correlation between crack length and potential drop. In any homogeneous test specimen of uniform thickness, the current will only flow in the plane of the specimen. The steady-state potential field produced is governed by the Laplace equation:

$$\frac{\partial}{\partial x} \left( k_x \frac{\partial V}{\partial x} \right) + \frac{\partial}{\partial y} \left( k_y \frac{\partial V}{\partial y} \right) = 0. \quad (2.2)$$

Where  $k_x$  and  $k_y$  are the electrical conductivity  $\sigma$ , of the conducting medium in the  $x$  and  $y$  directions respectively. By using conformal mapping techniques, Johnson [1] obtained an analytical solution to the potential field for a infinitely long conducting sheet of uniform thickness with a center crack modeled as a thin slit. The electric

potential far from the crack axis is uniform over the width of the sheet. This is referred to as a uniform current configuration. Potential measurement points are located symmetrically a distance  $y$  on either side of the crack centerline as shown in Figure 2.2. The equation governing the potential field for this configuration is:

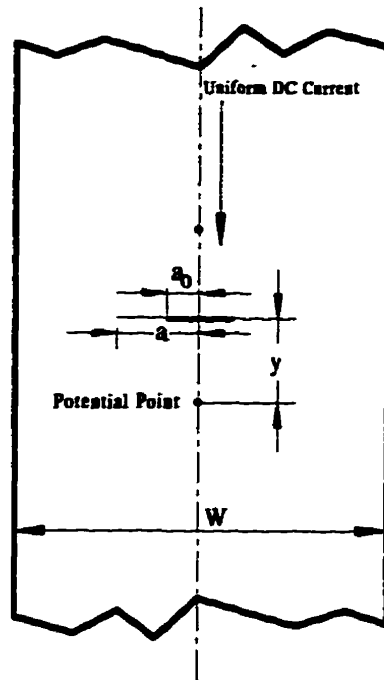


Figure 2.2: Geometry for Johnson's Solution

$$\frac{V}{V_0} = \frac{\cosh^{-1}\left(\frac{\cosh \frac{\pi y}{W}}{\cos \frac{\pi a}{W}}\right)}{\cosh^{-1}\left(\frac{\cosh \frac{\pi y}{W}}{\cos \frac{\pi a_0}{W}}\right)} \quad (2.3)$$

Where  $V_0$  is the potential difference at crack length  $a_0$  and  $V$  is the potential at crack length  $a$ . Better agreements with experimental data are found using a similar solution which modelled the crack as elliptical in shape [13].

Analytical solutions to single edge notch (SEN) specimen geometries were presented by Gilbey and Pearson [14]. The problem is modelled as an infinitely long strip of metal with a single transverse crack. Two potential field configurations are

investigated, the uniform current configuration (Fig. 2.3a) and the non-uniform current configuration (Fig. 2.3b). The solution to the potential field for both current configurations is solved using conformal mapping techniques. These solutions are equally applicable to center-cracked plates with symmetric crack extension as in Figure 2.2 due to the symmetry of the voltage field about the plate vertical centerline.

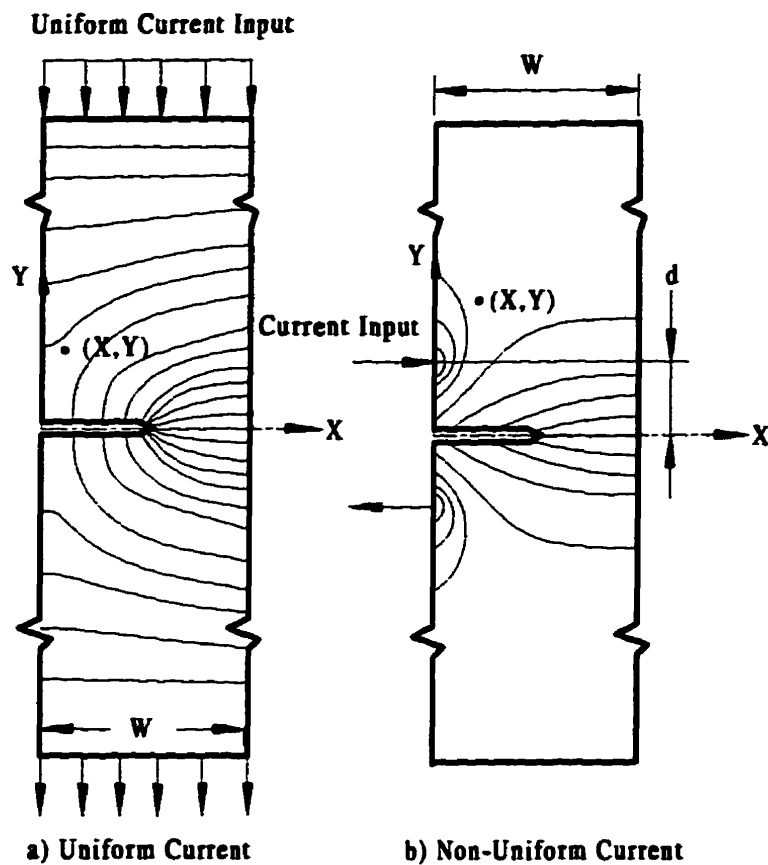


Figure 2.3: Potential Field Distributions in Single Edge Notch Specimens

By using conformal mapping techniques, the geometries shown in Fig. 2.3a and Fig. 2.3b are mapped into new geometries on which the governing Equation 2.2 can be easily solved. This involves the 'conformal transformation' of the physical coordinate system to another coordinate system in which the problem boundary conditions

become simplified. The solution is then transformed back the physical plane. To denote coordinates  $(x,y)$  in the physical plane, a complex variable  $z = x + iy$  is used. Both real and imaginary parts of any analytic function of  $z$  will satisfy Equation 2.2. For the uniform current configuration (a), the solution for the potential field is given by:

$$V_a = \Im \left[ K_1 \cos^{-1} \frac{\cos\left(\frac{\pi z}{2W}\right)}{\cos\left(\frac{\pi a}{2W}\right)} \right], \quad (2.4)$$

where  $W$  denotes the width of the strip and  $a$  is the length of the crack as shown in Figure 2.3a.  $K_1$  is a constant based on the conducting strip electrical properties. The value of  $K_1$  can be determined by measuring the PD at a known crack length and solving for  $K_1$  using Equation 2.4. For the non-uniform current configuration (b), the solution for the potential field is:

$$V_b = \Re \left[ K_2 \ln \frac{(\epsilon + ic)}{(\epsilon - ic)} \right], \quad (2.5)$$

where transformation between the  $z$ -plane and  $\epsilon$ -plane is given by:

$$\epsilon = \sqrt{\sec^2\left(\frac{\pi z}{2W}\right) \cos^2\left(\frac{\pi a}{2W}\right) - 1}. \quad (2.6)$$

Geometrical constant  $c$  is based on the distance  $d$ , between the point application of current and the axis of crack extension as shown in Figure 2.3b.

$$c = \sqrt{1 - \cos^2\left(\frac{\pi a}{2W}\right) \operatorname{sech}^2\left(\frac{\pi d}{2W}\right)} \quad (2.7)$$

Constant  $K_2$  is also based on the electrical properties of the conducting strip, and can be determined in a similiar method as described for  $K_1$ .

Specimens prepared utilizing the uniform current configuration realize a near-linear potential increase with crack length due to an increase in specimen resistance caused by a reduction in conducting cross section. The non-uniform current configuration indicates crack length change by an increase in the path length that current

must travel between current leads. This increase in path length increases the specimen resistance in a non-linear relationship with crack length. Of particular interest in this research is the solution for the non-uniform current potential field of a conductor of finite size, this is discussed in Chapter 5.

### **2.1.2 Experimental Methods of Calibration**

Calibration of specimens with complex geometries for which no theoretical calibration is available, is achieved using experimental methods. The calibration is performed by recording potential difference for various crack lengths. As in the theoretical calibration method, the calibration is made independent of current level, material electrical properties and specimen thickness by using a ratio of potential readings  $\frac{V}{V_0}$  and crack length as a fraction of total specimen width  $\frac{a}{W}$ . In this format, the calibration is valid for all proportional specimen geometries with current input and potential lead positions adjusted in proportion to size [15]. In addition, starter notch crack length  $a_0$  must be adjusted proportionally for the calibration to remain valid between specimens of the same geometry but different proportions. Calibration of large or thick specimens can be easily performed by performing calibration on a thin foil of conducting material [16]. This material is cut in a geometry and size proportional to the specimen and the crack is modelled as a thin slit which can be easily increased in length by using a razor. By performing a calibration on an electrical analogue difficulties involved in incrementing crack length in large or thick specimens is avoided.

When performing calibrations on full-size specimens crack extension is usually achieved by saw cutting [17] or fatigue [1, 7, 18, 5]. In general, crack fronts are not perpendicular to the front and back faces of the specimen but curved as shown in Figure 2.4. The curvature of the crack front is convex in the direction of propagation due

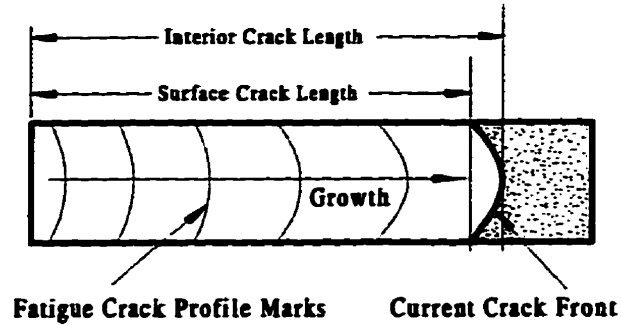


Figure 2.4: Typical Through-Thickness Crack Front Profile

to a through thickness stress state - plasticity variation [4]. The convex shape of the crack front can lead to underestimations of crack length when optical measurements of the surface crack length are used. Crack profile curvature can be measured by marking the fracture face during testing by a load change or heat tinting and examining the fracture surface after testing. The amount of crack profile curvature can be added to optical measurements of the surface crack length as a correction. Although crack profile curvature is not present when sawcutting is used for crack propagation, the wide square profile of the crack tip produces differences in the potential field when compared to thin cracks of the same length. Siverns and Price [19] suggest that this technique leads to a calibration which underestimates length when applied to narrow cracks.

Particularly at short crack lengths, measured potentials are sensitive to crack tip shape and size of the plastic zone surrounding the crack tip [4]. To avoid errors at short crack lengths, the measurement of potential  $V_o$  should be performed at a crack length  $a_o$  sufficient to distance the crack tip from the measurement points, starter notch or other irregularities which may locally affect the potential field.

## 2.2 Optimization of Lead Positions

The locations of both current and potential lead positions on the specimen have large effects upon the sensitivity and reproducibility of crack length measurement results. For a specimen with a non-uniform current distribution as shown in Figure 2.3b, maximum sensitivity (maximum  $\frac{dV}{da}$ ) occurs when current is applied near to the crack axis (small  $d$ ). This can be shown by evaluating  $\frac{dV}{da}$  using Equation 2.5 for various values of distance  $d$  between the point of current application and the crack axis. This configuration offers a sensitivity two to three times [14] that of the uniform current configuration shown in Figure 2.3a. In using a non-uniform current configuration with current supplied near the crack axis, care must be taken to ensure consistency of leadwire locations. Variation in leadwire position between test specimens will result in decreased reproducibility of results. Except in applications where maximum sensitivity is needed, moving the current leads further out from the crack axis produces increased reproducibility of results which more than compensates for the slight loss in sensitivity [4].

In both non-uniform and uniform current distributions, potential probe leads are usually placed adjacent to the axis of crack extension such that the Y-coordinate of the probe location is small. This positioning provides a high sensitivity to crack growth which increases as the probe location is moved towards the axis of crack extension. Similar to the effects of decreasing dimension  $d$  for the current input leads in Figure 2.3b, high sensitivity configurations require particular accuracy in positioning potential leads to avoid poor reproducibility of results between specimens. Alternate potential lead probe locations have been proposed for measuring asymmetric crack growth in center cracked plates [17], and providing an average crack length for specimens with significant through-thickness crack front curvature [20].

## **2.3 AC and DC Potential Difference Methods**

Potential difference methods of crack length measurement utilizing both AC and DC current supply have been in use since the early 1960's [18]. During this time, DC based systems have been the standard electrical method of crack length measurement primarily due to their simplicity, stability and ease of use when compared to similar AC systems. Although AC based systems of crack length measurement have been in use since the early 1960's, it was not until the late 1970's to early 1980's that electrical equipment needed for further development of this method became readily available. Subsequent AC systems offered increased sensitivity and additional capabilities not possible with comparable DC based systems. Performance differences between the two methods are related to the behavior of the voltage field and measurement of the potential difference signal. The calibration, resolution and operating characteristics for the AC and DC systems are discussed in this section, with particular attention to the relative advantages and disadvantages of each system.

### **2.3.1 The DC Potential Difference Method**

A typical layout for a DC based potential difference crack length measurement system is shown in Figure 2.5.

The constant-current DC power supply maintains a set level of current flow through the specimen. Lead connection locations on the specimen are selected to produce a uniform or non-uniform current distribution as shown in Figure 2.3. The test specimen must be completely electrically insulated from the load frame or other associated apparatus to produce the desired potential field within the specimen. Insulating sheaths around specimen loading pins are commonly used to insulate the specimen from external conductors. The fit of specimen to loading pins must not be

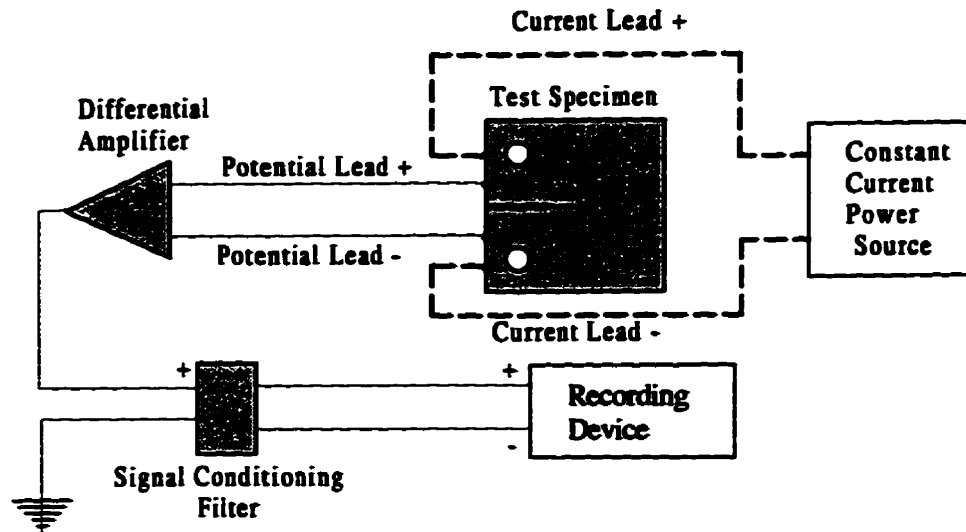


Figure 2.5: DC Potential Difference System Layout

too tight or the insulating sheaths may wear through during fatigue testing, causing grounding to occur through the load frame. Overload protection on the current leads is also recommended to prevent damage to experimental apparatus due to accidental grounding of the specimen.

Due to the large conducting cross section and high conductivity of most specimens, high current levels of 10 to 120 A [1, 4, 7, 17] are needed to yield modest PD readings, typically on the mV scale. To prevent resistance heating effects, flexible current leads of capacity in excess of 120 A are recommended. Resistive heating of the specimen or current leads produces erroneous PD readings through locally changing the specimen electrical resistivity ( $\rho$ ). Current leads are connected to the specimen by bolting, soldering or welding to ensure minimal resistance and avoid heating effects at contact points. Particular attention must be paid to reproducibility of contact area, resistance and location when selecting a means of lead attachment.

Temperature variations within the specimen or over time have been documented as major sources of error [4]. Since the resistivity of most metals is sensitive to tempera-

ture, variations in temperature produce significant differences in measured potential. Changes in temperature also produce changes in measured potential by influencing the voltage generated at bimetallic junctions within the circuit, especially at the point of potential lead contact with the specimen. To avoid these problems, temperature controlled rooms have been used to maintain a uniform and steady temperature for the potential drop equipment. Even if a temperature controlled room is used, equipment warm-up times of 24 hours are recommended to stabilize the temperature of the circuitry and the specimen before testing.

The signal amplifier shown in Figure 2.5 produces a PD reading large enough for input to the recording device. Amplification levels can vary between 10 to 1000 times. It is especially important that the amplifier produces a high signal to noise ratio even at maximum amplification. Since PD measurements are generally between  $10\ \mu\text{V}$  and  $100\ \text{mV}$ , amplification levels are usually quite high and even mild sources of electromagnetic interference can lead to erroneous data. Proper shielding of the potential leads, amplifier and other components in the measurement circuit is essential to preventing interference from nearby power sources and current leads. Although signal conditioning filters can be used to 'smooth' the output signal of the amplifier, it is the DC component of electromagnetic or temperature influenced potential variations that produces erroneous PD readings. Such sources of error cannot be filtered out and must be removed before reliable experimental results can be produced.

To record PD data, a strip chart recorder, digital voltmeter, or a computer with an analog-digital conversion card can be used. Regardless of the means of data acquisition and logging, the recorder should have variable full scale sensitivity, and capability for zero suppression of the initial potential reading. Thus, potentials are measured relative to the initial specimen condition and any potential change is related solely to crack propagation. Resolution of the recording instrument should be sufficient to detect crack length changes smaller than 1% of the total crack length over a wide

potential range. Overall system sensitivity is controlled by many factors: specimen thickness, excitation current level, recorder resolution, specimen resistivity, current and potential lead probe locations, crack length, and specimen shape and size.

### 2.3.2 The AC Potential Difference Method

A typical layout for an AC based potential difference crack length measurement system is shown in Figure 2.6.

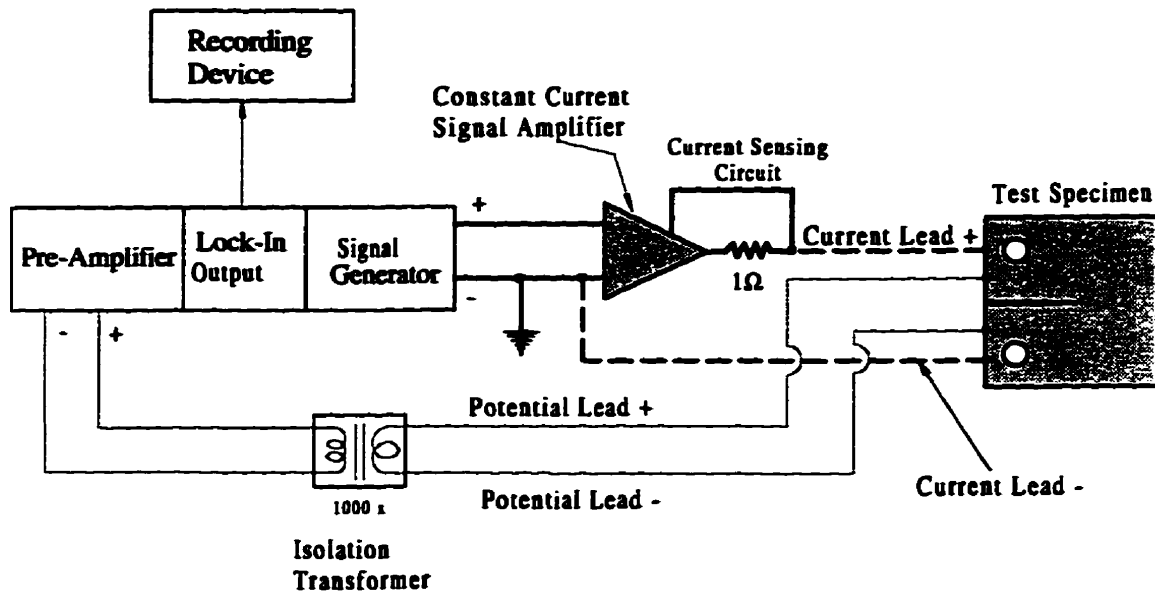


Figure 2.6: AC Potential Difference System Layout

An AC sine-wave of the desired reference frequency is produced by the signal generator for amplification through the constant current amplifier. The constant current amplifier amplifies the reference signal from the signal generator to produce the desired current flow through the specimen. The current sensing circuit provides voltage feedback to the amplifier proportional to current flow. The voltage drop through a high precision  $1\Omega$  resistor provides a 1V rms (root mean square) feedback

signal for 1A rms of current flow. This control system allows the amplifier to maintain the desired current flow through the specimen by adjusting the current lead voltage in response to changes in specimen resistance.

Current and potential leads are attached to the specimen by bolting or welding. For reasons discussed later, the AC systems typically use lower current levels than comparable DC systems, this allows smaller leads to be used and produces smaller, more precise connection points on the specimen. The lower current levels in AC systems also serve to prevent resistive heating of the specimen and current leads which introduce error in measured potential due to variations in specimen resistivity. To prevent electromagnetic 'crosstalk' between current and potential leads and signal interference from nearby power sources, it is essential that current and potential leads are properly shielded. Interference from nearby electromagnetic sources will produce significant error in potential measurements since potential difference at the specimen is normally on the  $\mu\text{V}$  scale.

The isolation transformer shown in Figure 2.6 serves to amplify potential readings, and isolate the lock-in amplifier from the potential measurement leads to prevent current flow to the amplifier. This allows the potential measurements to be 'transparent' to the specimen and not influence the potential field. The specimen potential difference is usually amplified by a factor of 1000, such that the signal at the lock-in input is on the millivolt scale. This input signal is further amplified in the preamplifier section of the lock-in amplifier and filtered through a band-pass filter to select only signal components which have the reference frequency produced by the signal generator.

The signal generator frequency is selected to produce a frequency which is sufficiently removed from that of nearby sources of electromagnetic interference such as power sources (60 Hz) to allow removal of these frequencies at the band-pass filter.

This noise rejection capability of the AC system allows high amplification levels to be used while maintaining a suitable signal-to-noise ratio after signal processing. By using higher amplification levels than comparable DC systems, AC systems require much lower current levels to produce measureable potential difference at the specimen. The current level for a typical AC system is typically 1 A rms [2, 3, 5, 21].

Another factor in the selection of the reference frequency for the signal generator is the influence of a 'skin effect' [3, 18] phenomenon at high frequencies in conducting materials (see Appendix A). As the reference frequency is increased, current flow distribution through the specimen thickness becomes non-uniform and begins to concentrate near the outer boundaries of the specimen. At frequencies producing strong skin effect, potential difference changes are indicative of surface crack growth while lower frequencies produce a uniform current distribution which is better suited to determining average through-thickness crack length [3]. Since the skin effect concentrates current flow in a smaller cross section of the specimen, the potential drop through the specimen will increase with increasing frequency. When studying surface crack growth, the skin effect can be used to produce increased resolution and sensitivity to crack growth. Wei and Brazill [3] studied the effects of reference frequency on AC potential difference measurements. Figure 2.7 shows the effects of skin depth on AC potential difference, where  $B$  is the specimen thickness and  $\delta$  is the skin depth.

The skin effect also has effects on the generated potential field within a cracked specimen. Current tends to concentrate near the crack [18], such that current flows in a 'U' shaped path around the crack tip. This produces high potential field gradients concentrated around the crack tip which diminish with distance from this location. At high reference frequencies, this effect decreases the dependence of calibration on specimen size and geometry and increases overall sensitivity to crack length change.

After the potential difference signal has been amplified and filtered to include

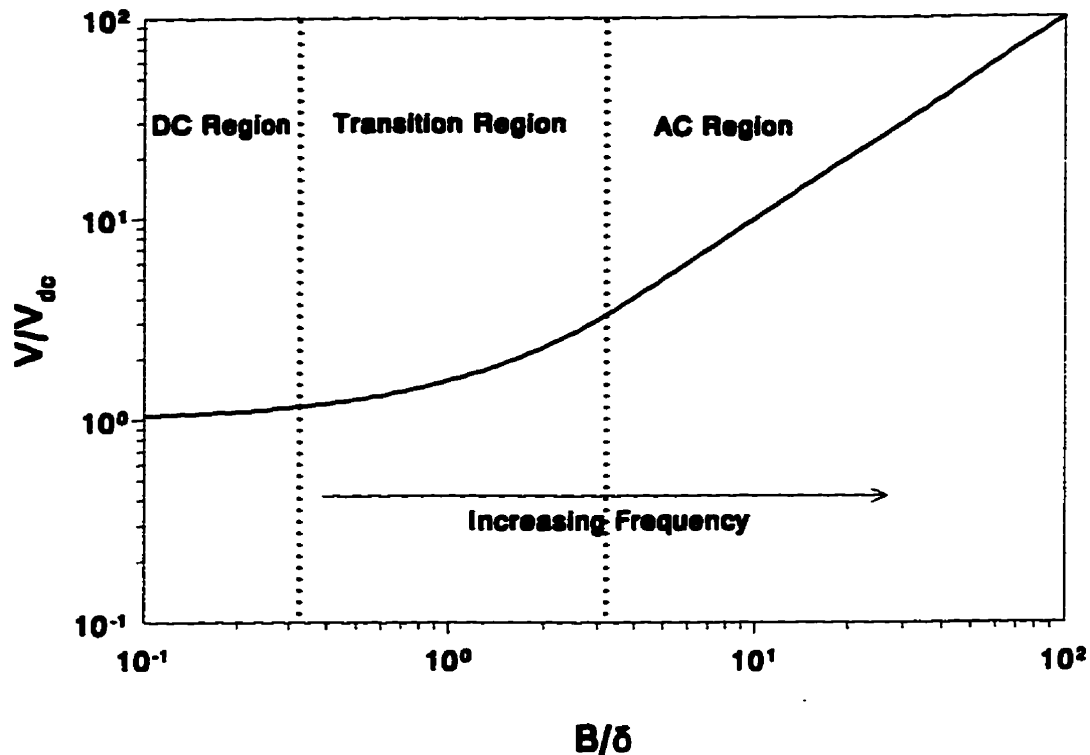


Figure 2.7: Normalized Potential vs. Normalized Thickness [5]

only components at the reference frequency, the peak to peak voltage is converted to a rms value for output to a suitable recording device. Since only the AC component is measured, DC contributions to the potential difference signal from voltage generated at bimetallic junctions do not produce erroneous results as in DC systems. However, changes in specimen temperature will affect specimen resistance and produce AC potential difference changes which will throw off results as observed in DC systems. Once again, it is important to maintain a steady and uniform specimen temperature during testing, this ensures all potential difference changes are associated only with crack extension. The alternating nature of the voltage in AC systems helps to prevent current flow from contributing to electrochemical processes such as stress corrosion cracking or corrosion fatigue [3].

As was mentioned for the DC system in the previous section, it is necessary that the specimen constitutes the only conducting path for the constant current signal. The test specimen must be electrically insulated from all connected conducting apparatus. In the event the specimen touches a conductor, distortion of the specimen potential field will result in erroneous PD measurements. If the charged specimen is shorted to ground, the AC PD measurement system can be damaged. For these reasons, insulated loading pins are used to prevent contact with the loading frame. Thermocouple probes for measuring specimen temperature must also be electrically insulated from the specimen. Shielding the wires with a ceramic coating is a useful technique in preventing contact.

### **2.3.3 Comparison of AC and DC methods**

To compare AC and DC potential difference methods the advantages and disadvantages of the AC system relative to the DC system are presented in point form below:

#### **AC System Advantages**

- Due to excellent noise rejection, filtering and higher amplification levels, lower excitation current is needed. Also, in using lower current levels, resistive heating effects are avoided.
- AC systems are not susceptible to errors from generation of DC voltage at bimetallic junctions of differing temperature. Only the AC portion of the voltage is measured.
- Due to the alternating nature of the current, AC systems do not contribute to electrochemical processes such as stress corrosion cracking and corrosion fatigue.
- The skin effect phenomenon of current flow at high reference frequencies can be

used to decrease dependence of calibration on specimen geometry and increase sensitivity to measurement of surface crack lengths.

### **AC System Disadvantages**

- AC Systems require more sophisticated and expensive equipment with higher measurement stability. Due to the use of high amplification levels, signal drift or distortion from electrical components can quickly introduce significant error in potential readings.
- Due to the alternating nature of the signal and high amplification levels, errors are more likely to be introduced due to lead 'crosstalk' [18] or interference from electromagnetic sources. Proper shielding of all leads and other sources of electromagnetic interference is more important than in comparable DC systems.

## **2.4 Problems and Limitations of Potential Difference Methods**

Although both AC and DC methods of crack length measurement may be used under a variety of testing situations with good results, one must be aware of the sources of error and difficulties associated with using potential difference techniques.

### **2.4.1 Problems Associated with the Shape of the Crack Front**

Gradients in the potential field are extremely high at the crack tip. Changes in the shape and through-thickness profile of the crack tip can lead to large changes in the surrounding potential field, even though the crack length has remained constant. The result of these effects are to produce crack length measurement errors by the potential

difference system. These situations are not accounted for during calibration, since the crack tip is usually considered perpendicular to the front and back faces of the specimen and very sharp at the tip.

Deviations from a theoretical or experimental crack length calibration for the potential difference system can occur in several ways. Severe crack tip blunting or the production of multiple radial cracks at the crack tip lead to large deviation of the potential field from the field predicted under calibration. Changes in the crack front profile shown in Figure 2.4, can occur due to the presence of inclusions or other discontinuities in the specimen and will normally have a varying convexity through the specimen from side face plasticity effects on crack motion [4]. Deviations between actual and predicted crack length will occur if the varying convexity through the specimen is not accounted for during calibration. Such situations arise when optical crack length measurement is used during experimental calibration of a thick specimen with significant crack front convexity, or theoretical calibration is used assuming a straight crack front profile.

#### **2.4.2 Problems Associated with Fracture Surface Touching**

Contact of the fracture surface behind the crack tip leads to an alternate path for current flow rather than around the crack tip. This results in a sudden change in the potential field within the specimen making PD measurements invalid under the calibrated situation. The end result is to produce deviations in the predicted and actual crack length.

Fracture surface touching has been shown to occur primarily in testing situations involving low mean stresses and specimens with large material inclusions or coarse microstructures [4]. Coarse microstructures or inclusions in the material matrix promote the formation of rough, jagged fracture surfaces by inducing sudden changes in

crack propagation direction from anisotropy of mechanical properties in the material. Under low mean stresses, the crack opening distance (COD) is minimized, increasing the likelihood of fracture surface touching as shown in Figure 2.8.

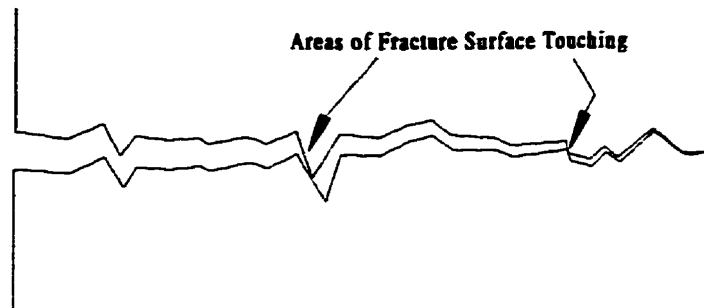


Figure 2.8: Fracture Surface Touching

During cyclic loading, fracture surface touching during the low stress portion of the loading cycle will produce some cyclicality to potential difference measurements.

### 2.4.3 Problems Associated with the Nature of Crack Extension

In studying crack propagation in a center cracked plate using either Johnson's [1] or Gilbey and Pearson's [14] calibration, asymmetric crack growth results in underprediction of crack length. Both calibrations are no longer valid since the potential field becomes asymmetric under asymmetric crack growth. For asymmetric crack growth, the calibration according to Read and Pfuff [17] which utilizes the asymmetric potential is applicable.

It is also of note that all theoretical calibrations assume straight crack growth. Situations where crack growth direction varies significantly from the calibrated condition produces error in crack length measurement. As was observed for asymmetric crack

growth, the voltage field deviates from the calibrated situation rendering the calibration relationship between voltage and crack length invalid. Similar consequences apply for testing in which the test crack propagation direction deviates significantly from the crack path taken during experimental calibration.

#### **2.4.4 Limitations of the Potential Difference Method**

The sensitivity of potential difference measurements to specimen temperature changes can produce significant measurement errors, as was discussed in previous sections. To maintain a steady and uniform temperature of the specimen, temperature controlled rooms are recommended. This source of error has prevented the extension of potential difference measurement systems to test situations with varying temperature. The requirement for such a controlled operating environment is a large inconvenience for precision crack length measurement using the potential difference method.

The need to fully charge the specimen and insulate it from connected apparatus makes the use of potential difference methods very difficult to apply to on-site monitoring of crack length outside a laboratory setting. Also, the dependency of calibration on specimen geometry requires calibration for each new application. For example, if a boiler was to be monitored for crack extension, calibration would have to be performed for the geometry of the boiler, the boiler insulated from connected apparatus, and the entire boiler would be charged. Obviously, these requirements can make it very difficult, if not impossible to monitor the crack length in any application outside a laboratory setting and still operate the machinery in a normal fashion.

The 'thin film' potential difference measurement technique discussed in Chapter 3 is designed to overcome the limitations associated with conventional potential difference methods. This involves extension of the technique to account for the effects of temperature variation on potential difference measurements. In addition, the system

is designed to allow application of the technique to on-site crack length monitoring of all materials regardless of electrical properties.

## **Chapter 3**

# **The 'Thin Film' AC Potential Difference System**

To overcome some of the disadvantages inherent in conventional potential difference systems, a new crack length measurement system is proposed. The system is designed to provide crack length feedback under variable specimen temperature with extremely low current levels and calibration independent of specimen geometry. The nature of the design also allows several other advantages over previous AC and DC potential difference systems which will be discussed later in this chapter. The new system is based on the AC potential difference method to take advantage of the increased noise rejection, sensitivity, and performance under varying specimen temperature as compared to DC systems. In this chapter, the design and operation of the proposed potential difference system is discussed.

### 3.1 Crack Length Measurement Using a Thin Conducting Film

The 'thin film' approach to measuring crack length involves a thin electrically conducting film bonded to the surface of a test specimen in the area of crack extension as shown in Figure 3.1. The film is insulated from the specimen by a thin barrier of insulating material. The film captures the crack, allowing potential difference through the film to be calibrated to the specimen surface crack length. The thin nature of the film/barrier deposit allows accurate transference of the specimen surface crack profile to the foil with negligible influence on the specimen behavior in the area occupied by the deposit. The attached current and potential leads allow the measurement of potential difference to determine the corresponding crack length in the foil.

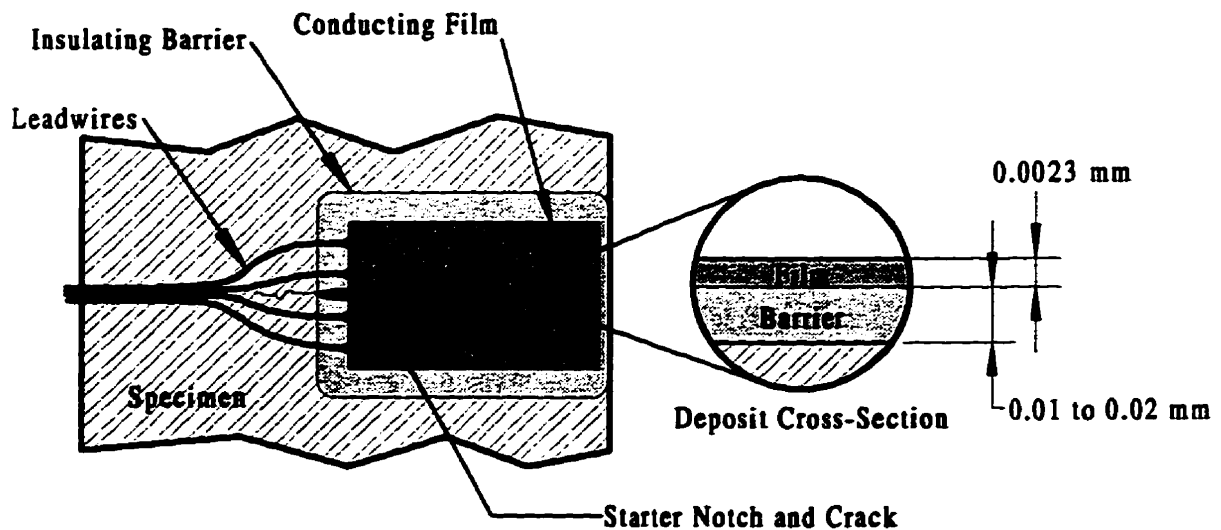


Figure 3.1: Crack Measurement Deposit On Specimen

The nature of the thin film method provides several important advantages over potential difference systems which use the specimen as the conducting circuit:

- Crack length in specimens composed of non-conducting material can be measured.
- Calibration is dependent upon the geometry of the film deposit only. Once calibration has been performed for the film deposit, crack length measurement can be applied to specimens of any geometry with no need for further calibration.
- Due to the thin nature of the conducting film, significantly lower current levels are used to yield acceptable potential difference readings. Also, current level need not be adjusted to suit specimen thickness, size, or material electrical conductivity.
- Since the specimen itself is no longer charged, the technique can be easily extended to on-site crack monitoring outside a laboratory setting.
- The ability of the method to measure the extension of only one crack tip eliminates problems associated with asymmetric crack extension as discussed in Section 2.4 of Chapter 2.

Although this method of crack length measurement provides surface crack length, a knowledge of the convexity of the crack front profile allows correction of surface crack length values to provide through-thickness crack length estimates.

### **3.1.1 Producing the Crack Measuring Deposit**

In producing the film deposit, the materials used and the method of application must be suited to the specimen operating environment during testing. Materials are

selected for high temperature stability, electrical properties, adhesion, and mechanical properties. Lack of material capability in any of these areas will ultimately lead to failure of the crack measurement system. In addition, the method of producing the film deposit is also important in determining the success of the deposit under harsh conditions. In this section, the method of producing the film deposit for testing a 6061-T6 aluminum alloy specimen at temperatures up to 300 ° C is presented.

First, the insulating barrier between the specimen and the foil is produced by brushing on a layer of M-BOND 610 solvent thinned epoxy. This is an epoxy typically used for attaching strain gages to metal specimens and is suitable for use up to 370 ° C. The epoxy is allowed to air dry and is cured at 200 ° C and 300 ° C for two hours at each temperature. This ensures that gases produced during the curing process are driven off before the conducting film is deposited on top of the epoxy. If the epoxy is not allowed sufficient curing time at high temperature, delamination of the conducting film will occur during testing from the production of curing gases in the epoxy. This delamination occurs in the form of bubbling of the film deposit. The thickness of the cured epoxy deposit is approximately 0.01 to 0.02 mm as shown in Figure 3.1.

After the epoxy has cured, thin strips of 0.0005 in. (0.013 mm) thick aluminum gage foil are glued to the cured epoxy layer using M-BOND 610 epoxy. The position of the tips of these strips corresponds to the location of the current and potential leads after the conducting film has been deposited as shown in Figure 3.2. Once the M-BOND 610 has air dried, teflon insulated wires are affixed to the aluminum strips using DuPont 5504N high-temperature electrically conductive silver epoxy. The assembly is baked at 300 ° C for one hour to cure the silver epoxy and the M-BOND epoxy holding the aluminum strips down.

Conducting film is applied on top of the insulating epoxy barrier using a vapor deposition method. The vapor deposition method allows extremely thin layers of

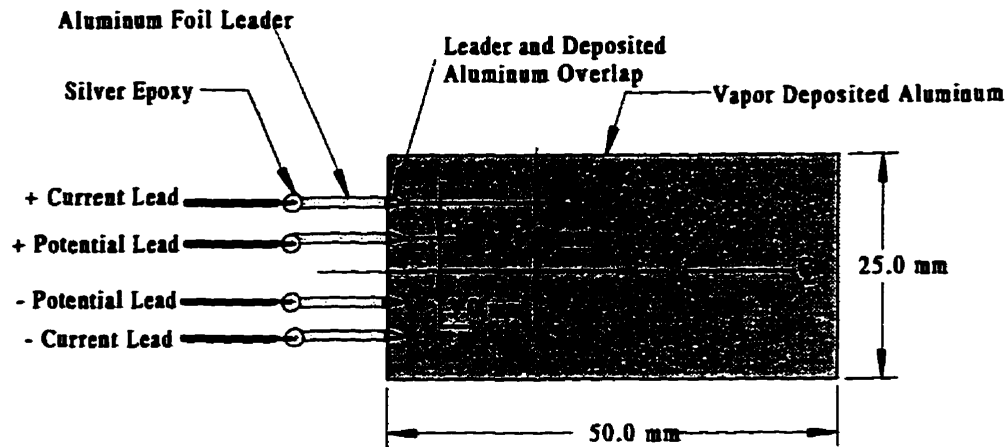


Figure 3.2: Potential Difference Circuit Through Conducting Film

conducting material to be uniformly deposited on the epoxy barrier. High purity (99.9% pure) aluminum is selected for deposition due to its linear conductivity with temperature and to minimize differences in thermal expansion between the specimen and conducting film. The aluminum is deposited to a thickness of 0.0023 mm in a 25 × 50 mm rectangle as shown in Figure 3.2. Once the aluminum is deposited, electrical contact is established with the thin aluminum strips which are connected to the potential and current leads. The total thickness of the epoxy and conducting film deposit ranges from 0.01223 to 0.0223 mm.

Figure 3.3 shows the vapor deposition apparatus. High purity aluminum pellets are heated to evaporation with 300 A of current inside an evacuated bell jar at  $8 \times 10^{-6}$  torr. The evaporated aluminum diffuses throughout the bell jar and condenses on the specimen. The surface of the specimen is shielded with aluminum foil to allow aluminum to be deposited only in the desired area. The deposit thickness is monitored using a MaxTek TM100 thickness monitor. Aluminum is deposited at a rate of  $40 \text{ \AA}/\text{sec}$  up to the desired thickness of  $23000 \text{ \AA}$  (0.0023 mm). The deposition of the aluminum under high vacuum prevents air entrapment beneath the deposited aluminum coating. Air entrapment leads to 'bubbling' delamination of the foil from

the insulating epoxy at high test temperatures.

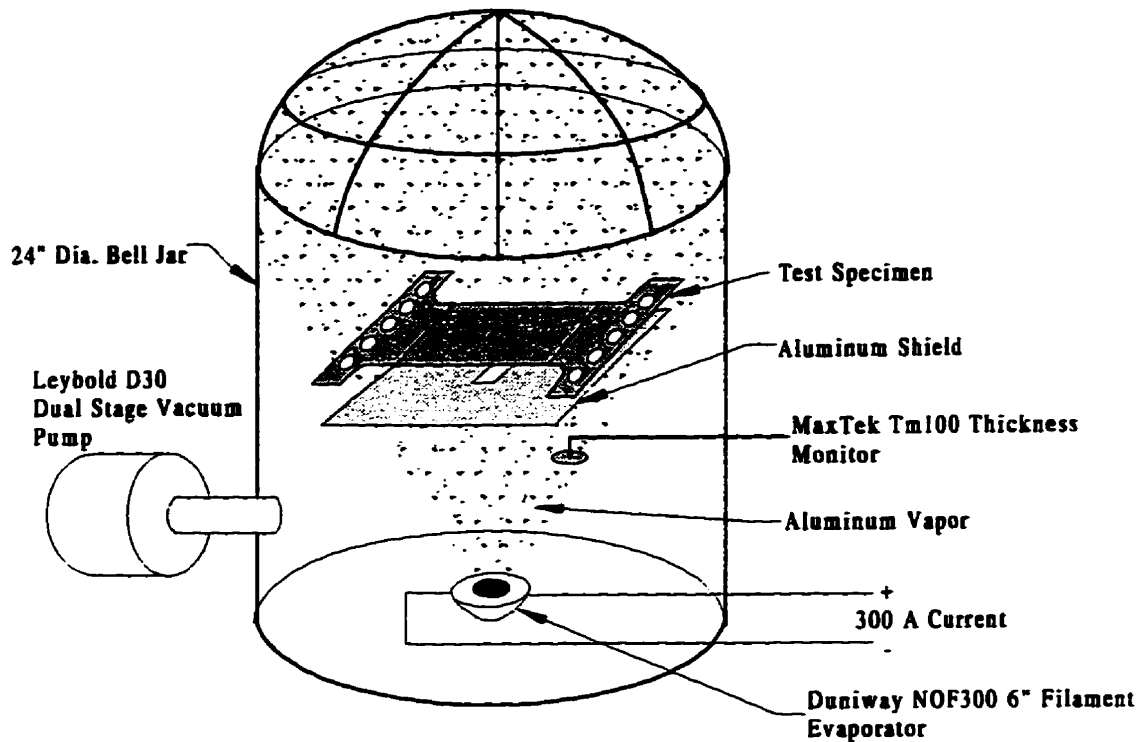


Figure 3.3: Vapor Deposition Apparatus

### 3.1.2 The Influence of Insulating Barrier Properties on Surface Crack Transference

Several factors are important in the selection of an epoxy or other material to be used as the insulating barrier between the conducting film and the specimen. In addition to selecting a material with high electrical resistivity, the influence of the barrier mechanical properties on the accuracy of crack length transference should be considered. These include the effects of deposit thickness, strength of the adhesive bond to the specimen, fracture toughness, shear modulus, elastic modulus and the

effects of temperature on these properties. The effects of varying these properties are discussed in relation to the accuracy of surface crack transference.

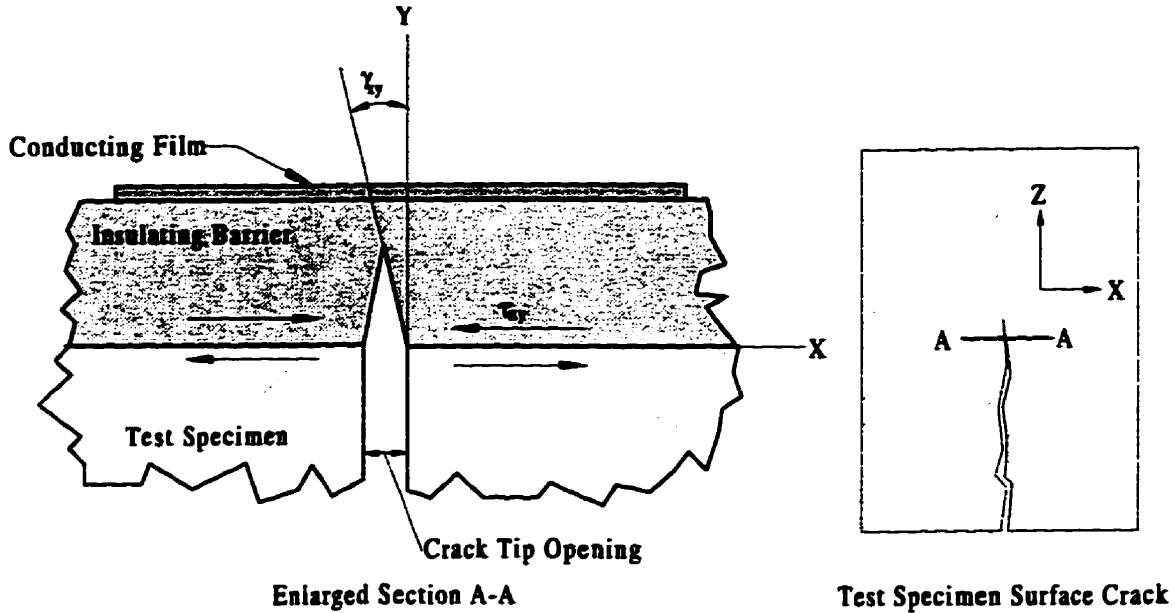


Figure 3.4: Behavior of Insulating Barrier Cross Section Near Crack Tip

### The Effect of Adhesive Bond Strength

In all cases, the adhesive bond strength of the insulating barrier to the specimen and the conducting film is desired to be maximized. Good adhesive bonding prevents delamination from occurring at material interfaces from high shearing stresses at the crack tip. Figure 3.4 shows a cross sectional view of crack propagation in the Z-direction (into the page). As shown in Figure 3.4 the crack opening distance (COD) and plastic strain ahead of the crack tip give rise to shearing stress in the insulating barrier which drive crack extension into the insulating barrier and the conducting film. Adhesive bond failure at the specimen or the conducting film can result in considerable underestimation of specimen surface crack length due to the loss of the ability to transfer these shearing stresses.

### **The Effect of Shear and Elastic Modulus**

In the ideal case, the shear and elastic modulus of the insulating barrier is desired to be close to that of the specimen. Unfortunately, this can be very difficult to achieve. Materials with moduli equal to or slightly below that of the specimen provide adequate results. Of concern are materials with moduli significantly higher or lower than that of the specimen. Barrier materials with shear modulus significantly lower than that of the specimen will transfer a shorter crack length by deforming under the transmitted shear forces as shown in Figure 3.4. The true specimen surface crack will 'tunnel' underneath the conducting film and transfer an erroneously short crack length. Materials with elastic modulus significantly higher than that of the specimen should also be avoided. These materials produce large shearing stresses at the specimen-insulating barrier interface which promote failure of the adhesive bond.

### **The Effect of Fracture Toughness**

The fracture toughness  $K_{Ic}$ , of the insulating boundary material plays an important role in determining what level of stress is required to propagate the surface crack into the insulating barrier. Materials with low fracture toughness are quite brittle and can produce a conducting film crack longer than the specimen surface crack. This occurs when plastic or elastic deformation ahead of the crack tip in the specimen produces sufficient stress in the adjacent insulating material to produce cracking. Conversely, if the fracture toughness of the material is quite high, crack transference is retarded and the film crack tip lags behind the specimen surface crack tip. Similar to the ideal case observed for the barrier shear and elastic moduli, it is desired that the barrier material have a fracture toughness close to that of the specimen material ( $K_{Ic}$  for aluminum alloys and most carbon steels ranges from 30 to 55  $\text{MPa}\sqrt{m}$  [22]). Understandably, the ideal case entails an insulating boundary which has mechanical

properties identical to those of the specimen. In this case crack transference is exact, since the boundary area becomes isotropic with respect to mechanical properties and crack propagation proceeds into the insulating barrier as if it were moving through the specimen material.

### **The Effect of Temperature**

All mechanical properties of the barrier material should stay within a satisfactory range during crack length monitoring involving temperature change. Materials which are resistant to softening, oxidation, and loss of adhesive properties at high temperatures are needed for testing under elevated temperature. Similarly, materials which are resistant to becoming too brittle at low temperatures are ideal for low temperature testing. Many epoxy resins give excellent crack transference at room temperature but soften and lose adhesive properties at high temperature. Relatively few commercially available epoxies are suitable for temperatures up to 300 ° C. Ceramic based insulating materials maintain properties over a wide temperature range, but commonly the fracture toughness of these materials is too low for use in the thin film potential difference method.

### **The Effect of Deposit Thickness**

The deposit thickness of the insulating barrier is important in controlling the accuracy of the crack transference through decreasing sensitivity to the effects of low shear and elastic moduli. By making the deposit thickness as thin as possible, the tendency for shear strain of the boundary material to retard crack transference as shown in Figure 3.4 is minimized. Also, in using a thin layer of insulating material, the shear stress transferred to the boundary layer is decreased, making the possibility of adhesive bond failure much less likely. In the limiting case, where the insulating barrier is

infinitesimally thin and the adhesive bond is very strong, crack transference is exact regardless of insulating material properties. By ensuring a good adhesive bond and a very thin insulating barrier (less than 0.05 mm), a wide range of materials can be used. Good crack transference will be obtained if deformation of the material remains largely elastic and fracture toughness is not so low that artificially long crack lengths are transferred to the conducting film. Crack transference accuracy can be verified by measuring film and specimen crack lengths under test conditions to determine whether a particular insulating barrier material will produce suitable results. Since many epoxies and other adhesives are transparent, the specimen and epoxy surface crack lengths are easily compared by optical measurement.

### **3.2 The Test Specimen**

Center cracked specimens made of 6061-T6 aluminum alloy are fabricated as shown in Figure 3.5. Specimens are used for calibration tests of the potential difference system and studies of system performance under complex thermal and mechanical loading schedules. The geometry of the center cracked plate provides a stress field within the loaded specimen which produces a purely mode I fracture [22] initiating from the sharp tips of the crack starter notch. The geometry of the specimen also allows surface crack length to be easily optically measured with reference to a vertical centerline scribed on the specimen.

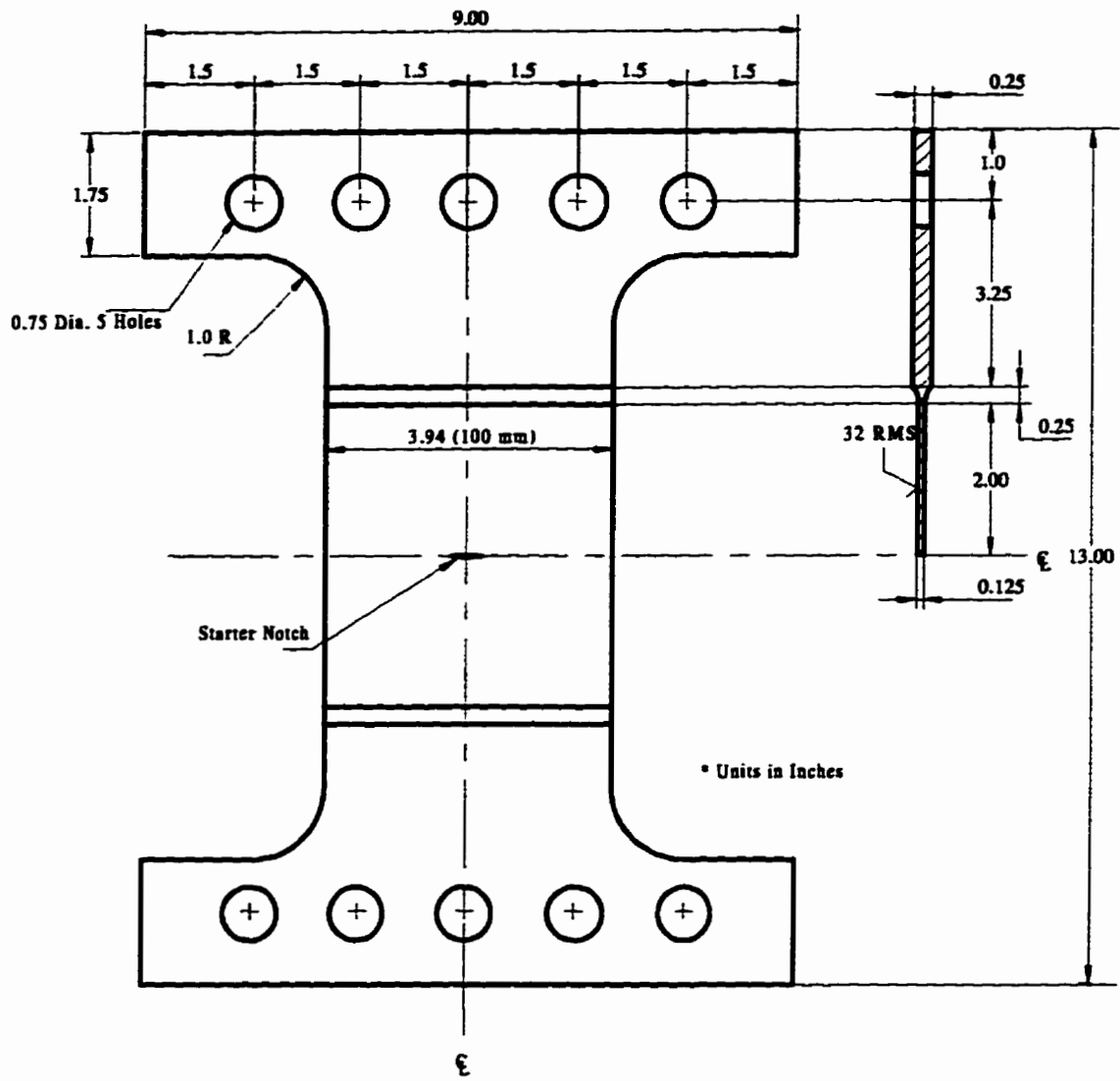


Figure 3.5: Aluminum Test Specimen

Figure 3.5 shows the reduced section thickness in the 100 mm wide test section of the specimen. Load applied using loading pins at the 5 upper and 5 lower load application holes will produce maximum stress at the tips of the starter notch and initiate crack propagation at these locations. The smooth radii at the top and bottom portions of the test section ensure stress concentration does not initiate failure or large strains in these areas. The horizontal and vertical symmetry of the specimen ensures that the stress and strain fields around the starter notch are symmetric about the centerlines. This will lead to ‘theoretically’ symmetric crack propagation along the horizontal axis. Actual crack extension is always slightly asymmetric and non-horizontal due to imperfections in specimen manufacturing, test section surface finish, and nonuniformity of specimen material properties. These problems are minimized by measuring the advance of only one crack tip and ensuring a smooth surface finish during specimen preparation.

The center crack starter notch is produced by electrodischarge machining (EDM). Subsequent fatigue loading of the specimen is used to sharpen the crack tip and extend the tip beyond the local geometrical irregularities of the starter notch. The crack measurement deposit is produced on the specimen as discussed in Section 3.1.1 and centered on top of the existing fatigue crack. Leadwires are bonded to the specimen using a general purpose high-temperature epoxy to prevent accidental damage to the fragile foil connection points. The finished specimen is shown in Figure B.1 of Appendix B.

### **3.3 AC Potential Difference Measurement Circuit**

The circuit used to measure potential difference through the conducting film is shown in Figure 3.6. The circuit is similar to that used by Wei and Brazill [3], except a constant current power amplifier is not required. Since potential difference is measured

through a thin metal film extremely low current levels are sufficient to produce measurable potential difference. The constant current signal generator provides an AC signal ranging from 0.5 to 2 mA rms. This level of current is sufficient for producing a potential difference of the order of  $10 \mu\text{V}$  through the conducting film. The frequency of the AC signal produced by the signal generator is 93 Hz as recommended by Wei and Brazill [3]. This reference frequency assists in filtering out interference from AC power sources at 60 Hz.

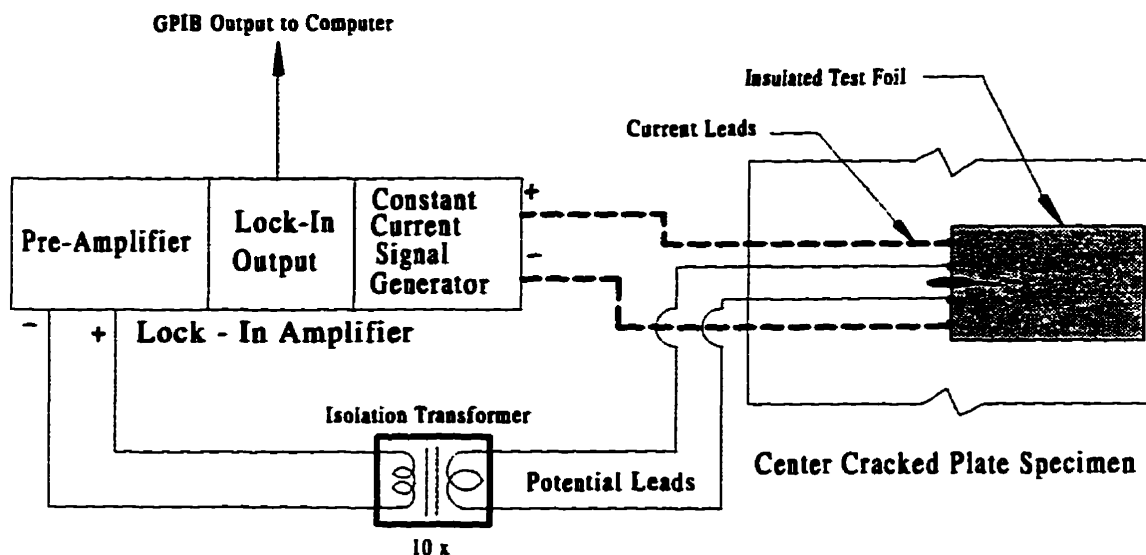


Figure 3.6: Potential Difference Measurement Circuit

Radio frequency (RF) shielded cable is used for current and potential leads to prevent crosstalk between adjacent leads and help minimize interference from power supplies and other sources of signal noise. The isolation transformer serves to amplify the potential difference signal by 10 times and isolate the potential measurement portion of the lock-in amplifier from the specimen. By isolating the lock-in amplifier from the specimen, the potential measurement circuitry is 'transparent' to the specimen and does not influence the potential field produced in the conducting foil.

The pre-amplifier section of the lock-in amplifier subtracts the waveforms between potential leads to produce a differential signal (potential difference). The potential difference waveform is filtered to remove signal frequencies other than the reference frequency using a band pass filter. The remaining signal, having a 93 Hz frequency is amplified according to the sensitivity setting of the instrument and sent to the lock-in output section. The lock-in output section measures the amplitude of the potential difference signal at the reference frequency and provides a corresponding rms value for output. The value of the potential difference is transmitted to a computer for recording.

## Chapter 4

# Experimental Calibration of the Thin Film AC Potential Difference System

To develop a relationship between potential difference and crack length, the thin film PD crack length measurement system must be calibrated. This chapter details the apparatus and method used for experimental calibration of the system. In addition, the extension of the calibration to account for variable specimen temperature is discussed.

Traditional theoretical and experimental calibrations have produced calibration relationships of the form:

$$a = f(V) \tag{4.1}$$

Where the potential difference  $V$  is related to crack length  $a$  at constant temperature. To extend calibration beyond constant temperature, the effects of temperature

change on the calibration relationship must be considered such that the relationship has the form:

$$a = f(V, T) \quad (4.2)$$

By recording potential difference over a range of crack lengths  $a$ , and temperatures  $T$ , a set of data is compiled which can be curve fit to provide a relationship of the form given by Equation 4.2.

## 4.1 Test Apparatus

In this section, the arrangement and operation of apparatus used to subject the specimen to a range of temperatures and propagate the crack to produce a range of crack lengths is discussed. The test station is designed to provide ease of use and accuracy in performing both calibration of the potential difference system, and subsequent tests indicating crack response to selected thermomechanical loading schedules. Once the PD system calibration relationship is determined, the test station is capable of performing fully automated testing of specimens under variable thermomechanical loading.

At the heart of the test apparatus, the test specimen can be subjected to any combination of load, strain, or temperature. To maintain control over test conditions there are also provisions for monitoring specimen temperature, load, strain and potential drop. Figure 4.1 shows a cross-section of the specimen test enclosure. Photos of the apparatus are included in Appendix B.

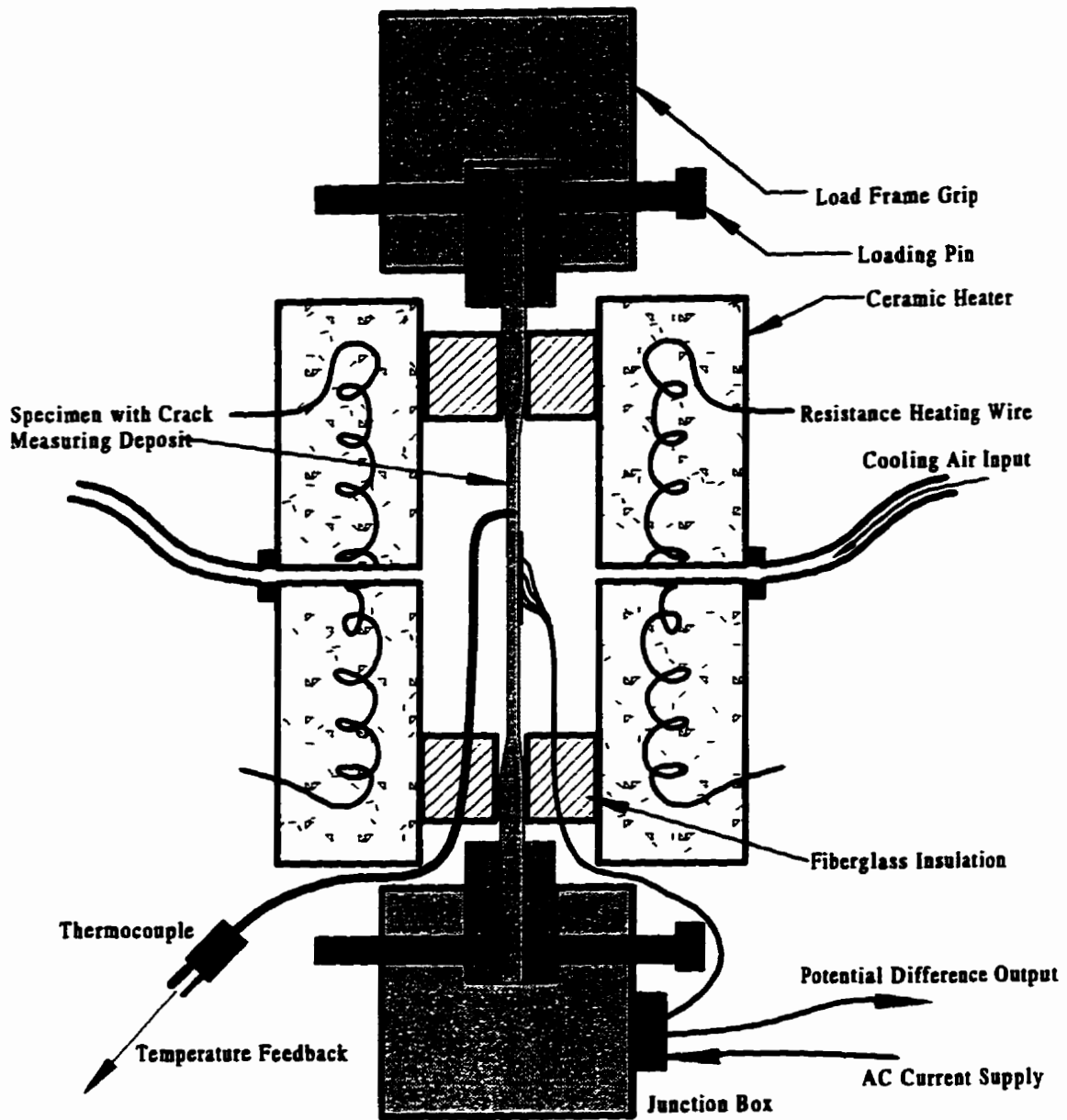


Figure 4.1: Cross Section of Specimen Test Enclosure

The Instron 8562 load frame connects to the specimen using five loading pins at the top and bottom of the specimen which fit snugly into the specimen load bearing holes. Unlike traditional potential difference systems, the specimen is not insulated from the loading frame at these holes since the potential difference measurement circuit is insulated from the specimen. The load frame operates under load or position control to maintain specimen load or position at a requested value. The load frame can also subject the specimen to a variety of cyclic load or position waveforms which are useful in producing controlled fatigue cracking in the specimen. Load frame grips and other load application components are of sufficient size and strength that elastic deformation within these components is negligible when compared to deformation of the specimen. Ceramic blocks on either side of the specimen center the specimen within the load frame grips and help prevent heat flow from the specimen to the surroundings outside the enclosure.

Two ceramic heaters on opposite sides of the specimen supply heat from resistance wire to control specimen temperature. These heaters are moveable to allow easy access to the specimen when not in use. When the heaters are in use, they are positioned to 'sandwich' the fiberglass insulation and seal off the enclosure to prevent heat loss. The specimen temperature is maintained at temperatures up to 500 ° C by an Omega digital temperature controller utilizing a specimen mounted thermocouple for feedback. Given adequate stabilization time, the furnace assembly provides a uniform temperature distribution throughout the test section of the specimen. This ensures the crack measurement film is maintained at a uniform temperature to prevent variations in resistivity within the film which can lead to crack length measurement error.

To provide rapid cooling of the specimen, chilled air is supplied by tubes which run through the core of the ceramic heaters. The chilled air exits the heater tube between 3 and 6 ° C and impinges on the test section of the specimen. The chilled

air is produced by circulating ambient air at 90 to 100 psi through a coiled  $\frac{3}{8}$  inch diameter copper tube immersed in a refrigerated ethelene glycol bath. The bath is controlled at temperatures as low as  $-20^{\circ}\text{C}$  by a Rosemount refrigeration system. The combination of ceramic heaters and chilled air cooling allows the specimen to be subjected to controlled temperature schedules involving rapid heating or cooling transients.

The length of the specimen surface crack can be optically measured by moving the ceramic heaters out of the way and rotating the specimen in the load grips by  $90^{\circ}$ . Optical measurement of the crack length is performed using a travelling microscope. Although the resolution of this measurement instrument is 0.01 mm, accuracy of crack length measurement is estimated at  $\pm 0.03$  mm due to difficulties in optically locating the crack tip.

An EG&G Princeton Applied Research lock-in amplifier is used to supply AC current flow to the crack measuring deposit and measure potential difference. Resolution of this instrument is below  $0.001\ \mu\text{V rms AC}$  on the maximum sensitivity setting. Unfortunately, the sensitivity of the instrument must be set at a level comparable to the magnitude of potential difference readings or overload of the signal pre-amplifier will occur. For this reason, tests normally occur on the  $300\ \mu\text{V}$  or  $1\ \text{mV}$  sensitivity settings with resolution ranging from  $0.03\ \mu\text{V}$  to  $1\ \mu\text{V}$ .

#### **4.1.1 Automated Control of Testing Apparatus**

The testing station includes a computer interface from which specimen testing is controlled. As shown in Figure 4.2, data acquisition and control of all test apparatus is achieved using a 386 personal computer. Programs written in the 'C' programming language direct test execution, record data, and prompt the user for input of test parameters. Automated control of the test apparatus provides uniformity of test

conduct, ease of acquisition and analysis of data, and continuous monitoring and control of tests of long duration.

The serial port of the computer is used to communicate with the temperature controller. Through this port, the temperature 'setpoint' of the controller may be changed or the specimen temperature reported. Communication with the lock-in amplifier and load frame control unit is achieved through the GPIB (General Purpose Interface Bus) interface. The GPIB interface is a controller card specifically designed to provide a high-performance hardware interface with instrumentation for computer control. Through the GPIB interface, the computer can set the current level flowing through the film, the reference frequency, and request potential difference measurements. Also, through the lock-in amplifier commands can be sent to activate or deactivate air cooling to the specimen. Two 12V DC output channels can be set on or off by the amplifier to control the operation of solenoid valves regulating chilled air flow.

All aspects of specimen loading and positioning are available for control through the GPIB interface. Specimen load and position may be read or set through this channel. In addition, the number of loading cycles in fatigue can be reported and test safety limits may be set and armed. Test programs discussed later, are comprised mainly of commands issued along communication pathways to test apparatus as shown in Figure 4.1.1.



## 4.2 Experimental Calibration

Calibration of the thin film technique using experimental means involves the collection of potential difference data over a range of temperatures  $T$ , and crack lengths  $a$ . Analysis and curve-fitting of the collected data provides continuous analytical expressions relating crack length to temperature and potential difference as in Equation 4.2. The calibration program 'calib.c' listed in Appendix C, provides automated control and data acquisition during most calibration steps. A program flowchart for 'calib.c' is shown in Figure 4.3.

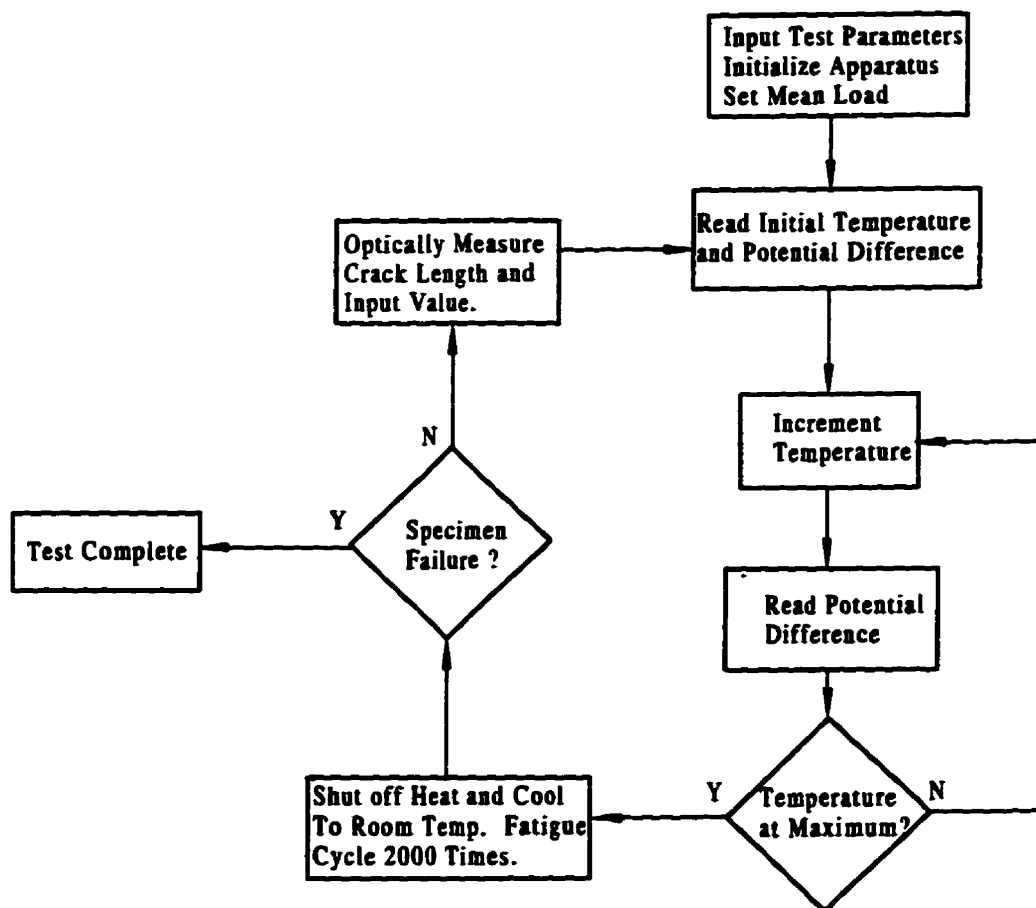


Figure 4.3: Flowchart for Calibration of Thin Film Technique

After the apparatus has been set up and the specimen installed, the initial crack length of the specimen is measured optically and input into the computer. Important test parameters (shown in Table 4.1) are requested by the program and input by the user. The calibration program proceeds to initialize the test parameters in instrumentation, set safety limits for the load frame, and apply the minimum load to the specimen. The use of a minimum load for the specimen throughout testing is important in ensuring a reasonable crack opening distance to prevent crack face touching and errors associated with this phenomenon.

Current ( $i$ )	0.897 mA
Reference Frequency ( $\omega$ )	93 Hz
Minimum Stress ( $\sigma_{min}$ )	36 MPa
Maximum Stress ( $\sigma_{max}$ )	144 MPa
# of Cycles for Crack Increment	2000
Initial Temperature ( $T_o$ )	30 ° C
Maximum Temperature ( $T_{max}$ )	200 ° C
Temperature Increment ( $\Delta T$ )	28 ° C
Initial Crack Length ( $a_o$ )	10.15 mm

Table 4.1: Calibration Parameters

The initial potential difference at temperature  $T_o$  and crack length  $a_o$  is measured and the temperature is incremented. Potential difference is measured after the specimen temperature has stabilized and the process is repeated until the specimen has reached its maximum temperature. Once the maximum temperature has been reached, air cooling is activated and the ceramic heaters are shut off. During cooling the specimen is fatigue cycled 2000 times using a sine waveform between  $\sigma_{min}$  and  $\sigma_{max}$ . Once the specimen temperature stabilizes at  $T_o$  and fatigue cycling is complete, the crack length is optically measured and input into the computer. The new crack

length is recorded and load levels are decreased to reflect the decreased load carrying section of the specimen and maintain proper minimum and maximum stress. By maintaining maximum and minimum stress constant over all crack lengths, the crack growth increment during the fatigue cycling portion of testing is uniform.

With each new crack length after the completion of fatigue cycling, temperature is incremented six times up to the maximum temperature of 200 ° C and potential difference is taken at all intervals. As the program proceeds, data is collected which 'maps' potential difference over the range of temperatures and crack lengths. The entire process is repeated until fatigue crack propagation initiates final fracture of the specimen and data can not be collected further.

### 4.3 Analysis of Calibration Data

The experimental test results provides a set of datapoints containing the voltage reading  $V$  for a corresponding crack length  $a$  and temperature  $T$ . This set of  $(a, T, V)$  data is expressed in terms of incremental quantities relative to the first data point  $(a_o, T_o, V_o)$  yielding  $(\Delta a, \Delta T, \Delta V)$ . Presenting the data in this manner eliminates variation between tests due to leadwire resistance differences and contact resistance variation. In this form, the data reflects voltage changes as influenced by temperature and crack length effects on the foil. This data is curve fit and the following equation is found to closely match experimental results.

$$\Delta V = K_1 V_o \Delta T + K_2 \Delta a + K_1 K_2 \Delta T \Delta a \quad (4.3)$$

Where  $K_1$  and  $K_2$  are curve fit constants found to be equal to 0.0033 and 0.001645 respectively.

### 4.3.1 Calibration Relationship Based on a Simplified Model

The form of Equation 4.3 is investigated in light of some governing equations for conductors and simplifying assumptions. The voltage drop through a conductor of length  $\ell$  with cross sectional area  $A$  and electrical resistivity  $\rho$  which is carrying a current  $i$  is given by:

$$V = \rho \frac{i\ell}{A}. \quad (4.4)$$

If the temperature of a metal is above  $0.2\theta_D$ , where  $\theta_D$  is the Debye temperature of the metal, the change in resistivity varies linearly with temperature change [6, 24]. Then the temperature coefficient  $\alpha$  can be used to yield the resistivity of the conductor at any temperature above a reference temperature  $T_o$  through the relation:

$$\rho = \rho_o(1 + \alpha\Delta T). \quad (4.5)$$

If all other variables remain constant in Equation 4.4, Equation 4.5 can be written:

$$V = V_o(1 + \alpha\Delta T). \quad (4.6)$$

Using Equations 4.4 and 4.6, we can write a relation which gives the final voltage through the conductor for any change in conductor length  $\Delta\ell$  and temperature variation  $\Delta T$ .

$$V = \left[ V_o + \rho_o \frac{i\Delta\ell}{A} \right] \left[ 1 + \alpha\Delta T \right] \quad (4.7)$$

Expanding equation 4.7 allows easy comparison with equation 4.3.

$$\Delta V = \alpha V_o \Delta T + \rho_o \frac{i\Delta\ell}{A} + \alpha \left( \rho_o \frac{i\Delta\ell}{A} \right) \Delta T \quad (4.8)$$

### Assumptions of the Linear Conductor Model

Upon comparing equations 4.3 and 4.8, we see  $K_1 = \alpha$  and  $K_2 = \rho_o \frac{i f(\Delta a)}{A}$  where  $f$  is a function relating  $\Delta \ell = f(\Delta a)$ . These associations are reasonable if the thin film can be modelled as a linear conductor of length  $\ell$  and conducting cross sectional area  $A$ . The potential difference through the film will approximate the behavior of a linear conductor if the following requirements are met:

- 1) the potential and current density through the cross sectional area perpendicular to current flow are uniform. This implies that the influence of the 'skin effect' phenomenon is negligible for the specified film thickness, material and AC operating frequency.
- 2) the foil electric field strength  $\epsilon = -\frac{\partial V}{\partial l}$  is constant in a 'U' shaped path of length  $\ell$  around the crack tip, and  $\epsilon = 0$  perpendicular to this path (ie. the foil can be approximated as a curved one-dimensional conductor).
- 3) the AC system foil deposit has negligible inductance and capacitance so  $V_{rms} = i_{rms} R$
- 4) the width of this conductor is constant. (ie. the crack propagates straight, and does not approach the end of the foil).
- 5) the temperature of the foil  $T$ , remains above  $0.2\theta_D$  ( $0.2\theta_D = 24.2^\circ \text{C}$  for aluminum). Above  $0.2\theta_D$ ,  $\alpha$  remains constant and the variation of resistivity with temperature is linear.

To check the validity of the first requirement, Section A.1 of Appendix A investigates the influence of the skin effect on the proposed crack length measurement system. This study indicates that the magnetic susceptibility of aluminum is very low

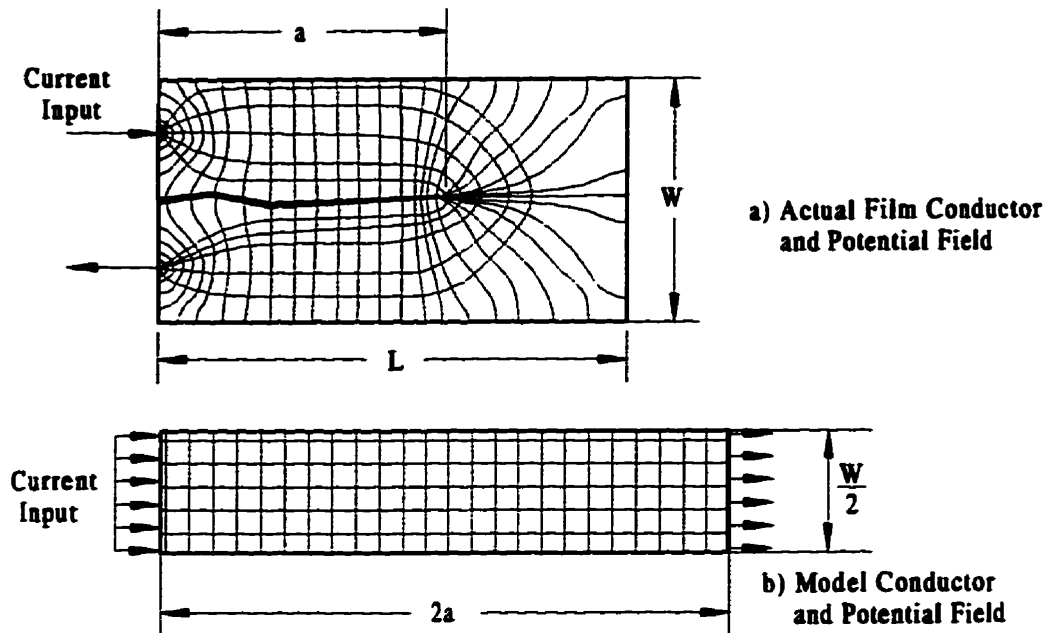


Figure 4.4: Representation of Simplified Model

and therefore is termed a paramagnetic material. The skin effect in such materials is very weak compared to ferromagnetic materials and does not result in appreciable changes in current density through the conducting cross section of the material. Calculations show that the ratio of film thickness to the skin depth is  $2.31 \times 10^{-4}$ . Figure 2.7 of Chapter 2 shows that for ratios below 0.1 the surface potential is identical to the DC potential and there is no variation in potential through the conductor cross section.

The validity of the second requirement is assessed in Chapter 5 following numerical studies of the film potential field. Since the foil acts as a solid conductor (like a wire), the inductance and capacitance will be negligible. The fulfillment of the remainder of the requirements is achieved through control of the material used in the film deposit and the nature of testing.

From the second requirement,  $\Delta\ell = 2\Delta a$  is an obvious first order approximation which neglects the localized non-uniformity of the potential field around the current input leads. This models the foil as a one dimensional conductor of length  $2a$  as shown in Figure 4.4. The conducting cross sectional area of this conductor would be one half the width of the foil strip  $W$  multiplied by the thickness  $t$ . Since the model represents a one-dimensional conductor, there is no variation in potential in the y-direction as shown in Figure 4.4b. From the simplified model;  $\Delta\ell = 2\Delta a$  and  $A = t\frac{W}{2}$  then Constants  $K_1$  and  $K_2$  can be written as:

$$K_1 = \alpha \text{ and} \quad (4.9)$$

$$K_2 = \rho_o \frac{4i}{Wt}. \quad (4.10)$$

Therefore the theoretical approximation for the voltage drop using this model is:

$$V = V_o + V_o\alpha\Delta T + \rho_o \frac{4i\Delta a}{Wt}(1 + \alpha\Delta T). \quad (4.11)$$

Rearranging Equation 4.11 provides a simple equation for predicting crack length in the foil:

$$a = a_o + \frac{Wt}{4i\rho_o} \left( \frac{\Delta V - V_o\alpha\Delta T}{1 + \alpha\Delta T} \right). \quad (4.12)$$

By using equations 4.9 & 4.10 and curve fit coefficients  $K_1$  and  $K_2$ , we can solve for two physical constants of aluminum. Equation 4.9 suggests a temperature coefficient of resistivity ( $\alpha$ ) of  $3.3 \times 10^{-3} \text{ } ^\circ\text{C}^{-1}$ , the value of this physical constant for aluminum is reported being  $3.9 \times 10^{-3} \text{ } ^\circ\text{C}^{-1}$  [6, 25]. Equation 4.10 contains the resistivity of the deposit at the reference temperature ( $30 \text{ } ^\circ\text{C}$  in the experiment). All other variables are experimental constants;  $i = 8.97 \times 10^{-4} \text{ A}$ ,  $W = 2.5 \times 10^{-2} \text{ m}$  and  $t = 2.3 \times 10^{-6} \text{ m}$ . Subbing these values into equation 4.10 and solving for  $\rho_o$  with  $K_2 = 0.001645$  yields  $\rho_o = 2.64 \times 10^{-8} \text{ } \Omega \cdot \text{m}$ , which is near the expected value of  $2.75 \times 10^{-8} \text{ } \Omega \cdot \text{m}$

for aluminum at 30 ° C [6, 25]. The close vicinity of these constants to their actual physical values suggests that equation 4.11 is an accurate model for predicting voltage drop in the foil conductor.

Table 4.3.1 summarizes the findings of the theoretical model when used with calibration results to calculate the initial resistivity  $\rho_o$ , and temperature coefficient of resistivity  $\alpha$ , for aluminum. The good agreement between the theoretical model and experimental results suggest the requirements outlined for the model have been met during calibration.

	Calculated Value	Physical Constant
Resisitvity at 30 ° C ( $\Omega \cdot m$ )	$2.64 \times 10^{-8}$	$2.75 \times 10^{-8}$
Temperature Coefficient of Resistivity ( $C^{-1}$ )	$3.3 \times 10^{-3}$	$3.9 \times 10^{-3}$

Table 4.2: Actual and Calculated Electrical Constants for Aluminum

## 4.4 Accuracy and Resolution of the Crack Length Measurement System

Using Equation 4.12 with actual and calculated values for constants  $\rho_o$  and  $\alpha$ , Figure 4.5 shows the accuracy of predicted crack lengths when compared to experimental values. The deviation for each crack length is based on the average difference between actual and predicted crack lengths over 6 temperatures from 30 to 200 ° C. Figure 4.5 suggests increased deviations for actual values of  $\rho_o$  and  $\alpha$ . This is due to the fact that the foil voltage field does not exactly meet the idealized case on which Equation 4.11 is based. The calculated (curve fit) values of  $\rho_o$  and  $\alpha$  are compensating for the slight deviation of the actual foil voltage field from the ideal model. Accuracy of the model using calculated  $\rho_o$  and  $\alpha$  is shown to be within 1.0 mm over the range of crack

lengths investigated as indicated in Figure 4.5.

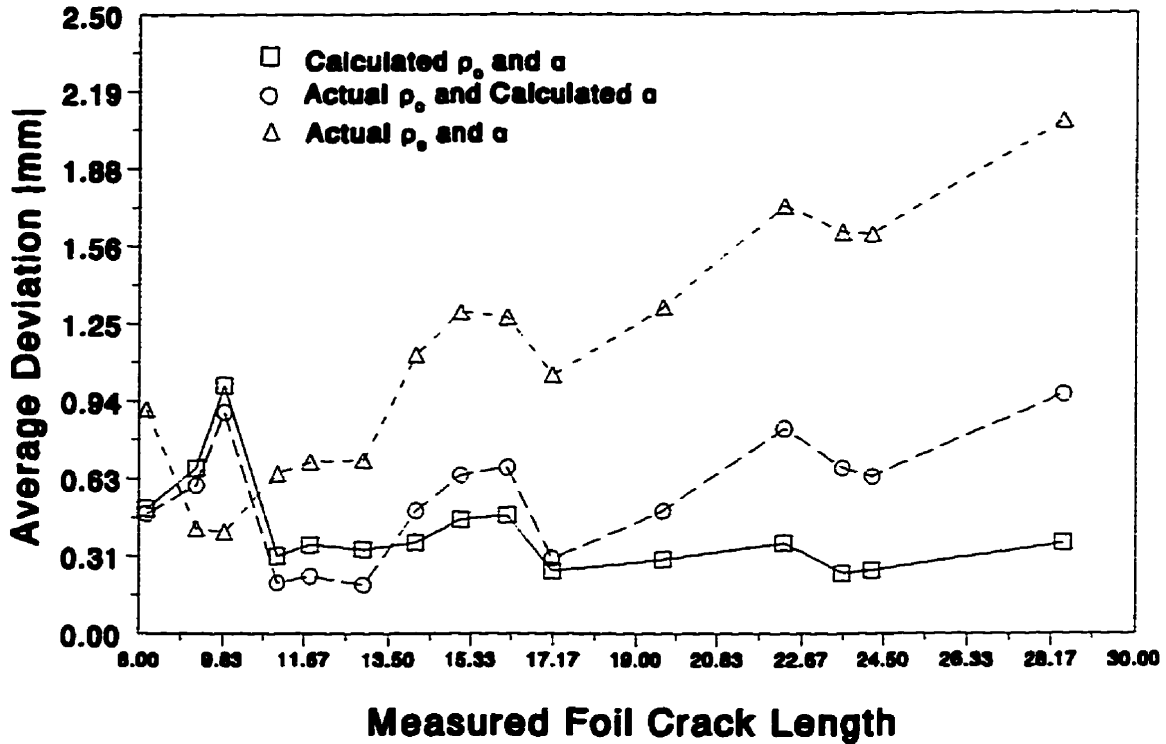


Figure 4.5: Accuracy of Crack Length Predictions

Over the majority of crack lengths, accuracy of the system is within 0.3 mm for calculated values of  $\rho_0$  and  $\alpha$ . Decreased accuracy at shorter crack lengths is suggested by Figure 4.5, this phenomenon is investigated in Chapter 5.

The overall sensitivity of the potential difference system can be determined by differentiating Equation 4.11 to yield the slope of the calibration curve. By differentiating Equation 4.11 with respect to crack length we obtain:

$$\frac{\partial V}{\partial a} = \rho_0 \frac{4i}{Wt} (1 + \alpha \Delta T). \quad (4.13)$$

Equation 4.13 indicates that the slope of the calibration curves are constant and

independent of crack length. Thus, the relationship between PD and crack length is linear. Equation 4.13 also shows that the sensitivity of the system can be increased by decreasing the film width or thickness, increasing the current or temperature, and using a conducting film with a high resistivity. Subbing in the calculated value of constants  $\rho_o$  and  $\alpha$  from Table 4.3.1 and  $i = 8.97 \times 10^{-4}$  A,  $W = 2.5 \times 10^{-2}$  m and  $t = 2.3 \times 10^{-6}$  m as used in calibration into Equation 4.13, and using an average calibration temperature ( $85^\circ\text{C}$ ,  $\Delta T = 55^\circ\text{C}$ ) we find that the average sensitivity of the system during calibration is  $1.95 \frac{\text{mV}}{\text{m}}$ . The voltage resolution of the lock-in amplifier is  $0.1 \mu\text{V}$  during calibration, thus the system can reliably detect a crack length change of  $0.051$  mm. In experimental testing discussed in Chapter 6, the current level  $i$  is increased beyond  $0.897$  mA to  $1.96$  mA, providing a higher sensitivity.

## **Chapter 5**

# **Numerical Analysis of the Film Potential Field**

To further explore the accuracy of Equation 4.12 in producing calculated crack length from temperature and potential values, numerical solutions for the film potential field are developed. By examining the nature of the potential field and comparing potential difference results with the model developed in Chapter 4, the accuracy and validity of the assumptions made by the linear conductor model can be evaluated. By using numerical solutions to the film potential field, results can be quickly produced when compared with experimental means. Of course, the results produced using numerical methods should be shown to verify existing experimental data before these techniques can be used.

The potential field distribution has been shown to be independent of film electrical properties, thickness, temperature and current flow when presented in a normalized form [1]. This suggests that these variables have a linear effect on all points of the potential field and do not control the 'shape' or distribution of the field. The factors which control the distribution of the potential field are the geometry of the film

deposit, the length of the crack within the film, and the location of the current input leads [4]. The location of the potential leads are also of importance since the location of potential measurement is known to influence the sensitivity and linearity of results [13, 4]. By determining the potential field and associated potential difference curves over a range of crack lengths, film geometries, and leadwire positions, the suitability of the 'linear conductor' model proposed in Chapter 4 can be evaluated within a range of these parameters.

## 5.1 Numerical Simulation of the Voltage Field

The deviations of the foil potential field from the ideal case are investigated using a finite difference solution. The potential field is governed by the Laplace equation:

$$\frac{\partial}{\partial x} \left( k_x \frac{\partial V}{\partial x} \right) + \frac{\partial}{\partial y} \left( k_y \frac{\partial V}{\partial y} \right) = 0. \quad (5.1)$$

In potential field problems,  $k_x$  and  $k_y$  are the electrical conductivity  $\sigma$ , of the material in the x and y directions respectively. Electrical conductivity and resistivity are inversely related to each other by the definition:

$$\rho \equiv \frac{1}{\sigma}. \quad (5.2)$$

Essentially, Equation 5.1 satisfies the law of conservation of electrical charge. The quantity of charge per second ( $\frac{C}{s}$ ) or current flowing out of an incremental volume of film of size  $dy$  by  $dx$  and thickness  $t$  (shown in Figure 5.1), in the x-direction is written as:

$$i_{x+dx} = t \frac{1}{\rho_x} \frac{\partial V}{\partial x} \Big|_{x+dx} dy. \quad (5.3)$$

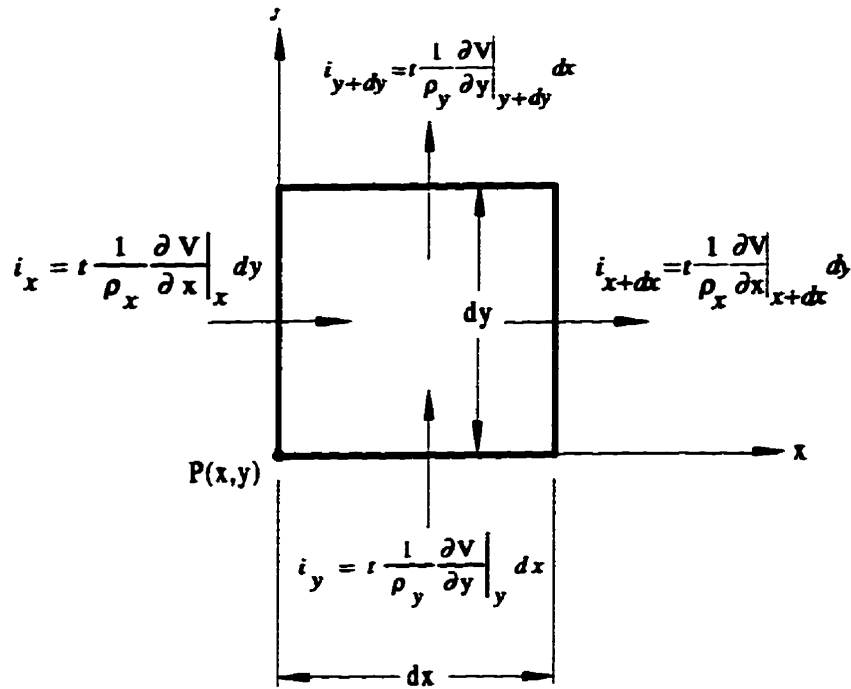


Figure 5.1: Conservation of Charge in the Control Volume

Using similar equations at boundaries  $x = x$ ,  $y = y$  and  $y = y + dy$  and performing a summation to indicate conservation of charge, Equation 5.1 is recovered. In the case of the vapor deposited aluminum film, electrical resistivity is uniform in all directions throughout the film. This means that constants  $k_x$  and  $k_y$  are equal, and may be removed from Equation 5.1 giving a simplified governing equation for the film potential field.

$$\frac{\partial^2 V}{\partial x^2} + \frac{\partial^2 V}{\partial y^2} = 0 \quad (5.4)$$

Using the Fortran program 'aspect.f' (listed in Appendix C), a finite-difference solution to the film potential field is calculated for various crack lengths and film geometries. Since the potential field is anti-symmetric about the x-axis, we need only solve for half of the problem. The boundary conditions and the geometry of the half-

field are shown in Figure 5.2. Due to the irregularity of the boundary conditions, an analytical solution was not found for the voltage field.

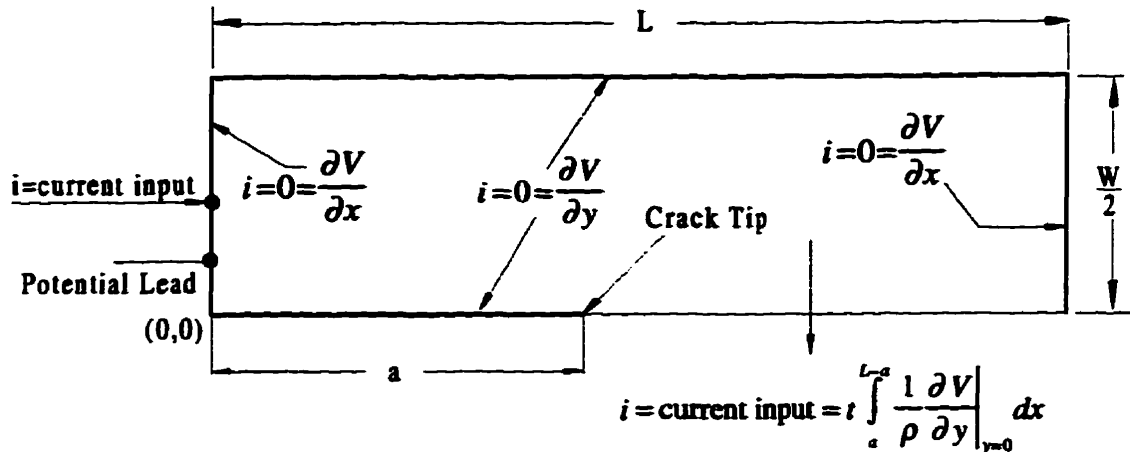


Figure 5.2: Boundary Conditions of Potential Field Problem

The problem is broken up into a ‘mesh’ of control volumes or elements which have finite difference equations that individually satisfy Equation 5.4. The finite difference mesh uses mesh refinement around the point of current input and the crack tip to accurately capture the high potential gradients in these areas. The simultaneous solution of all the elemental equations yields a nodal solution to the potential field throughout the finite difference mesh. However, upon assembling the elemental equations, we find that there are an insufficient number of equations to solve the problem. Additional information supplied by the boundary conditions is needed to complete the solution.

Boundaries at  $x = 0$ ,  $y = \frac{W}{2}$ ,  $x = L$ , and  $x = 0$  to  $a$  along  $y = 0$  require that current does not cross these boundaries. This is equivalent to setting the potential gradients perpendicular to these boundaries equal to zero as shown in Figure 5.2. One additional equation is supplied by conservation of current flow within the problem boundaries. This requires that the current supplied at the point of current application

is equal to the current exiting the problem boundary between  $x = a$  and  $x = L$  along  $y = 0$ . By summing the current flux in the  $y$ -direction along this line, the equation is written as:

$$i = t \int_a^{L-a} \frac{1}{\rho} \frac{\partial V}{\partial y} \Big|_{y=0} dx. \quad (5.5)$$

For any current input into the film, the problem may be satisfied by an infinite number of solutions. This is because the problem is specified in terms of potential gradients and point values of the solution are not specified. Since we seek the potential difference between potential leads, and the relative difference between all point values remains the same regardless of the solution, any of the possible solutions is acceptable. By arbitrarily specifying the potential at the coordinate  $(x = L, y = 0)$  equal to zero, the potential at the point of the potential lead connection is made to yield exactly one half of the potential difference reading. This is possible due to the anti-symmetric nature of the film potential field.

The computer program generated the solution for the half field for a given crack length  $a$ ,  $\rho_o$  and  $\alpha$ . For each crack length, potential fields were generated for the reference temperature of  $30^\circ \text{C}$ , and six temperature increments up to  $200^\circ \text{C}$  as in the calibration testing. Using these voltage fields, potential lead differential voltage can be determined and compared against experimental findings. The values of  $\rho_o = 2.7 \times 10^{-8} \Omega \cdot m$  and  $\alpha = 3.3 \times 10^{-3} \text{ } ^\circ \text{C}^{-1}$ , are found to give the best correlation with experimental data. The close vicinity of these constants to the curve fit values from experimental results found in Chapter 4, and the physical constants for aluminum suggests the numerical solutions are indeed accurate.

Figure 5.3 shows a typical half potential field solution for a 32 mm crack produced by the finite difference program 'aspect.f'. It is important to note the electric field strength in the  $x$  direction ( $\epsilon_x$ ) is constant from approximately 6 mm to 30 mm along

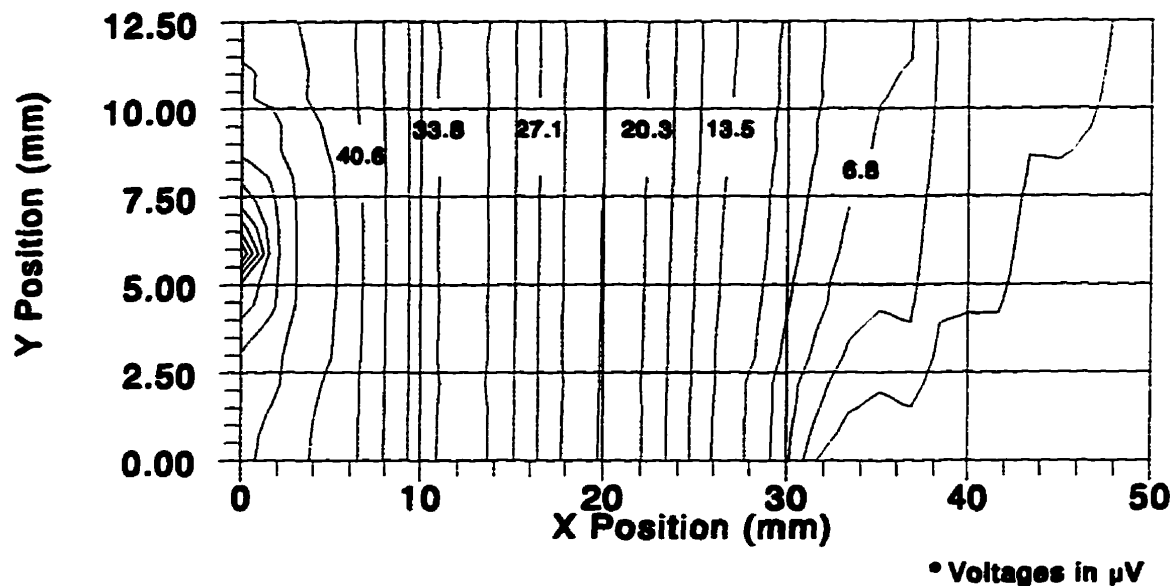


Figure 5.3: Half Potential Field for 32mm Crack

the x axis. In this region,  $\epsilon_y$  is zero. This shows that the second requirement of the simplified model is met within the majority of the voltage field. In this region, the potential field is behaving as if the film were a one dimensional conductor. In the voltage field outside this region, the field is not behaving according to the simplified model. However, the potential change through these regions remains relatively constant with crack length change and is accounted for in the  $V_0$  term of Equation 4.11.

The potential change in the foil with increasing crack length is dominated by the potential change in the region of constant electric field strength. Potential drop as predicted by Equation 4.11 and the finite difference program are compared to experimental results in Figure 5.4. Both methods are shown to accurately predict the potential change as the constant  $\epsilon_r$  region increases in size due to crack advance. Slightly higher potential values are suggested by Equation 4.11 and the experimental results since these values include small potential contributions from leadwire and

contact resistance outside the foil.

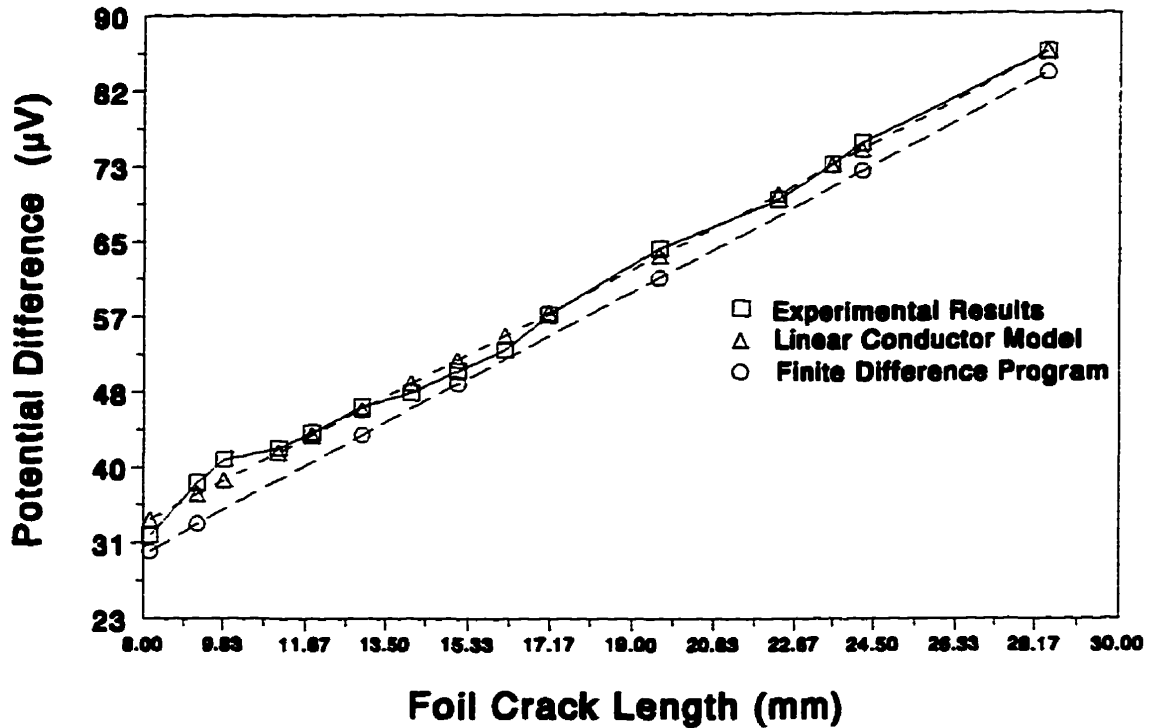


Figure 5.4: Potential Drop in Foil at 200 °C

## 5.2 The Effect of Crack Length

Using the finite difference program, potential fields are generated for a range of crack lengths at constant temperature. The potential fields are used to extract the corresponding potential difference between potential lead locations on the foil for each crack length. The potential differences suggested by numerical results are compared to those predicted by Equation 4.11. Differences between the two methods under particular crack lengths would suggest that the model is invalid for predicting potential drop at these crack lengths. In understanding the deviations from the idealized

model in these situations, the model can be refined or the crack measurement foil modified to provide better accuracy in predicting crack length.

### 5.2.1 Deviation at Short Crack Lengths

The computer program is used to study the agreement of Equation 4.11 with numerical results under short crack lengths at constant temperature as shown in Figure 5.5.

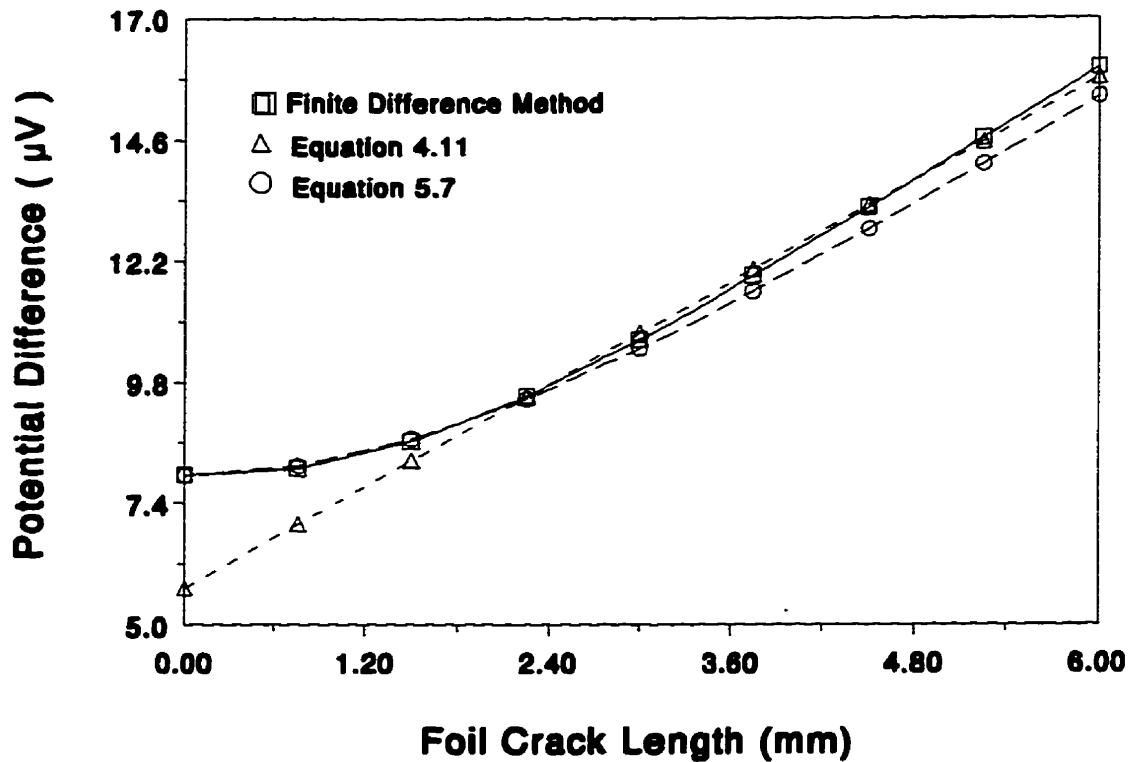


Figure 5.5: Predicted Potential at 30 °C - Short Crack

Sizeable deviation between the program results and Equation 4.11 are apparent for crack lengths below approximately 2.4 mm. This deviation reflects the change in direction of current flow from the 'simplified model' at short crack lengths such that

$\epsilon_x \approx 0$  and  $\epsilon_y = \text{constant}$ . To account for this change in the potential field at short crack lengths, the following corrected crack length is substituted into Equations 4.11 and 4.12.

$$a_{\text{corr}} = \sqrt{a^2 + s^2} \quad (5.6)$$

Where  $s$  denotes the distance between the potential leads and the centerline of the foil (3 mm in calibration specimens). Equations 4.11 and 4.12 incorporating this short crack length correction become:

$$V = V_o + V_o\alpha\Delta T + \rho_o \frac{4i(\sqrt{a^2 + s^2} - \sqrt{a_o^2 + s^2})}{Wt} (1 + \alpha\Delta T) \quad \text{and} \quad (5.7)$$

$$a = \sqrt{\left[ \frac{Wt}{4i\rho_o} \left[ \frac{\Delta V - V_o\alpha\Delta T}{1 + \alpha\Delta T} \right] + \sqrt{a_o^2 + s^2} \right]^2 - s^2}. \quad (5.8)$$

Where  $a_o$  denotes the crack length at the starting reference point. Figure 5.5 shows the improved accuracy of Equation 5.7 in calculating potential difference at short crack lengths.

### 5.2.2 Deviation at Long Crack Lengths

Deviation from the model is also expected for crack lengths longer than 37.5 mm, since this would result in a varying conducting area along the current path. This violates the fourth requirement of the model as detailed in Section 4.3. The potential is seen to approach infinity asymptotically as the crack length approaches 50 mm. This effect is shown in Figure 5.6. Note that the equations based on the simplified model do not predict this rapid increase in potential difference at long crack lengths.

To avoid errors due to conducting area reduction at long crack lengths, the width of the foil deposit must be made at least the maximum crack length expected plus one half the foil width. By decreasing the overall width of the foil deposit, nonlinear regions at short and long crack lengths are decreased. Although decreased foil width

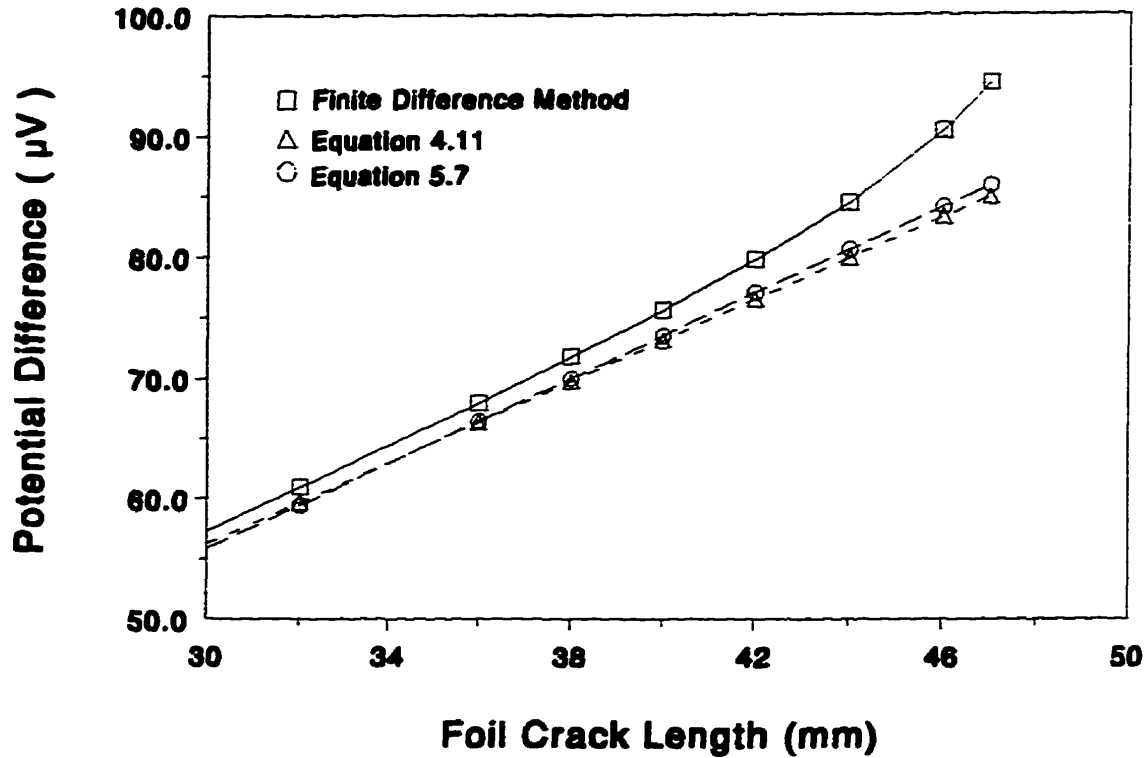


Figure 5.6: Predicted Potential at 30 ° C - Long Crack

may increase tendency towards linearity, it becomes more difficult to contain a propagating crack within foil boundaries such that the crack is roughly centered within the foil width. Thus, optimum dimensions of the foil deposit are largely dependent on the expected maximum crack length and direction of propagation.

### 5.3 The Effect of Film Aspect Ratio on Calibration Curves

The finite difference program 'aspect.f' is used to determine the shape of the potential difference vs. crack length curves for various film aspect ( $\frac{W}{L}$ ) ratios. The curves are

produced by determining the associated potential difference of various crack lengths for films with aspect ratios ranging from 0.5 to 4.0 at 30 ° C with a fixed foil length of 50 mm. The results produced by the program are plotted and shown in Figure 5.7. Aspect ratios which minimize the deviation of the potential field from the simplified model at short and long crack lengths will produce the best agreement with the model.

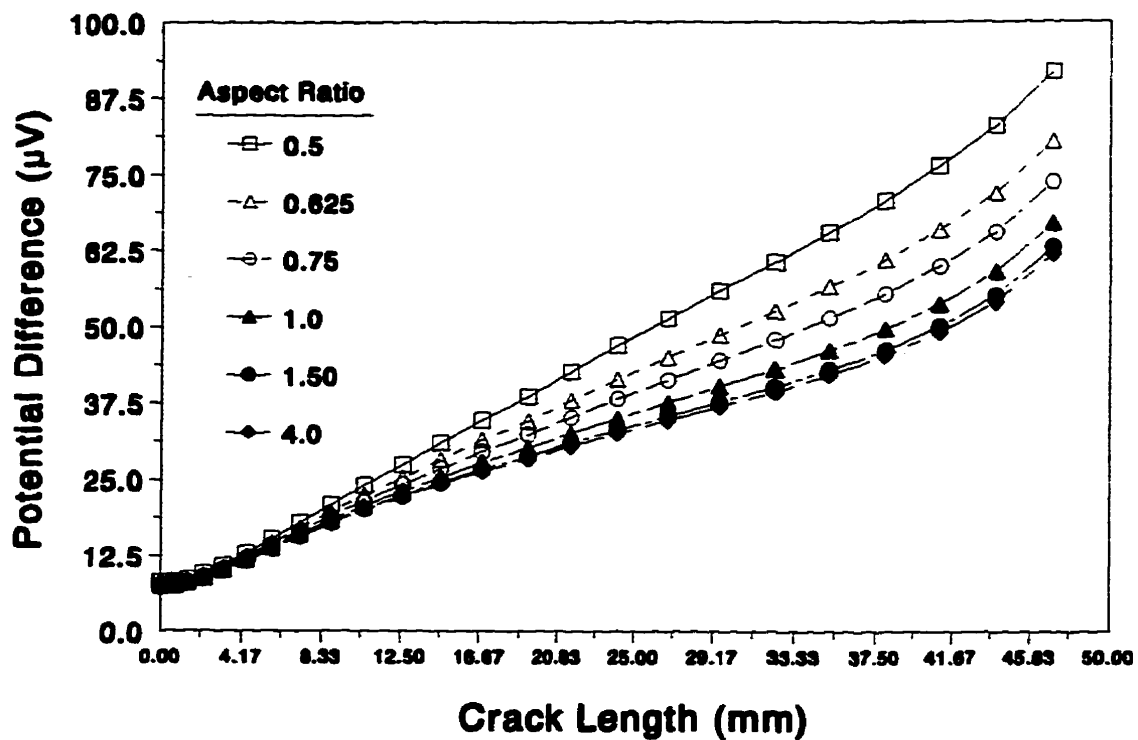


Figure 5.7: Effect of Film Aspect Ratio on Calibration Curves

As the aspect ratio is increased, results approach the analytical solution for the non-uniform current distribution in a strip of infinite width as discussed in Section 2.1.1 of Chapter 2. Obviously, using high aspect ratios leads to calibration curves which have a very small linear portion in the middle of the curve. Figure 5.7 shows the significant increase in linearity of results through the range of crack lengths as the aspect ratio is decreased. An aspect ratio of 0.5 gives a linear calibration curve

for cracks 8 to 38 mm in length (60% of the foil gage length) and provides good agreement with the linear conductor model over this range. Figure 5.7 also shows the gradual increase in sensitivity ( $\frac{dV}{da}$ ) of the system to crack length extension. This increase in sensitivity is due to the reduction of the conducting cross section as the aspect ratio is decreased. This trend is in agreement with Equation 4.13 which yields the sensitivity of the linear conductor model.

## **5.4 The Effect of Current and Potential Lead Location on Calibration Curves**

By using a modified version of 'aspect.f' potential difference curves for various locations of the potential and current leads are produced. By examining the potential difference curves for various lead locations, configurations which provide maximum sensitivity and linearity of results can be noted. Such configurations will provide the best agreement with the linear conductor model and yield the highest accuracy in crack length prediction.

Numerical results simulate the calibration curves for a 50 mm  $\times$  25 mm aluminum film which is  $2.3 \times 10^{-6}$  m thick carrying 0.897 mA current at 30 ° C.

### **5.4.1 The Effect of Current Lead Location**

By varying the vertical distance of the current leads from the crack centerline, the distribution of the film potential field is changed. Similar to the experimental calibration configuration, the potential leads are symmetrically located  $\pm 3$  mm from the crack centerline. Potential difference curves are generated for symmetrically placed current leads ranging from  $\pm 1$  mm to  $\pm 12.5$  mm from the crack centerline as shown

in Figure 5.8.

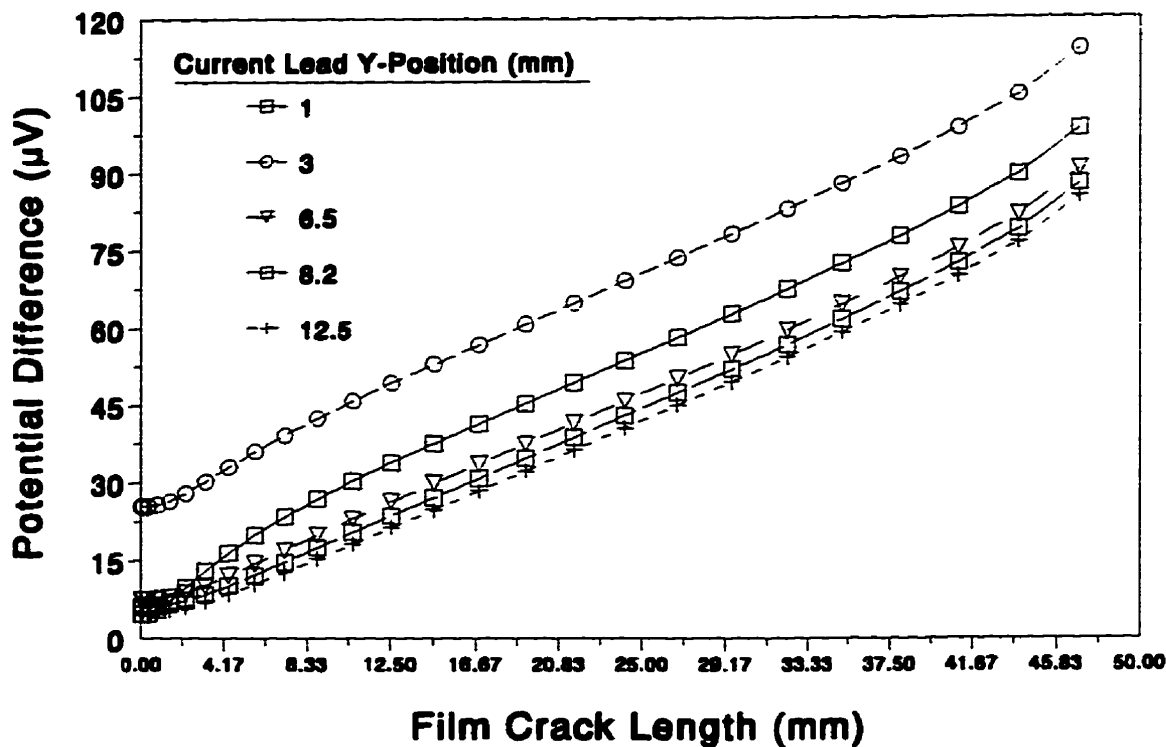


Figure 5.8: Effect of Current Lead Location on Calibration Curves

Figure 5.8 suggests that the effect of current lead location on the sensitivity of the crack length measurement system is negligible. It is important to note that this observation only applies to a film deposit of a finite size with an aspect ratio of approximately 0.5. Sensitivity was found to be dependent on the location of the current leads in the study of a non-uniform current carrying conductor by Gilbey and Pearson [14] as discussed in Chapter 2.

The magnitude of potential difference readings are shown to change with the location of the current leads. As the current leads get closer to the location of the potential leads ( $\pm 3$  mm), measured potentials increase. This does not influence the sensitivity of the system or the agreement of results with the linear conductor model,

since calibration is based on potential change from a reference point. Figure 5.8 suggests a decrease in linearity of the potential curves at short crack lengths as the current leads are moved closer to the axis of crack extension. Numerical results suggest that positioning the current leads farther than 5 mm from the crack axis minimizes the size of this nonlinear region at short crack lengths.

#### **5.4.2 The Effect of Potential Lead Location**

Potential difference curves are generated for various locations of the potential leads. All test parameters are the same as in the current lead position investigation except the current lead positions are held constant at  $\pm 6$  mm from the crack centerline. Potential difference curves are generated by varying the location of the potential leads from  $\pm 0$  mm to  $\pm 12.5$  mm from the crack centerline as shown in Figure 5.9.

The similar slope of all the curves in Figure 5.9 suggests that sensitivity of the crack length measurement system cannot be enhanced by varying the position of the potential leads. The magnitude of the potential difference readings increase as the potential leads are moved closer to the location of the current leads. This effect was observed in the studying the effect of moving the current lead positions. Figure 5.9 shows that configurations using a potential lead positions less than  $\pm 3$  mm from the crack centerline have an increased region of nonlinearity at short crack lengths. By using potential lead positions farther than  $\pm 3$  mm from the crack centerline, better agreement with the linear conductor model is achieved.

### **5.5 Summary of Numerical Findings**

Table 5.1 summarizes the findings of the effects of various aspects of the film configuration on the agreement of results with the linear conductor model. By presenting

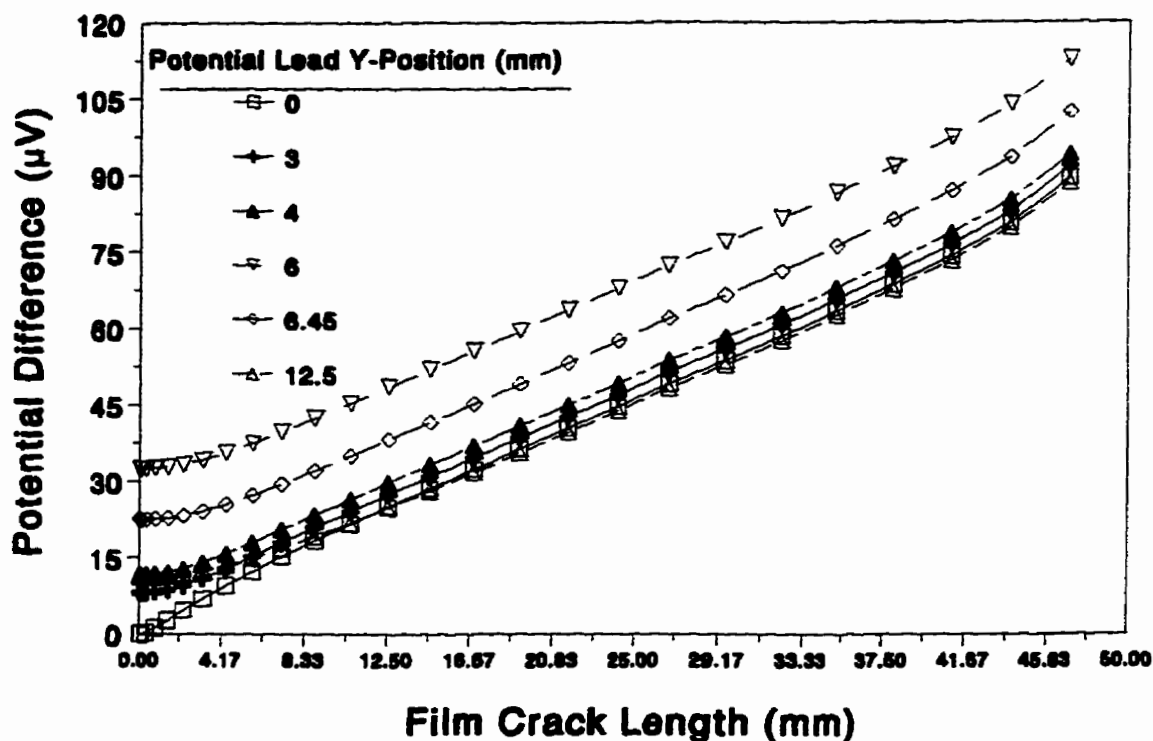


Figure 5.9: Effect of Potential Lead Location on Calibration Curves

the results in a normalized form, the results are applicable to rectangular conducting film deposits of any proportional size. These recommendations should be used as guidelines to maintain good agreement of potential difference measurements with the linear conductor model. This will serve to produce the highest level of accuracy and sensitivity in using Equations 4.12 or 5.8 to predict crack length based on potential difference.

It is of note that the film configuration used during the experimental collection of calibration data falls within acceptable bounds of the parameters suggested in Table 5.1. It was only by chance that this had happened, and would help to explain the good correlation of experimental results with relations developed using the linear conductor model. Essentially, the range of parameters shown in the Table represent

<b>Parameter</b>	<b>Range</b>	<b>Effect</b>
Crack Length $a$	0.16L to 0.76L	Best Accuracy
Aspect Ratio $\frac{W}{L}$	$\leq 0.5$	Best Sensitivity and Accuracy
Current Lead Position ( $\pm$ )	$\geq 0.2W$	Best Accuracy
Potential Lead Position ( $\pm$ )	$\geq 0.12W$	Best Accuracy

**Table 5.1: Optimal Film Parameters**

limits in which the film potential field behaves similarly to the assumptions of the linear conductor model. Under these situations, Equations 4.12 and 5.8 provide a simple and accurate means of crack length prediction based on potential difference.

## **Chapter 6**

# **Application of the Crack Measurement System to Fatigue and Creep Induced Crack Growth**

To investigate the performance of the crack length measurement system under typical testing situations, several tests are performed. Experimental results are collected from constant temperature fatigue testing, and both constant and variable temperature creep testing. The experimental results produced by these tests are indicative of the sensitivity, resolution, and long term stability of the testing station. Knowledge of the performance of the crack length measurement system is important in the evaluation of the possible application of this system to other types of testing involving crack length measurement.

From each test, results are collected which record the potential difference, load, temperature and strain of the specimen. Potential difference results are translated into crack length using Equation 5.8 and discussed in light of the test conditions. In particular, the crack growth response to temperature and loading changes is discussed.

## 6.1 The Fatigue and Creep Testing Program 'Creep.c'

Fully automated control of the test procedure is provided by 'creep.c', a C-based program included in Appendix C. Similar to the calibration program 'calib.c', 'creep.c' is comprised mainly of commands issued to external test apparatus through control pathways to conduct testing and record results. A flowchart of the execution of 'creep.c' is shown in Figure 6.1.

The specimen response to thermomechanical loading is recorded through the changes in strain and potential difference over time. The test parameters input at the start of program execution control the nature of testing. Several test styles may be selected; constant temperature fatigue, constant temperature creep, and variable temperature creep. In addition to specifying the test type, pertinent test parameters listed in Table 6.1 are input.

Parameter	Symbol	Units
Maximum Stress	$\sigma_{max}$	MPa
Relaxation Stress	$\sigma_{min}$	MPa
Fatigue Loading Frequency	$\omega$	Hz
Loading Duration	$t_{load}$	min
Relaxation Duration	$t_{relax}$	min
Maximum Temperature	$T_{max}$	°C
Minimum Temperature	$T_{min}$	°C
Initial Crack Length	$a_o$	mm

Table 6.1: User Specified Test Parameters

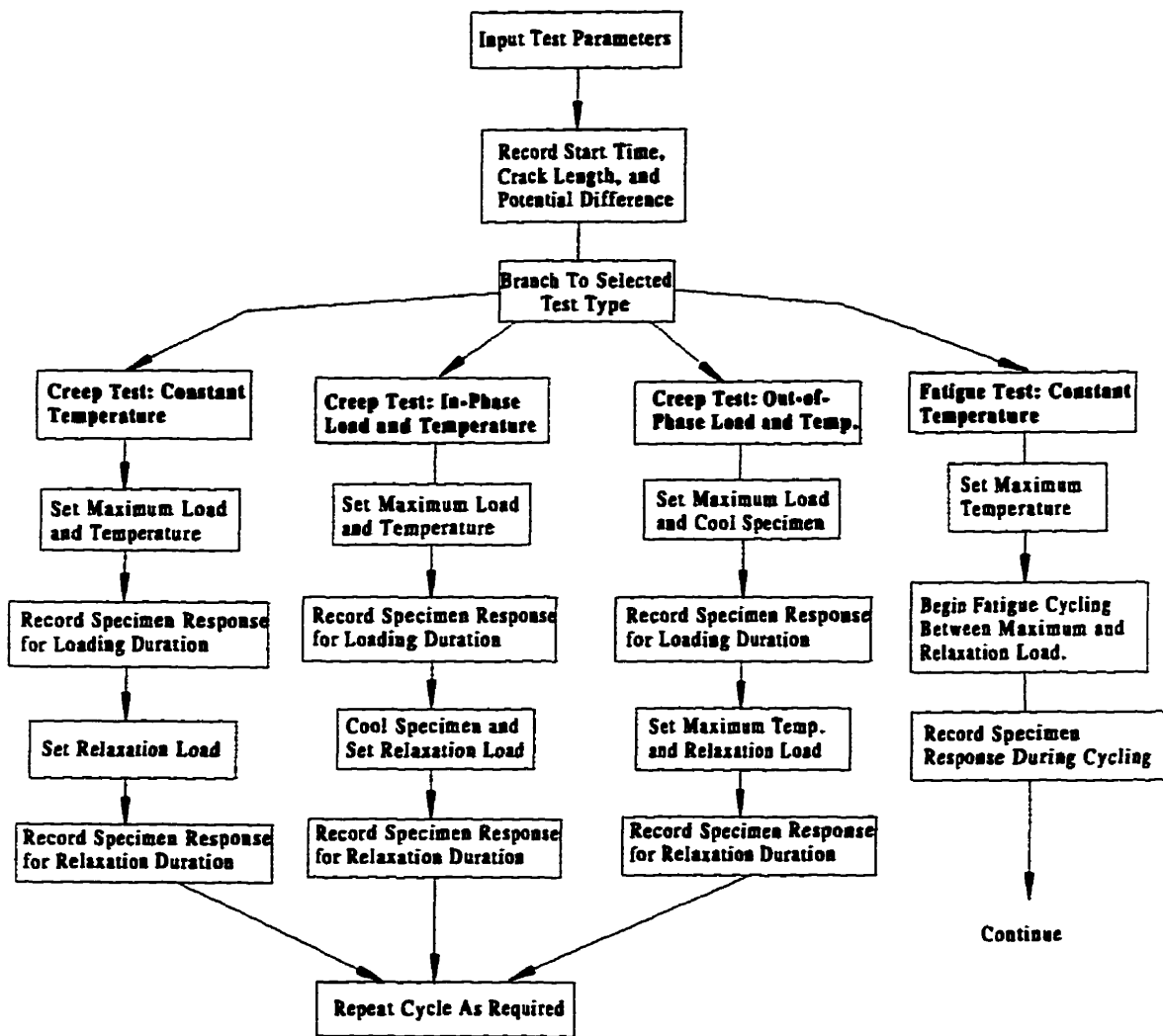


Figure 6.1: Program Flowchart for 'creep.c'

The stresses  $\sigma_{max}$  and  $\sigma_{min}$  control the maximum and minimum load the specimen is cycled between during loading and relaxation cycles. These stresses apply to both creep and fatigue test configurations. The fatigue loading frequency  $\omega$ , applies only to fatigue testing and is not requested if a creep test type is specified. The loading and relaxation duration  $t_{load}$  and  $t_{relax}$  apply only to creep testing and are not used for fatigue testing. The maximum and minimum testing temperatures  $T_{max}$  and  $T_{min}$  control the limits of temperature during testing. During variable temperature creep testing, the temperature can be varied using air cooling and furnace heating to produce both in-phase and out-of-phase thermomechanical loading as shown in Figure 6.2. In the case of a constant temperature creep test or a fatigue test, only  $T_{max}$  is required. Finally, the initial crack length  $a_0$  is needed to calculate suitable load values which produce stresses  $\sigma_{max}$  and  $\sigma_{min}$ .

After the required information has been input by the user, test execution proceeds automatically until halted. This feature allows fatigue and creep tests of long duration to be performed automatically with no requirement for user interaction. This feature also helps to maintain uniformity of test execution between specimens subjected to the same test schedule.

## 6.2 Potential Difference System Configuration

During all testing, the configuration of the AC potential difference system is not changed. As in previous calibration testing, a 93 Hz excitation frequency is used. The thin film deposit on the specimen is of the same dimensions as in calibration with the potential and current leads positioned at  $\pm 3$  mm and  $\pm 6$  mm from the crack centerline respectively.

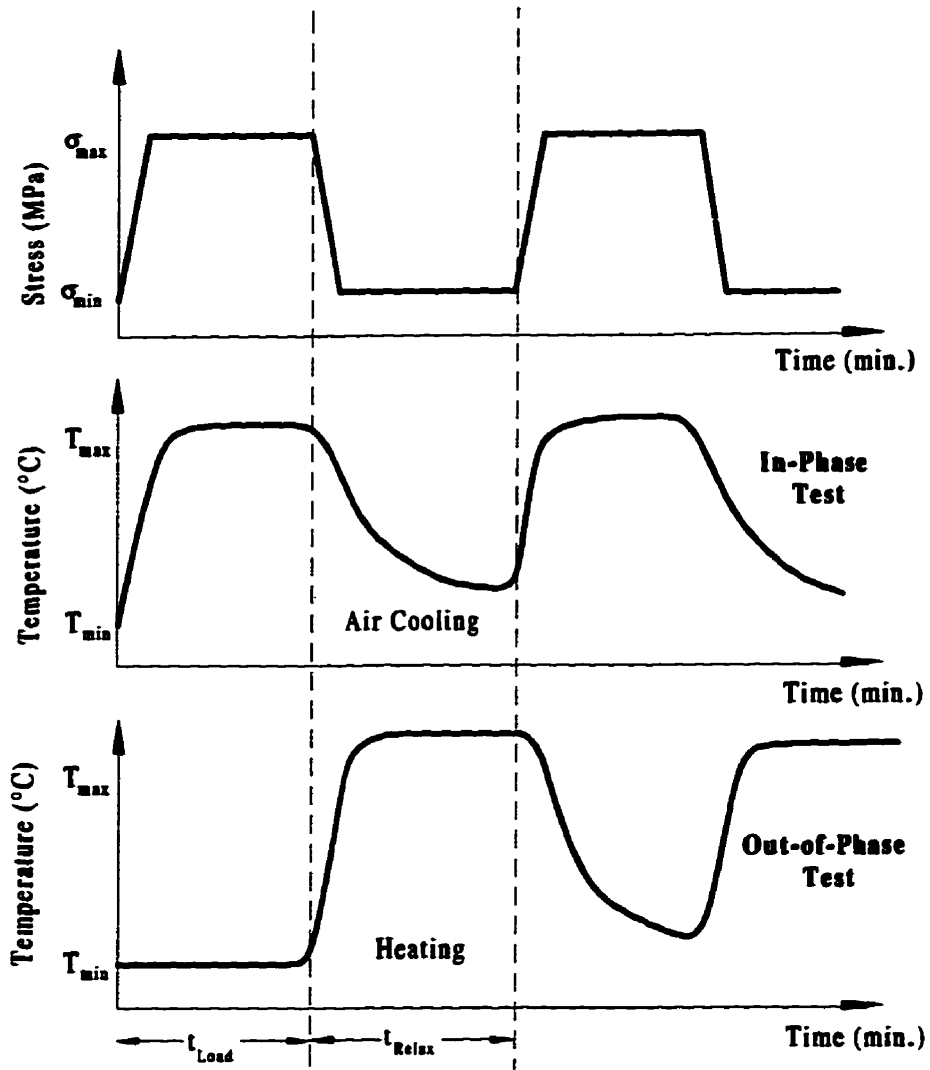


Figure 6.2: Creep Testing under Variable Temperature

To increase the resolution of the crack length measurement system, the current level is increased from 0.897 mA rms (used during calibration) to 1.96 mA rms. Equation 4.13 suggests that the average sensitivity of the system in this configuration is  $5.27 \frac{mV}{mm}$  for tests ranging from 30 ° C to 300 ° C. The resolution corresponding to this sensitivity level 0.0188 mm with a lock-in amplifier resolution of 0.1 $\mu$ V. Thus, the sensitivity and resolution of the system is increased by 2.5 times over the configuration used for calibration testing.

## 6.3 Fatigue and Creep Testing Results

The test procedure and important test parameters are discussed along with test results for each of the four test types. Crack response to the various types of thermomechanical loading as indicated by the potential difference system is evaluated with respect to what sort of results should be expected. Test results indicate potential difference, temperature, stress and strain change over time during testing. With the potential difference and temperature data collected over time, a corresponding plot of crack length over the test period can be constructed using Equation 5.8.

Through all the tests, the 6061-T6 aluminum test specimens are prepared identically as was previously done for calibration testing.

### 6.3.1 Fatigue Induced Crack Growth under Constant Temperature

During fatigue cycling of the test specimen, the test temperature is preset to  $T_{max}$  and cycling proceeds at the requested frequency  $\omega$ . The load cycling waveform for the specimen is sinusoidal with minimum and maximum stresses of  $\sigma_{max}$  and  $\sigma_{min}$

respectively. Fatigue cycling and data recording begins when the specimen temperature has had time to stabilize. Test parameters for the fatigue test are listed in Table 6.2.

Parameter	Symbol	Magnitude
Maximum Stress	$\sigma_{max}$	144 MPa
Minimum Stress	$\sigma_{min}$	36 MPa
Fatigue Loading Frequency	$\omega$	0.75 Hz
Test Temperature	$T_{max}$	21 ° C
Initial Crack Length	$a_o$	26.56mm

Table 6.2: Fatigue Test Parameters

Potential difference measurements collected during testing are plotted in Figure 6.3. The oscillation of the potential difference data about the linear curve fit indicates some slight crack face touching near the crack tip. Crack face touching which occurs while specimen stresses are low temporarily decreases the potential difference measurements as discussed in Section 2.4 of Chapter 2. The effects of crack face touching can be quite pronounced, especially during fatigue loading with low values of  $\sigma_{min}$ .

After approximately 90 minutes of fatigue cycling the specimen crack length was measured optically and found to be 27.43 mm. After translating the potential difference data into calculated crack length using Equation 5.8, the final calculated crack length is 27.38 mm as shown in Figure 6.4. This represents a difference of only 0.05 mm between measured and calculated results. Using the calculated results, the crack growth over the 90 minutes of fatigue cycling is 0.82 mm.

The uniform rate of crack growth shown in Figure 6.4 is typical of fatigue crack growth under uniform stress cycling. With this type of loading, the crack front moves a uniform distance increment per fatigue cycle.

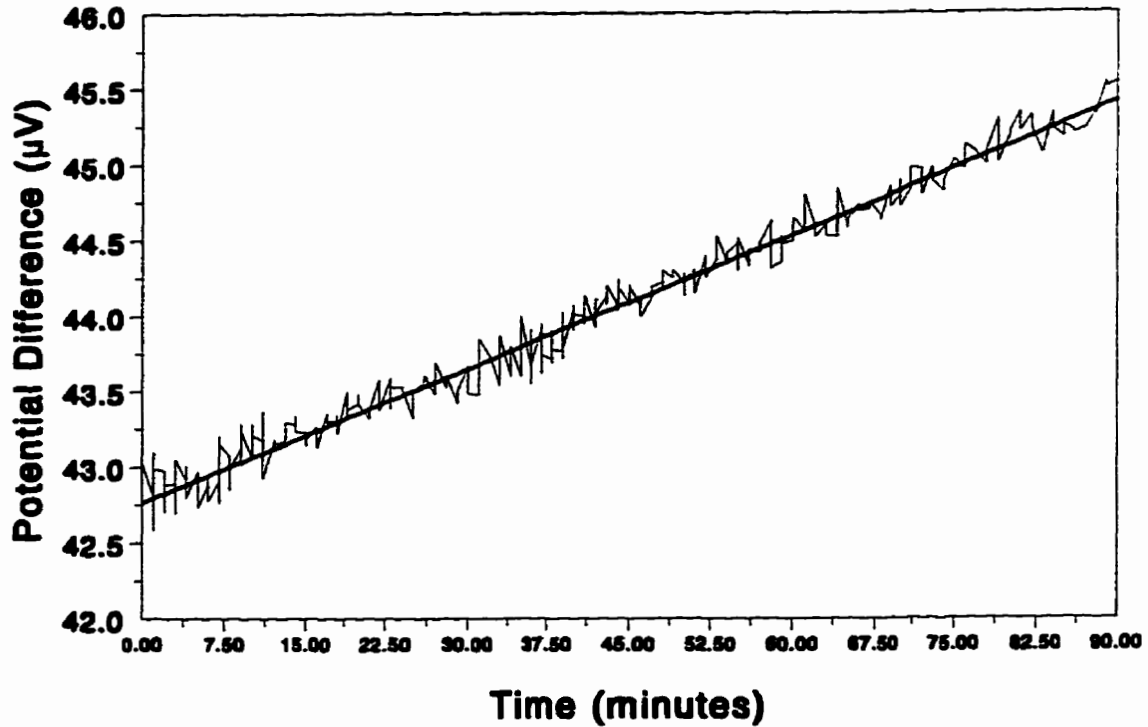


Figure 6.3: Potential Change with Fatigue Crack Growth

### 6.3.2 Creep Induced Crack Growth

During creep testing of the specimen, the temperature is preset to  $T_{max}$  and the specimen stress is set to  $\sigma_{max}$ . The response of the specimen is recorded through changes in potential difference and strain. In creep testing, it is important to ensure that the size of the plastic zone at the crack tip is kept reasonably small to prevent plastic strains from producing delamination or premature cracking in the film ahead of the crack tip. Loading stress  $\sigma_{max}$  is selected to ensure a small plastic zone.

From linear elastic fracture mechanics [22] for a center cracked plate of width  $W$  with half crack length  $a$  we can determine the stress in the  $y$ -direction at any polar coordinate  $(r, \theta)$  using;

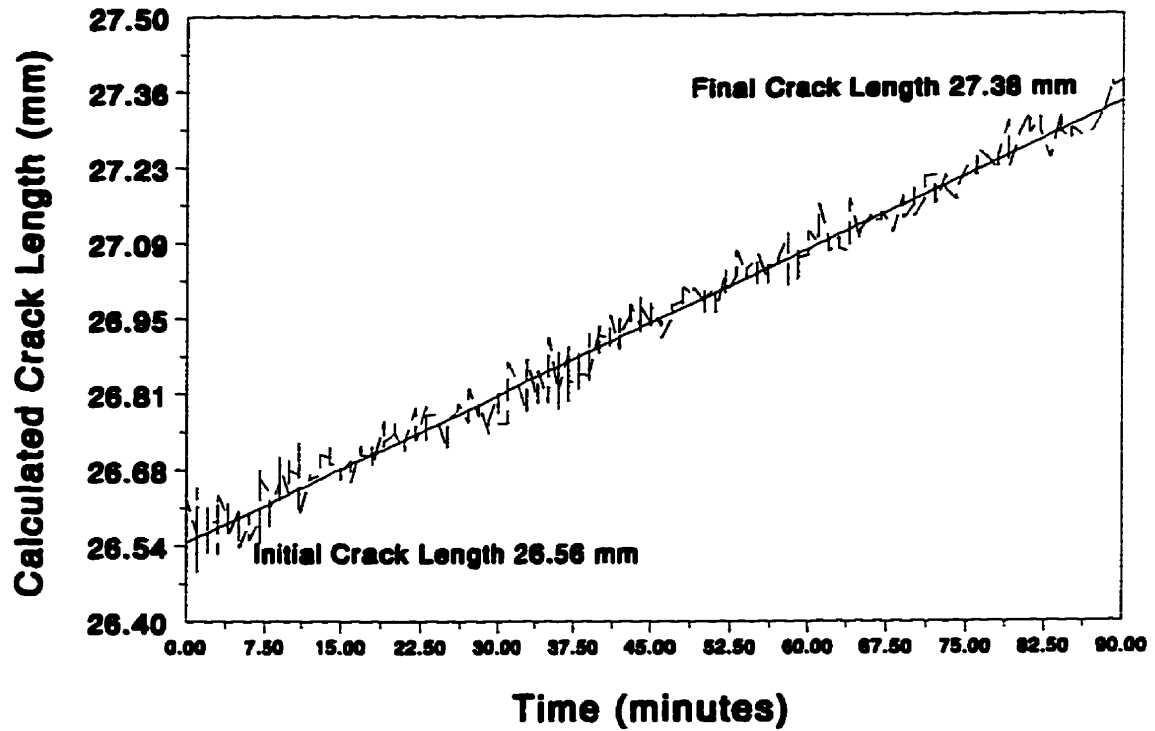


Figure 6.4: Fatigue Crack Growth at 21 ° C

$$\sigma_y = \frac{K_I}{\sqrt{2\pi r}} \cos \frac{\theta}{2} \left[ 1 + \sin \frac{\theta}{2} \sin \frac{3\theta}{2} \right]. \quad (6.1)$$

If we set Equation 6.1 equal to the yield stress of the material  $\sigma_{yld}$ , and using  $\theta = 0$ , we can determine the distance of the plastic radius  $r_p$  from the crack tip in the x-direction.

$$r_p = \frac{K_I^2}{2\pi\sigma_{yld}^2} \quad (6.2)$$

The stress intensity factor  $K_I$  for a center cracked plate is obtained by the expression;

$$K_I = \sqrt{\sec \frac{\pi a}{W}} \sigma_y \sqrt{\pi a}. \quad (6.3)$$

Using Equations 6.2 and 6.3, the plastic radius according to linear elastic fracture mechanics can be determined. This plastic radius has been shown to be precisely one half the actual plastic radius due to stress redistribution and crack tip blunting. These findings are valid if  $r_p \ll a$ .

To minimize the possibility of foil delamination or premature cracking ahead of the crack tip, the load to produce a plastic radius of 0.20 mm is determined. Using Equations 6.2 and 6.3 with  $r_p = 0.05\text{mm}$ ,  $W = 100\text{mm}$ ,  $a = 17\text{mm}$  and  $\sigma_{yld} = 240\text{MPa}$  we can determine the desired loading stress  $\sigma_{max}$ . Subbing in these values and solving for  $\sigma_{max}$  we find that a loading stress of 24.2 MPa is required to produce a 0.2 mm plastic radius for a crack of 17 mm length. Based on these calculations, stress levels  $\sigma_{max}$  and  $\sigma_{min}$  are set at 25 MPa and 5 MPa respectively. These stresses are sufficient to drive creep crack extension and maintain the plastic radius within approximately 0.20 mm for cracks up to 17 mm in length.

To induce significant creep behavior in most metals, the test temperature must exceed  $0.4T_m$  where  $T_m$  is the melting point of the primary metal constituent in the alloy [8]. In the case of the 6061-T6 aluminum alloy specimens used for testing, the melting point of the alloy is  $650^\circ\text{C}$ , then test temperatures above  $260^\circ\text{C}$  ( $0.4T_m$ ) are expected to produce significant and measureable creep response to loading. In creep induced crack growth testing using the crack measuring film, the maximum testing temperature  $T_{max}$  is  $300^\circ\text{C}$  ( $0.46T_m$ ).

For aluminum at temperatures exceeding  $300^\circ\text{C}$ , creep testing curves for aluminum [27] have shown that primary creep response is apparent up to 600 minutes into testing. After approximately 500 to 600 minutes, constant rate or secondary creep dominates the specimen response as shown in Figure 6.5. For investigative testing needed to evaluate the operation of the crack measurement system, the primary creep regime will be sufficient for the purposes of inducing creep crack growth response. In

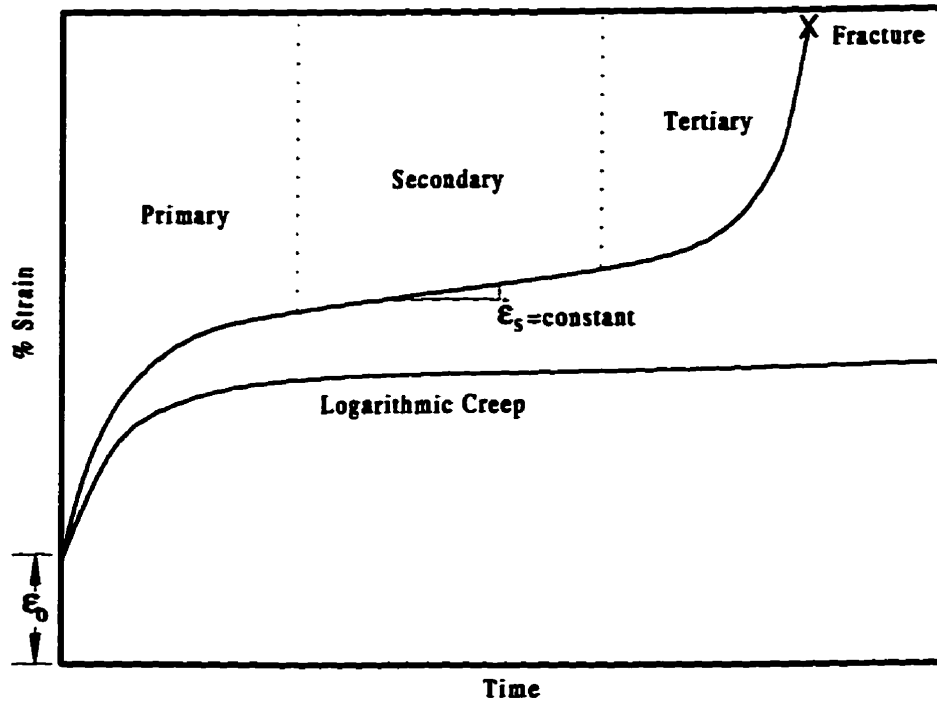


Figure 6.5: Strain-Time Curves for Logarithmic ( $T < 0.4T_m$ ) and Normal Creep ( $T > 0.4T_m$ ) Response [8]

testing, both loading and relaxation time will be 480 minutes to allow sufficient time for measurable specimen response. Overall test times range from 8 to 42 hours to show the time dependent response of the crack tip to the varied thermomechanical loading patterns.

Test parameters used in creep testing are listed in Table 6.3.

### Constant Temperature Constant Load Creep Test

Specimen response was recorded for a constant temperature of  $300^\circ\text{C}$  while under 25 MPa stress. The test duration of approximately 9 hours allowed completion of the primary creep regime and transition from primary to secondary creep in the specimen. The specimen response during the test is shown in Figure 6.6.

Parameter	Symbol	Magnitude
Maximum Stress	$\sigma_{max}$	25 MPa
Relaxation Stress	$\sigma_{min}$	5 MPa
Test Temperature	$T_{max}$	300 ° C
Loading Duration	$t_{load}$	420 min
Relaxation Duration	$t_{relax}$	420 min
Initial Crack Length	$a_o$	13.4 to 17 mm

Table 6.3: Creep Test Parameters

Figure 6.6 shows the logarithmic shape of the creep strain curve with time. The final specimen strain was 0.35% after approximately 525 minutes of testing. The crack growth response can be seen in the potential difference portion of the graph. Since the specimen temperature is constant, changes in potential difference correspond to crack length change. Similar to the specimen strain plot, the crack growth response is approximately logarithmic in shape and seems to correspond with the creep strain rate in the specimen. The plot shows the typical rapid creep induced crack growth associated with primary creep at time ranging from 0 to approximately 200 minutes. Using Equation 5.8, potential difference values are transformed to provide crack length data for the test over time. The calculated crack growth is shown in Figure 6.7.

Figure 6.7 shows rapid creep crack growth until approximately 200 minutes into testing. At 200 minutes, crack growth slows considerably until the final crack length of 14.54 mm. The calculated crack growth indicates a 1.14 mm increase in crack length over the 525 minute test period.

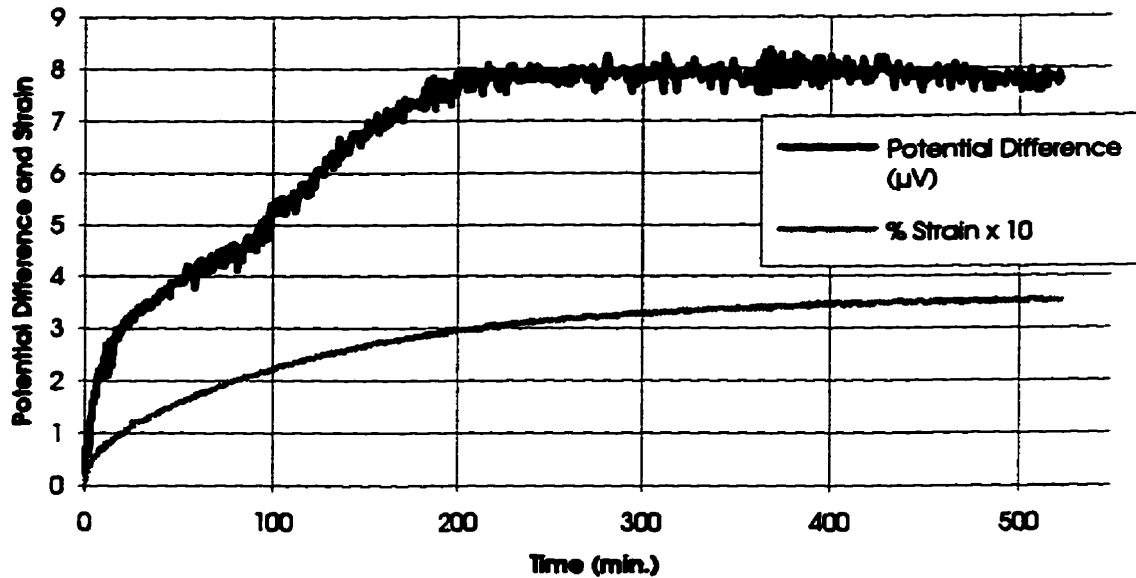


Figure 6.6: Specimen Response During Constant Temperature Creep Test

### Constant Temperature Variable Load Creep Test

Specimen response was recorded for a constant temperature of 300 ° C while under variable load ranging from 5 MPa to 25 MPa. Loading and relaxation durations for the test are both equal to 420 minutes. The test duration of approximately 45 hours allowed completion of the primary creep regime and transition from primary to secondary creep in the specimen. The specimen response during the test is shown in Figure 6.8.

The variable nature of the loading in this test is apparent from the plot of specimen strain. Nearly all of the creep strain developed in the specimen occurs during the peak loading cycle which produces 25 MPa average stress in the specimen. The potential difference portion of the plot shows sudden changes in potential readings during periods of load change. This is likely due to crack face touching effects or sudden elastic advance of the crack tip. During the relaxation portion of the loading cycle, very little creep of the specimen is observed.

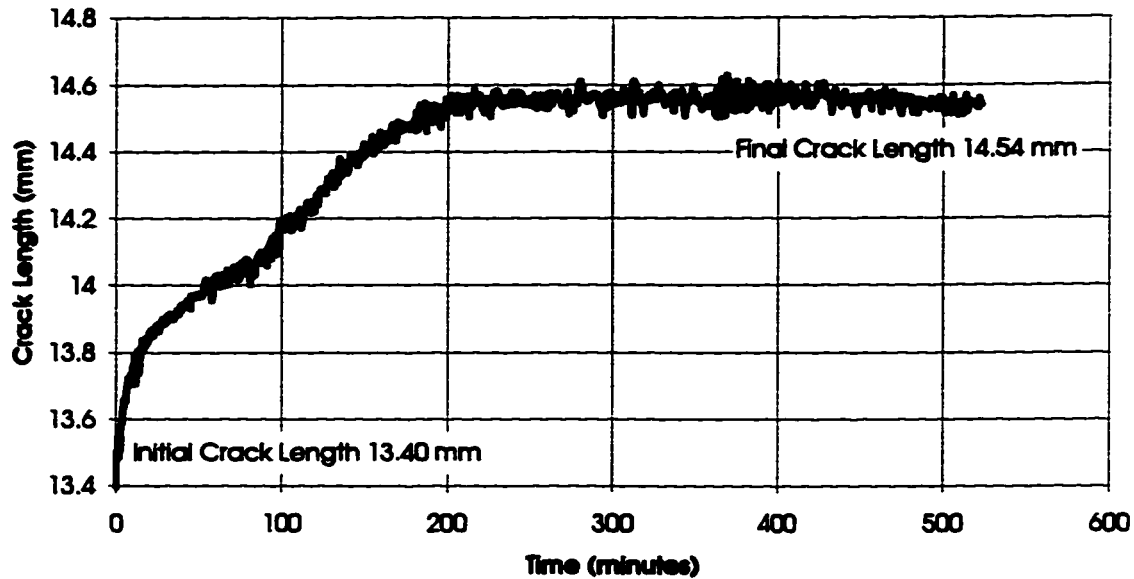


Figure 6.7: Crack Growth During Constant Temperature Creep Test

The crack growth response corresponding to potential difference and temperature data is shown in Figure 6.9. Primary creep crack growth is maximum during the peak loading cycle and is shown to continue at a decreased rate during the relaxation portion of the loading cycle. The relaxation portion of the loading cycle results in a decreased overall crack growth rate due to a reduction in the driving stresses at the crack tip. The calculated results indicate crack growth from 13.4 mm to 14.85 mm, a 1.35 mm growth over the 45.8 hour test period. Nearly all the crack growth occurs from 0 to 1500 min in the primary creep crack growth regime.

It is of note here that the results shown in Figure 6.9 do not indicate as rapid initial crack growth as in Figure 6.7. Although the initial conditions of both tests are nearly identical ( $T_{max} = 300^{\circ} \text{C}$ ,  $\sigma_{max} = 25 \text{ MPa}$ ,  $a_o \approx 13.5 \text{ mm}$ ), variation in crack growth response is likely due to differences in the shape and material conditions of the crack tip. Results shown in Figure 6.9 may be indicative of a more blunt initial crack tip or a larger plastic zone around the crack tip as compared to the specimen used for

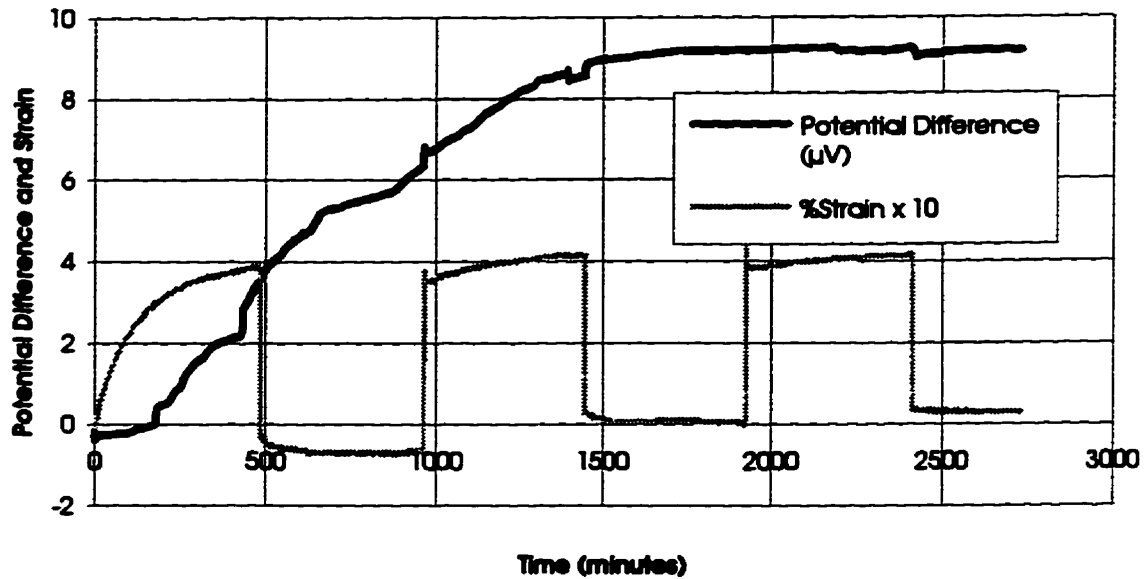


Figure 6.8: Specimen Response During Variable Load Creep Test

producing Figure 6.7. These conditions would explain the crack growth delay (0-200 minutes) and decreased growth rate (200-1500 minutes) observed in Figure 6.9.

### Variable Temperature Variable Load Creep Test

In this test, average stress in the specimen is varied between 5 MPa and 25 MPa between loading and relaxation portions of the loading cycle. The temperature of the specimen is also varied from room temperature to 300 ° C such that the temperature variation is in-phase with loading as shown in Figure 6.2. Once again, the loading and relaxation durations are 480 minutes in length. During the relaxation and cooling portion of the thermomechanical loading cycle the temperature of the specimen is dropped rapidly to the lowest temperature possible before the heating and loading portion of the cycle begins. Potential difference results for this thermomechanical loading pattern are shown in Figure 6.10.

The marked effect of temperature on potential difference results is shown in Fig-

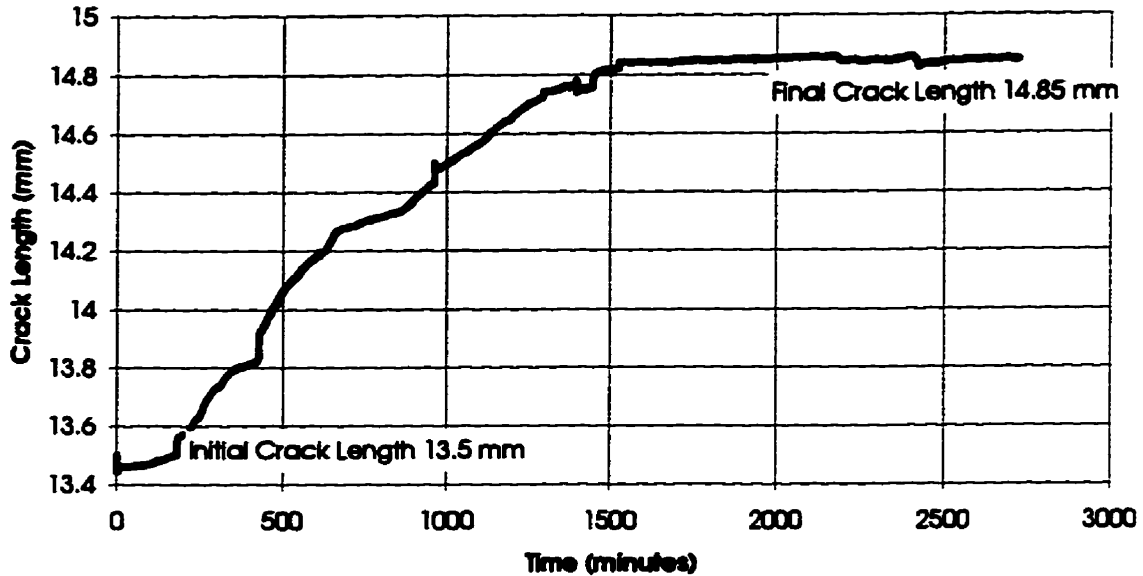


Figure 6.9: Crack Growth During Variable Load Creep Test

ure 6.10. During cooling, the resistivity of the material drops significantly and the potential difference drops in response to this change in film properties. The effects of temperature change on the data shown in the graph make it difficult to determine the crack growth response by simply viewing potential difference results as was done for constant temperature tests. Equation 5.8 must be used to transform the data and account for the effects of temperature on potential difference measurements. The calculated crack length over the test period is shown in Figure 6.11.

Figure 6.11 shows the crack response to the thermomechanical loading cycle over the test period of approximately 24 hours. To average out the effects of potential difference signal noise and provide a smoother representation of the crack growth data, a sixth order polynomial curve fit is shown. During the loading portion of the cycle, crack growth is quite rapid which is typical of primary creep response shortly after load application. This behavior has been observed in both of the previous creep tests. During the relaxation portion of the cycle appreciable crack growth is not

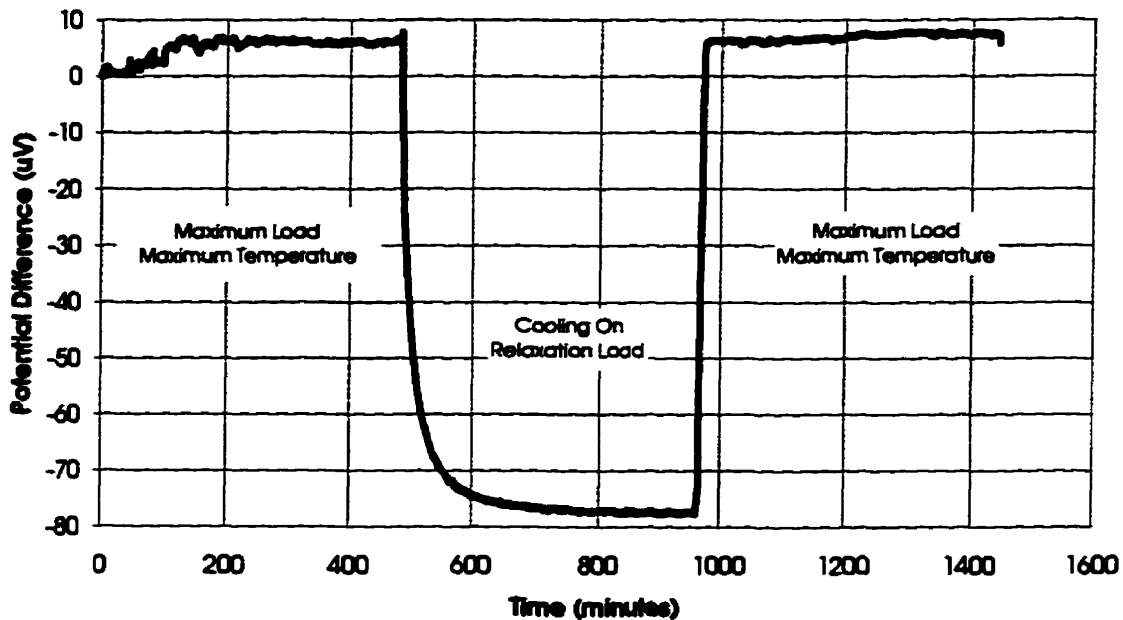


Figure 6.10: Potential Difference During In-Phase Thermomechanical Loading

observed due to the low specimen temperature caused by the air cooling. At the start of specimen cooling, the temperature dropped  $180^{\circ}\text{C}$  over 19 minutes. Obviously, measurable creep crack growth during the relaxation period would not be expected due to the sudden drop of temperature below  $0.2T_m$  ( $130^{\circ}\text{C}$ ) to a lower limit of  $19^{\circ}\text{C}$ .

Once the temperature of the specimen is returned to  $300^{\circ}\text{C}$  and the load is reapplied, creep crack growth is observed again. During the second loading cycle, crack growth of approximately 0.21 mm is recorded. The final calculated crack length is 18.14 mm, making a crack growth over the entire 24 hour period of 1.1 mm. At the latter stages of this loading cycle it appears that crack growth is slowing until crack length reaches a maximum value. This was also observed in previous creep tests.

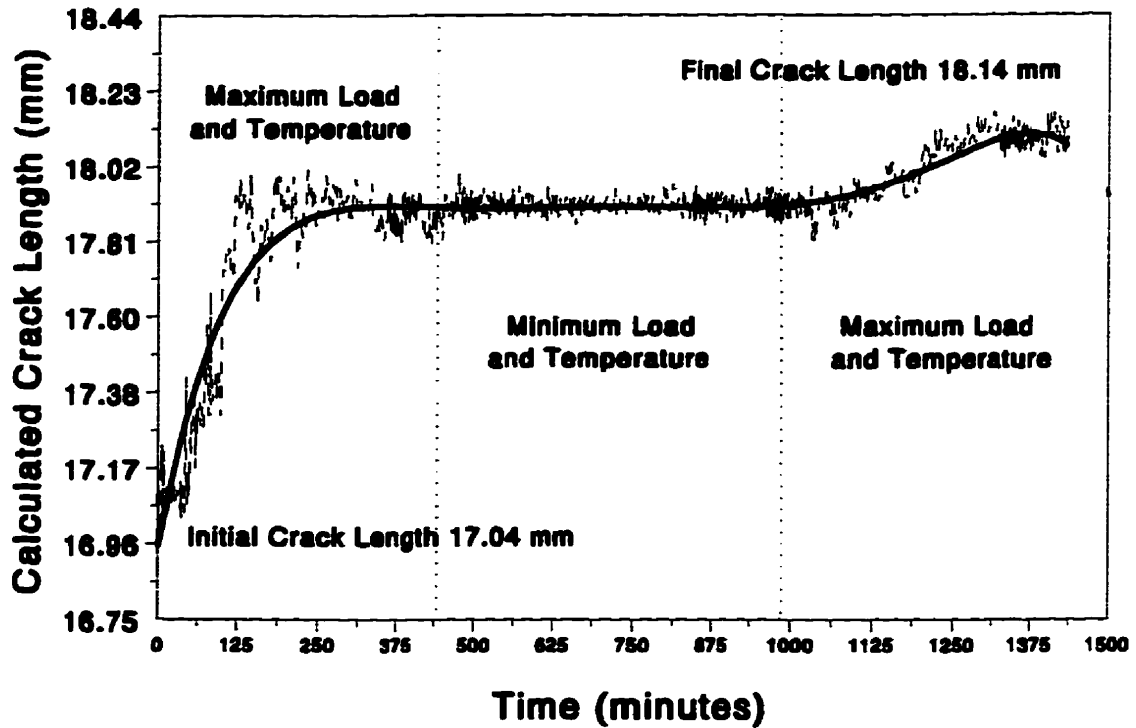


Figure 6.11: Crack Growth During In-Phase Thermomechanical Loading

### 6.3.3 Summary of Creep Test Findings

Test results suggest that a drop in load or temperature both decrease the rate of creep crack growth. Crack growth is re-established after temperature and load are restored. The test results also show that the specimen strain and creep crack growth appear logarithmic and reach a constant value over time. The crack growth is seen to slow considerably after propagating approximately 1.2 mm. The secondary or constant rate creep regime was not apparent from results. This would indicate that the test temperature was not sufficient to produce the traditional primary, secondary and tertiary creep behavior observed at higher temperatures. This form of creep response occurs when the temperature of the metal is not sufficient to produce the removal of dislocations generated through creep strain by recovery processes. This accumulation

of dislocations within the metal results in a gradual decay of creep rate towards zero [8]. Similar tests at higher temperatures should produce a visible constant (secondary) creep rate regime where the generation of dislocations is balanced by the rate of removal by recovery processes.

In terms of creep induced crack growth, the accumulation of dislocations in the plastic zone at the crack tip through crack tip blunting and stress redistribution increase the stress required for further propagation. Similar to the creep strain response of the specimen, the rate of crack growth decays with the accumulation of dislocations at the crack tip until the growth rate reaches zero.

## **6.4 Performance of the Crack Measurement System during Testing**

During both fatigue and creep testing using the crack length measurement system, experimental results showed that the system provided the sensitivity, resolution and long term stability to produce accurate real-time measurement of crack length. Oscillation of potential difference readings due to crack face touching (primarily during fatigue testing) and signal noise produced calculated crack length oscillation within  $\pm 0.07$  mm on all tests. This level of measurement stability was observed for up to 12 hours with no obvious mean potential difference drift during periods while crack length and temperature remained constant.

Through all testing, the integrity of the conducting film deposit and the connected leads was maintained. Bubbling or other forms of delamination of the film from the specimen was not observed. Potential difference measurements did not change with variations in specimen load (similar to strain gages), exposure to radiative heating from the furnace, or chilled air from the cooling system. There is no evidence to

suggest that the potential difference measurements are affected by any factors except specimen temperature and crack length.

If we incorporate the effects of signal noise observed during testing with the maximum resolution of the potential difference system configuration we can arrive at the accuracy of the system as observed during testing. This would equate to  $\pm 0.07$  mm plus  $\pm 0.02$  mm or  $\pm 0.09$  mm. This would be representative of the accuracy of the crack length measurement system configuration as used for the creep and fatigue crack growth measurement tests. During calibration, experimental results suggested the accuracy of the system was  $\pm 0.3$  mm over the majority of crack lengths measured. The increased accuracy of the system during creep and fatigue testing is due to the 250% increase in current used in the potential difference circuit as compared to the calibration configuration.

The accuracy suggested by experimental results indicates that for a potential difference measurement circuit current of 1.96 mA the crack length measurement system can be applied to any application in which crack length is expected to change in excess of  $\pm 0.09$  mm. The maximum test temperature is dictated by the temperature stability of the conducting film and epoxy barrier used.

# **Chapter 7**

## **Summary, Conclusions, Contributions and Recommendations**

### **7.1 Summary**

An AC potential difference (PD) method of crack length measurement incorporating a conducting film bonded to the surface of a test sample in the region of crack extension is developed. Due to the thin nature of the film, cracking induced in the specimen is transferred to the film and captured within the film boundaries. By flowing an electrical current through the film and measuring the change in measured electrical potential with crack extension, correlations with crack growth are formed.

The development of analytical relations between measured potential and crack length involved the development of a predictive model and evaluation of the model against experimental and numerical results. The effects of crack length and temperature on potential difference measurements are studied by collecting PD data over a

range of crack lengths and temperatures. In performing this task, specially prepared center-cracked specimens made of 6061-T6 aluminum alloy were subjected to a range of temperatures with various crack lengths by a computer controlled test program. The effect of temperature on potential difference is incorporated into calibration relations to allow continuous crack growth measurement through variable temperature. Through numerical studies of the film potential field, optimization of the film geometry and leadwire locations is performed to maximize the sensitivity and accuracy of the measurement system.

A series of studies are performed to evaluate the stability, resolution and accuracy of the crack measurement system under various test scenarios. Potential difference data is collected through testing involving fatigue and creep induced crack growth under constant and varied thermal and mechanical loading schedules. Test execution and data acquisition is fully computer controlled for uniformity of testing and ease of operation. Using the calibration relations to calculate crack length based on PD and temperature data, plots of crack length over time are produced. For each test the calculated crack growth response is compared against known fatigue and creep cracking behavior under similar conditions.

## **7.2 Conclusions**

The following conclusions can be drawn from this research work:

- 1) The thin film AC potential difference system provides several important advantages over conventional AC and DC potential difference methods of crack length measurement:
  - a) Crack length in non-conducting materials can be monitored.

- b) Calibration equations relating potential difference to crack length are dependent upon film properties only. Once calibration is performed for the film deposit, the system may be applied to specimens of any material and geometry with no need for further calibration.
  - c) Due to the thin nature of the conducting film, current levels required are 500 to 1000 times lower than conventional AC potential difference systems. Also, there is no need to adjust the current level to account for the specimen geometry or electrical properties.
  - d) The ability of the system to measure the extension of only one crack tip eliminates problems associated with asymmetric crack extension in center-crack tests.
  - e) Since the specimen itself is no longer electrically charged, the technique may be easily applied to on-site crack length monitoring outside a laboratory setting.
  - f) The feedback signal of the thin film system is linear with crack length over more than 60% of the film gage length for film aspect ratios below 0.5. Many conventional potential difference systems provide feedback which is nonlinear with crack extension.
  - g) The ability of the system to produce crack length measurements over a range of temperature, extends the application of the potential difference method beyond constant temperature testing.
- 2) The optimum configuration for a rectangular film deposit of dimensions  $L \times W$ , with the crack tip centered within the film width and current and potential leads placed symmetrically on either side of the axis of crack extension is as follows:

<b>Aspect Ratio (<math>\frac{W}{L}</math>)</b>	$\leq 0.5$
<b>Current Lead Position(<math>\pm</math>)</b>	$\geq 0.2W$
<b>Potential Lead Position(<math>\pm</math>)</b>	$\geq 0.12W$
<b>Crack Length</b>	0.06L to 0.86L

Table 7.1: Optimal Film Configuration

By maintaining the film configuration and crack length within these limits, sensitivity and accuracy of the crack length measurement system is maximized.

3) Using a current level of 1.98 mA rms and a 25 mm  $\times$  50 mm aluminum film of  $2.3 \times 10^{-6}$  m thickness, the AC potential difference system was used in measuring fatigue and creep crack growth in center-cracked 6061-T6 aluminum test specimens. Test results indicated that the system provided the following performance:

- **Long Term Stability:** No noticeable drift in PD readings over a 12 hour period.
- **Resolution:** 0.02 mm
- **Accuracy:**  $\pm 0.09$  mm

4) The performance of the proposed crack measurement technique is sufficient for application to both fatigue and creep induced crack growth monitoring over extended periods. The ability of the technique to account for the effects of temperature change make it a valuable tool in the study of crack growth under complex thermomechanical loading schedules.

## **7.3 Original Contributions**

The original contributions of this research involve the development and testing of the thin film AC potential difference system and its implementation into a automated test station. The test station is capable of performing crack growth studies in specimens under various thermal and mechanical loading patterns.

- **Development of the thin film AC potential difference system:**
  - 1) Design of a technique for producing potential difference change in a thin film bonded to a specimen in response to crack length change at elevated temperatures.
  - 2) Derivation of calibration equations based on both experimental and numerical studies of the relationship between measured potential, temperature, and crack length.
  - 3) Evaluation of the agreement of the calibration equations with numerical and experimental results.
  - 4) Numerical studies of the film potential field to optimize the sensitivity and accuracy of the system.
  
- **Implementation of the crack length measurement system into an automated test station:**
  - 1) The development of an automated calibration program to aid in the calibration of the thin film technique.
  - 2) The development of a testing program 'creep.c' used for automated control of tests investigating both fatigue and creep induced cracking under various thermomechanical loading schedules.

- 3) The evaluation of the crack length measurement system performance when used in studies of fatigue and creep induced crack growth.

## **7.4 Recommendations for Further Research**

- The need for temperature compensation in calibration relations may be eliminated by using a conducting film composed of a material which provides a constant resistivity over a wide temperature range. The use of constantan alloy or a carbon coating may meet this requirement.
- The use of a thinner insulating barrier material such as a high temperature spray-on coating will help to prevent premature cracking in the barrier. More accurate and reliable crack transference may be achieved.
- Application of the technique using higher current levels will yield higher sensitivity and accuracy of crack length measurements. Determination of the highest possible current without problems associated with arcing or burnout of the conducting film would provide useful data on the performance limitations of the technique.
- The application of the crack length measurement system to the study of the combined effects of thermal and mechanical loading schedules on fatigue and creep induced cracking.

# Bibliography

- [1] Johnson, H.H., *Calibrating the Electric Potential Method for Studying Slow Crack Growth*, Material Research and Standards, Vol. 5 (1965), pp. 441-445.
- [2] Saka M., Nakayama, M. and Kaneko T., *Measurement of Stress-Intensity Factor by Means of AC Potential Drop Technique*, Experimental Mechanics, Vol. 31 No. 3, Sept 1991, pp. 209-212
- [3] Wei R.P. and Brazill R.L., *An AC Potential System for Crack Length Measurement*, The Measurement of Crack Length and Shape During Fracture and Fatigue, ed. C.J. Beevers, pp. 190-201 (1980)
- [4] Halliday M.D. and Beevers C.J., *The DC Electrical Potential Method for Crack Length Measurement*, The Measurement of Crack Length and Shape During Fracture and Fatigue, ed. C.J. Beevers, pp. 85-112 (1980)
- [5] Nakai Y. and Wei R.P., *Measurement of Short Crack Lengths by an AC Potential Method*, Engineering Fracture Mechanics, Vol. 32, No. 4, 1989, pp. 181-189
- [6] Weasat R.C. et al, *CRC Handbook of Chemistry and Physics*, CRC Press, 1988
- [7] Hartman G.A and Johnson D.A, *DC Electric-Potential Method Applied to Thermal/Mechanical Fatigue Crack Growth*, Experimental Mechanics, March 1987, pp. 106-112

- [8] Evans R.W and Wilshire B, *Creep of Metals and Alloys*, The Institute of Metals, 1985
- [9] Skelton R.P., *Crack Initiation and Growth in Simple Metal Components During Thermal Cycling*, Fatigue at High Temperature, ed. R.P. Skelton, pp. 1-62 (1983)
- [10] Sinclair G, *Structural Reliability Through Fracture Mechanics*, Mechanical Engineering, June 1993, pp. 79-84
- [11] Barnett W.J. and Troiano A.R. *Crack Propagation in the Hydrogen-Induced Brittle Fracture of Steel*, J. of Metals, Vol. 9, pp. 486-494, 1957
- [12] Steigerwald E.A. and Hanna G.L. *Initiation of Slow Crack Propagation in High-Strength Materials*, Proc. ASTM., Vol 62, pp. 885-905, 1962
- [13] Knott J.F., *The Use of Analogue and Mapping Techniques with Particular Reference to Detection of Short Cracks*, The Measurement of Crack Length and Shape During Fracture and Fatigue, ed. C.J. Beevers, pp. 113-135 (1980)
- [14] Gilbey D.M. and Pearson S., *Measurement of the Length of a Central or Edge Crack in a Sheet of Metal by an Electrical Resistance Method*, Royal Aircraft Establishment Technical Report No. 66402, December 1966
- [15] Austen I.M. and Walker E.F, *Calibration of the Electrical Resistance Technique for Crack Growth Monitoring in CKS Type Test Pieces*, BSC Tech. Rep. PMC/6795/6/76/B. Rotherdam, U.K. (1976)
- [16] Smith R.A., *Calibrations for the Electrical Potential Method of Crack Growth Measurement by a Direct Electrical Analogy*, Strain, Vol. 10, (1974), pp. 183-187.
- [17] Read D.T. and Pfuff M., *Potential Drop in the Center-Cracked Panel with Asymmetric Crack Extension*, International Journal of Fracture Vol. 48, No. 3, Apr. 1 1991, pp. 219-229

- [18] Watt K.R., *A Consideration of an A.C. Potential Drop Method for Crack Length Measurement*, *The Measurement of Crack Length and Shape During Fracture and Fatigue*, ed. C.J. Beevers, pp. 202-221 (1980)
- [19] Siverns M.J. and Price A.T., *Crack Growth under Creep Conditions*, *Nature*, Vol. 228, (1970), p. 760.
- [20] Priest A.H. and McIntyre P. *Measurement of Sub-Critical Flaw Growth in Stress Corrosion, Cyclic Loading and High Temperature Creep by the D.C. Electrical Resistance Technique*, BSC Tech. Rep. MG/54/71, Rotherdam, U.K. (1971).
- [21] Gibson G.P., *The use of Alternating Current Potential Drop for Determining j-Crack Resistance Curves*, *Engineering Fracture Mechanics*, Vol 26, No. 2, pp 213-222, 1987
- [22] Saouma V.E., *Lecture Notes in Fracture Mechanics*, Dept. of Civil Engineering, University of Colorado, Sept 13, 1994.
- [23] Sun B., *Characterization of Creep Deformation and Damage of Metallic Materials at High Temperature*, Ph.d thesis, Dept. Of Mechanical and Industrial Engineering, University of Manitoba, June 10, 1994.
- [24] Pollock D.D., *The Physics of Engineering Materials*, Prentice Hall, 1990
- [25] Frick J.P., *Woldman's Engineering Alloys*, 7th. ed., ASM International, 1990
- [26] Kinloch A.J., *Adhesion and Adhesives: Science and Technology*, 1st ed., Chapman and Hall, pp. 46, 230, 342-350, 1987
- [27] Conway J.B. and Flagella P.N., *Creep Rupture Data for the Refractory Metals to High Temperatures*, Gordon and Breach, pp. 1971

[28] Serway R.A., *Physics for Scientists and Engineers*, 2nd ed., Saunders College Publishing, pp. 603-689, 1986.

# Appendix A

## The Skin Effect Phenomenon

An alternating current (AC) flowing in a conductor is affected by the magnetic field that it induces. This produces a current density in the conductor which varies with depth. The maximum current density occurs at the surface of the conductor with decreasing current density towards the center [5]. This is termed the 'skin effect' in AC current flow. Wei and Brazill [3] analyzed the effect of operating frequency on the AC potential. The following discussion is based on their results.

The total current,  $I$ , passing through the unit width of a conductor is:

$$I = 2\delta J_o [1 - \exp(-B/\delta)] \quad (\text{A.1})$$

where  $J_o$  is the surface current density,  $B$  is the film thickness, and  $\delta$  is the skin depth. The value of  $\delta$  is a function of the conducting film resistivity  $\rho$ , absolute magnetic permeability  $\mu$ , and cyclic operating frequency  $f$  given by the following equation:

$$\delta = \left( \frac{\rho}{\pi f \mu} \right)^{1/2}. \quad (\text{A.2})$$

By assuming the AC potential at the surface  $V$ , is proportional to the value of  $J_o$ :

$$V = \frac{C}{2\delta}[1 - \exp(-B/\delta)] \quad (\text{A.3})$$

where  $C$  is a proportionality constant. By using the condition that  $V = V_{dc}$  when  $B \ll \delta$ , Equation A.3 can be simplified as follows:

$$\frac{V}{V_{dc}} = \frac{(B/\delta)}{[1 - \exp(-B/\delta)]}. \quad (\text{A.4})$$

The graph shown in Figure 2.7 of Chapter 2 shows the relation given by Equation A.4. When  $B \gg \delta$  (high frequency), the value of  $V$  is proportional to  $f^{1/2}$  or  $1/\delta$ , and approaches  $V_{dc}$  when  $B \ll \delta$  (low frequency).

## A.1 Evaluation of Skin Effect in an Aluminum Film

The extent of the influence of the skin effect on the current density and potential distribution in an aluminum film can be evaluated using the equations governing this phenomenon. Using constants representative of the aluminum film used for crack length measurement in this research, the influence of the skin effect on potential values at the film surface can be assessed.

The absolute magnetic permeability  $\mu$ , of a conductor can be determined from the permeability of free space  $\mu_o$ , and the magnetic susceptibility of the conductor  $\chi$  according to the relation [28]:

$$\mu = \mu_o(1 + \chi). \quad (\text{A.5})$$

The magnetic susceptibility of aluminum is  $2.3 \times 10^{-5}$  and the magnetic permeability of free space is  $1.256637 \times 10^{-6} \text{ N/A}^2$  [28]. Using these constants along

with Equation A.5 we find that the absolute magnetic permeability of aluminum is  $1.256666 \times 10^{-6} \text{ N/A}^2$ . Aluminum is called a paramagnetic material because its magnetic permeability is very low, and the magnetic field induced within aluminum is not appreciably 'magnified' by its magnetic properties (as observed for ferromagnetic materials).

Using Equation A.2, the skin depth for current flow can be determined at an average test temperature of  $135^\circ \text{C}$  (tests range from  $30$  to  $300^\circ \text{C}$ ). At this temperature, the resistivity of the aluminum is  $3.635 \times 10^{-8} \Omega \cdot \text{m}$ . The operating frequency of all tests were  $93 \text{ Hz}$ . With these values, the skin depth is calculated to be  $9.95 \times 10^{-3} \text{ m}$  or  $9.95 \text{ mm}$ . Since the thickness of the film deposit is  $2.3 \times 10^{-6} \text{ m}$  we find that the ratio  $B/\delta$  is  $2.31 \times 10^{-4}$ . If we use this ratio with Equation A.4, the ratio of surface AC potential to DC potential  $V/V_{dc}$ , for current flow through the conducting film is  $1.00012$ . This clearly shows that the skin effect upon potential measurements in the aluminum film is negligible. Figure 2.7 in Chapter 2 of the thesis shows for the ratio  $B/\delta = 2.31 \times 10^{-4}$ , we are firmly in the DC region of the plot. This indicates that the current density through any cross section of the film is uniform, as is observed for DC current flow. This is an important requirement of the linear conductor model for predicting the potential difference within the thin film as discussed in Chapter 2.

Obviously, if a ferromagnetic material is used in the conducting film, the influence of the skin effect upon potential difference measurements must be taken into account. This would involve including Equations A.4 and A.2 in the calibration equation to account for the change in surface potential due to the skin effect. This would lead to increased complexity in the calibration equation which could be avoided by using a paramagnetic material.

## **Appendix B**

### **Photos of Experimental Apparatus**

This appendix contains various photos of the experimental apparatus which show the physical arrangement of the apparatus in the testing station and finished appearance of the aluminum test specimens.

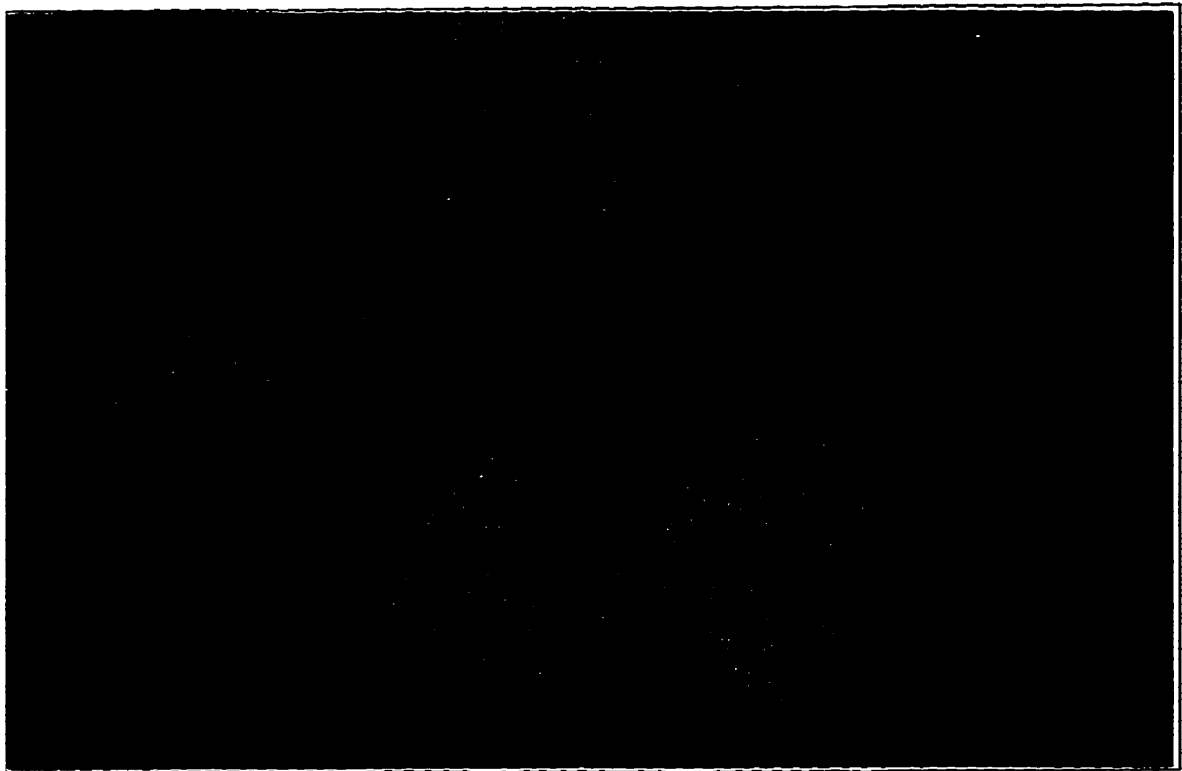


Figure B.1: Finished Test Specimen

Figure B.1 shows a finished test specimen with wire clip and thermocouple installed. The wire clip and the reinforcing epoxy (dark circle) serve to prevent accidental damage to fragile lead connection points on the film. The insulating epoxy layer is visible as a tan colored layer surrounding the aluminum film deposit.

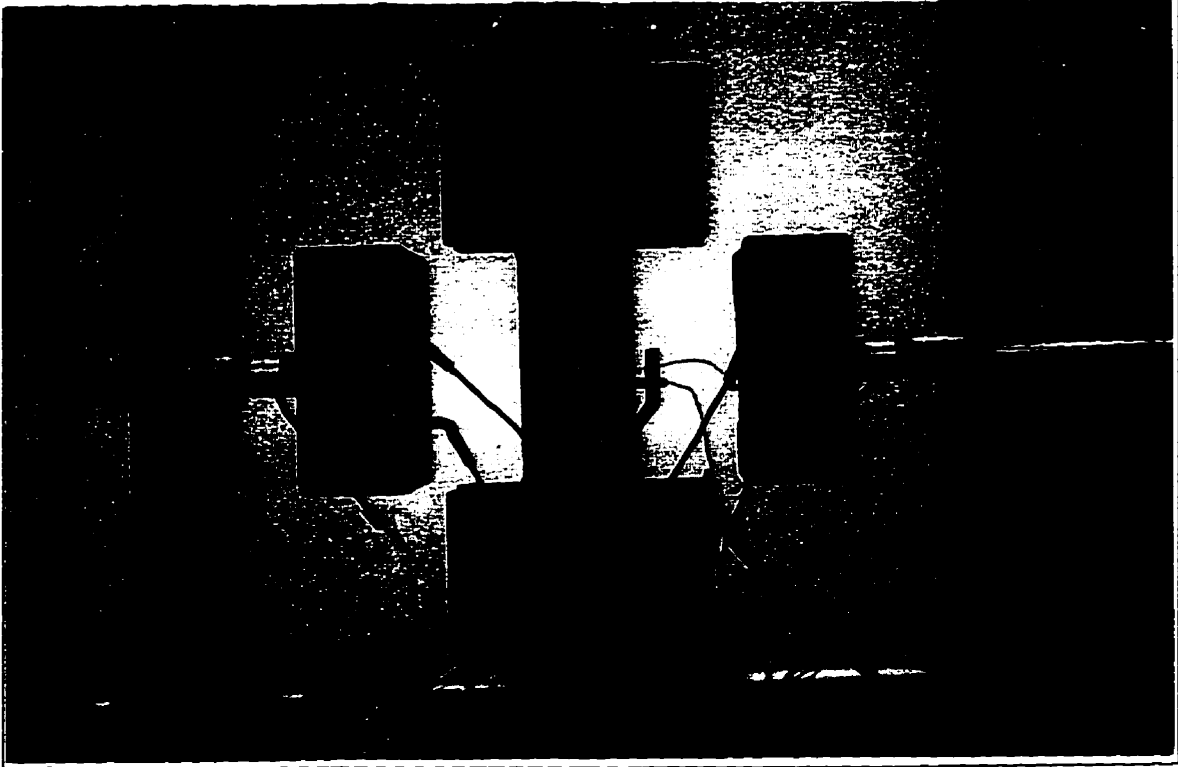


Figure B.2: Installed Specimen

Figure B.2 shows the installation of the specimen in the load frame. The specimen is rotated 90° from the heaters to allow easy measurement of the crack length in the film.

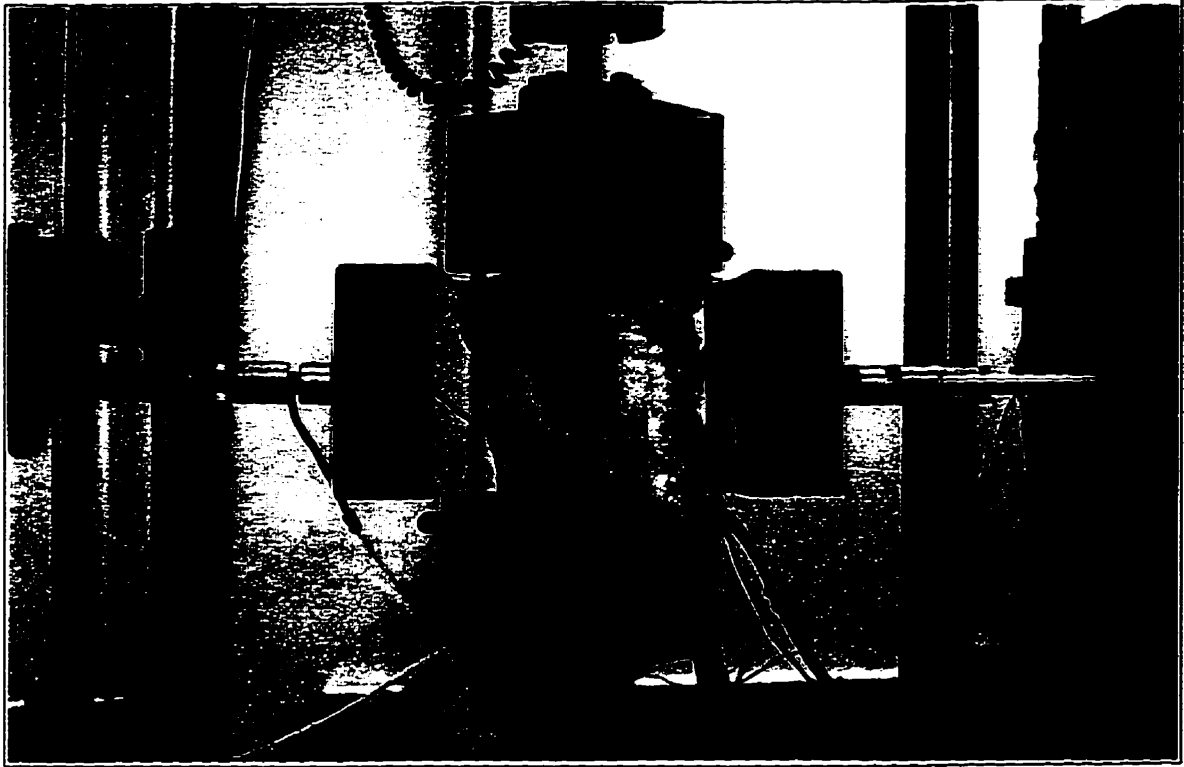


Figure B.3: Specimen Insulation

To maintain a uniform specimen temperature by preventing heat loss during testing, square pieces of insulation are used as shown in Figure B.3. Leadwires are visible coming from the specimen to the terminal block on the right side of the lower grip.

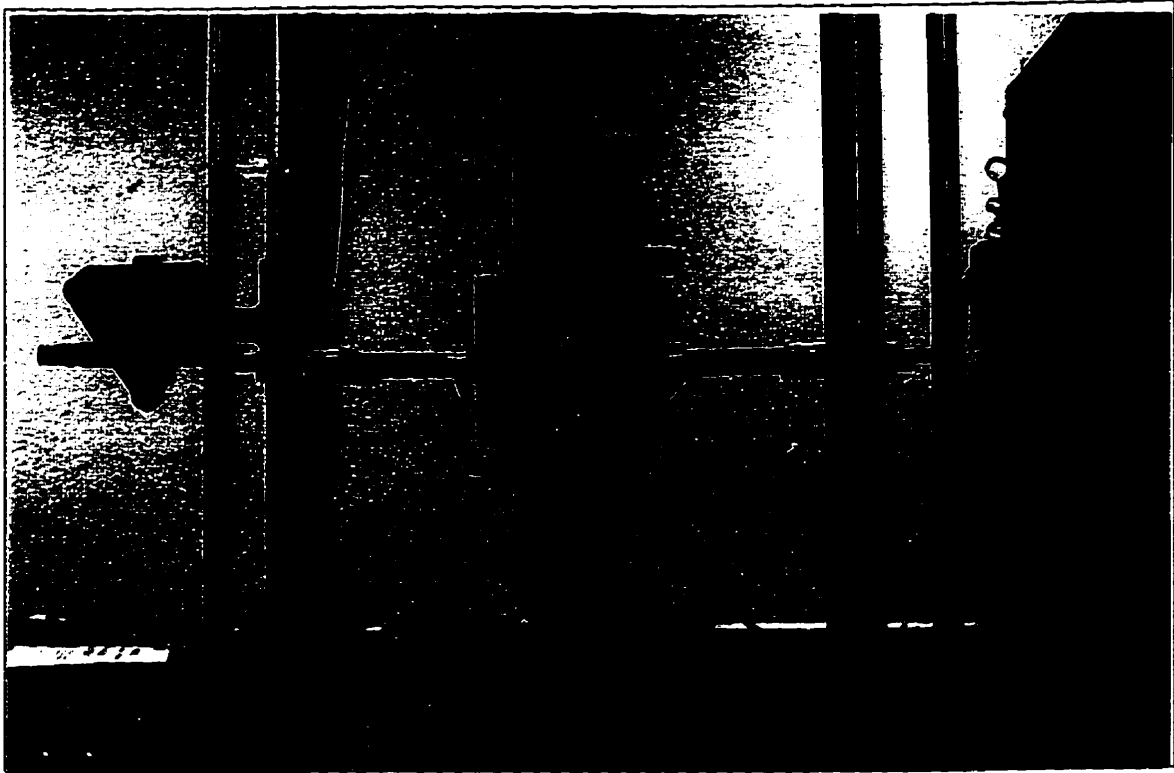


Figure B.4: Test Configuration

Figure B.4 shows the position of the specimen during testing. The moveable furnaces are now in position to 'sandwich' the insulation in place and prevent heat loss. Leadwires come from between the layers of insulation and are connected to the terminal block. Black RF shielded cables travel between the terminal block and the isolation transformer. The travelling microscope is clamped to the left post of the load frame and may be rotated into position for optical measurement of crack length.

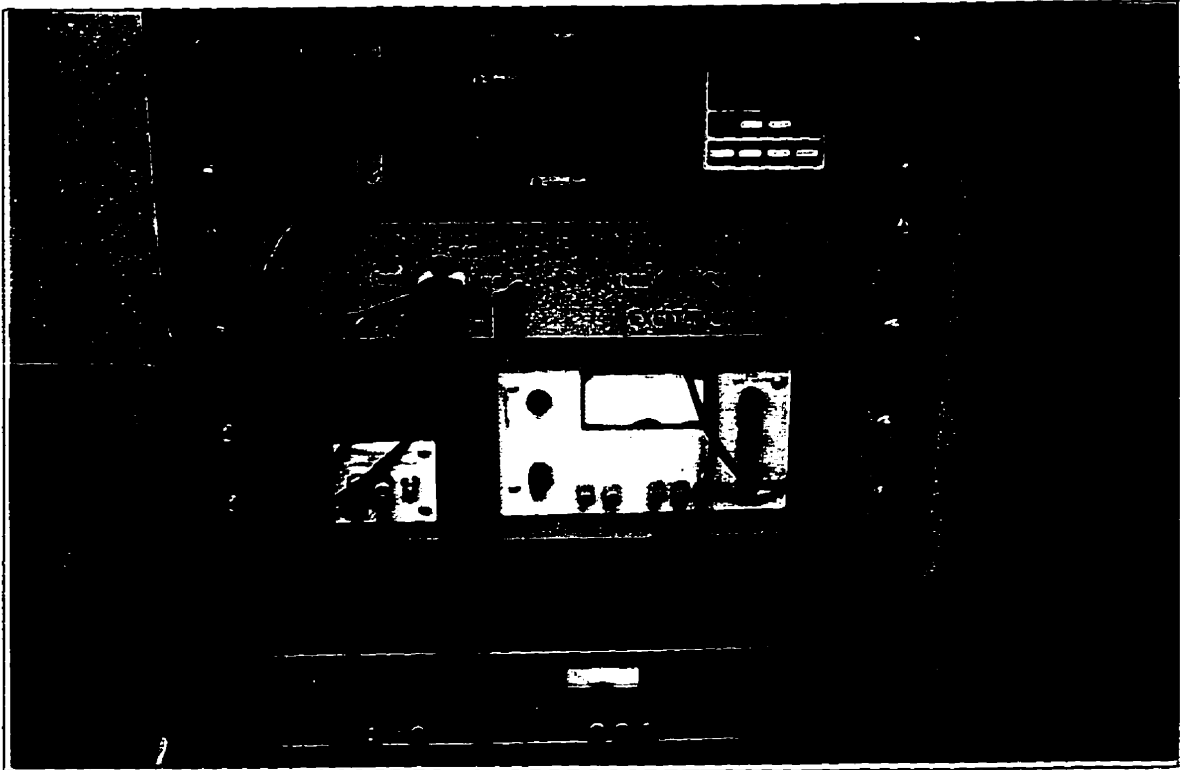


Figure B.5: Control and Measurement Apparatus

Figure B.5 shows the control and measurement apparatus used in the test station. The temperature controller is visible at the upper right of the photo. The isolation transformer is the silver unit at the center-left of the photo. Leads from the isolation transformer travel to the lock-in amplifier shown at the bottom of the photo.



Figure B.6: Testing Station

Figure B.6 gives an overall view of the testing station. The control panel for the load frame is shown at the left while the controlling computer is shown at the right. The current flow through the film is monitored using the multimeter shown to the left of the computer keyboard.

# Appendix C

## Program Listings

This appendix contains program listings of the C++ programs 'calib.c' and 'creep.c' used for control of testing and data acquisition during calibration and creep/fatigue testing respectively. The Fortran program 'aspect.f' used for solving the potential field within the conducting film for various aspect ratios is also included.

## C.1 Program Listing For 'calib.c'

The C++ program 'calib.c' controls the execution and data acquisition during the collection of calibration data. The program subjects the specimen to a wide range of temperatures under various crack lengths and records potential difference measurements. A flowchart of program execution is found in Figure 4.3 of Chapter 4.

```
#include <decl.h>
#include <stdio.h>
#include <stdlib.h>
#include <dos.h>
#include "math.h"
#include "serial.h"
#include "instron.h"

void main(void){
    FILE *stream;
    short lockamp, instrn;
    int airdrop,tinc, ntinc, nprop,msens,tmp, cycle, rtemp, ttemp
        , i, ncycle;
    char f1[25], cycle[15],msen[20],szero[10],smax[15],stamp[15]
        ,sfreq[15],llimit[16],ulimit[16], flag[1],sncycle[5]
        ,coffset[10];
    float peak,mean,ilen,amp,freq,zero,noffset,voffset;
    double volt,mvsens;
    s_open("COM1 12 n 8 2");
    find(&instrn, &lockamp);
    clrscr(); //collect test parameters from user//
    printf("\nCrack Length Calibration Program Rev 2 - July 1995\n\n");
    printf("Enter Data Storage Filename: ");
    scanf("%s", &f1);
    printf("Input Temperature Step (C): ");
    scanf("%d", &tinc);
    printf("Input #of Temp. Steps: ");
    scanf("%d", &ntinc);
    //Take Control of Instron//
    ibwrt(instrn, "C909,0", 6);
    ibwrt(instrn, "C909,1", 6);
```

```

printf("\npress the remote key for computer control\n");
printf("and then press any key to continue\n");
getch();
clrscr();
//Set Watchdog To off//
ibwrt(instrn, "C904,0", 6);
//Calibrate Zero On Instron//
printf("Calibrating Load Cell... Please Wait\n");
ibwrt(instrn, "C108,2,4", 8);
delay(20000);
//Set up Waveform//
printf("\n\nEnter Current Half Crack Length (mm): ");
scanf("%f", &ilen);
printf("Enter mean stress for Test (MPa):");
scanf("%f", &zero);
zero=zero/1000.0;
printf("Enter peak stress for test (MPa): ");
scanf("%f", &amp);
amp=amp/1000.0;
printf("Enter desired loading frequency (hz): ");
scanf("%f", &freq);
printf("Enter # of Cycles for Propagation (#): ");
scanf("%d", &cycle);
//Zero Actuator//
ibwrt(instrn, "C300,2", 6); //Transfer to Load Control//
mean=zero*3.0*(100.0-ilen*2.0)/100.0;
peak=amp*3.0*(100.0-ilen*2.0)/100.0;
sprintf(szero, "C3,2,%f", mean);
sprintf(smax, "C3,2,%f", peak);
sprintf(stamp, "C203,2,%f", peak-mean);
ibwrt(instrn, szero, strlen(szero));
printf("Setting Mean Load, press a key to continue\n");
getch();
//Arm Safety Limits//
sprintf(ulimit, "C122,2,1,%f", (peak+0.1*peak));
//Define Upper and Lower limits
sprintf(llimit, "C122,2,0,%f", (0.01*peak));
ibwrt(instrn, "C326,0", 6); //Disable & clear all safety limits
ibwrt(instrn, "C121,2,0,0", 10); // Unlock minimum limit
ibwrt(instrn, "C121,2,1,0", 10); // Unlock max limit

```

```

    ibwrt(instrn, llimit, strlen(llimit)); // Set minimum limit
    ibwrt(instrn, "C123,2,0,1", 10); // Disable actuator on min limit
    ibwrt(instrn, "C121,2,0,1", 10); // Arm minimum limit
    ibwrt(instrn, ulimit, strlen(ulimit)); // Set maximum limit
    ibwrt(instrn, "C123,2,1,1", 10); // Disable actuator on max limit
    ibwrt(instrn, "C121,2,1,1", 10); // Arm maximum limit
    ibwrt(instrn, "C326,1", 6); // Enable Safety limits
//Select Haversine Shape Loading//
    ibwrt(instrn, "C201,2,3", 8);
//Select Amplitude//
    ibwrt(instrn, stamp, strlen(stamp));
//Select Frequency//
    sprintf(sfreq, "C202,2,%f", freq);
    ibwrt(instrn, sfreq, strlen(sfreq));
//Set up Lockin Amp//
    senlock(lockamp, "REMOTE 1"); //set remote control on
    senlock(lockamp, "FLT 3"); //Set Filter to Band Pass//
    senlock(lockamp, "OA 1000"); //Set Oscillator Amplitude to 1v//
    senlock(lockamp, "OF 9300,2"); //Set Oscillator Freq to 93 hz//
//Get Current Temperature & Perform Automeasure//
    i=0;
    nprop=0;
Temp:;
    rtemp=30;
    senlock(lockamp, "ASM"); //Perform Automeasure
    delay(1600);
    senlock(lockamp, "AXO"); // Perform Auto Offset
    ibwrt(lockamp, "XOF", 3); // Request offset value
    ibrd(lockamp, coffset, 10);
    sprintf(coffset, " %c%c%c%c ", coffset[2], coffset[3], coffset[4],
coffset[5]);
    sscanf(coffset, "%f", &noffset);
    ibwrt(lockamp, "SEN", 3);
    ibrd(lockamp, msen, 10);
    sscanf(msen, "%d", &msens);
    sense(msens, &mvsens);
    if (nprop<1) {
    voffset=mvsens*noffset/1000.0;
    printf("Test Offset: %f V\n", voffset);
    stream=fopen(fl, "a+");

```

```

    fprintf(stream,"Offset: %f V\n", voffset);
    fclose(stream);
}
noffset=mvnsens*noffset/1000.0;
printf("noffset %f\n",noffset);
//Increment Temperature Loop//
while(i<=ntinc){
    if (i>=0) {
        int ttemp=rteap+i*tinc;
        if(ttemp>(15+rtemp+ntinc*tinc)) {
printf("Caught Program Fault - Target
Temperature Error\a\a");
writetemp(0);
solenoid(lockamp,2,1);
solenoid(lockamp,1,1);
goto end;
        }
        printf("Incrementing Temp to %3d Degrees C\n",ttemp);
        writetemp(ttemp);
        readtemp(&tmp);
        while(tmp<ttemp){
readtemp(&tmp);
delay(500);
        }
        delay(10000);
        readtemp(&tmp);
        while(tmp>ttemp+1||tmp<ttemp-1){
readtemp(&tmp);
delay(500);
        }
        delay(10000); //soak time for specimen
    }
    readtemp(&tmp);
    readlock(lockamp,noffset,&volt);
    volt=volt+noffset-voffset;
    stream=fopen(fl,"a");
    printf("Temp: %d Deg C   Voltage: %f V   Length: %f mm\n"
           , tmp,volt,ilen);
    fprintf(stream, "%f   %f   %d\n", ilen, volt, tmp);
    fclose(stream);

```

```

    i++;
}
airdrop=5;
readtemp(&tmp);
writetemp(0);
printf("\nCooling Specimen Down, airdrop = %d C\n\n",airdrop);
//Open Up Cooling Solenoid and Wait Till Temperature Returns to Room//
solenoid(lockamp,2,1);
printf("Solenoid #2 Activated\n");
delay(3000);
solenoid(lockamp,1,1);
printf("Solenoid #1 Activated\n");
//If Temperature is cool enough Propagate Crack//
while(tmp>rtemp+20){
    readtemp(&tmp);
    delay(2000);
}
printf(" Proceeding with crack propagation\n");
ibwrt(instrn, szero, strlen(szero)); //re-establish zero
ibwrt(instrn, "C210,0", 6); //Set quarter cycle counter to zero
ibwrt(instrn, "C200,1", 6); //Begin Cycling
ncycle=0;
while(ncycle<cycle*4){
    ibwrt(instrn, "Q210", 4);
    delay(300);
    sncycle[1]=' ';
    sncycle[2]=' ';
    sncycle[3]=' ';
    sncycle[4]=' ';
    sncycle[5]=' ';
    ibrd(instrn, sncycle, 5);
    sscanf(sncycle,"%d", &ncycle);
    printf("    %f cycles complete\r", ncycle/4.0);
}
ibwrt(instrn, "C200,4", 6); //finish current cycle and stop
ret;;
while(tmp>rtemp-airdrop){
    readtemp(&tmp);
    delay(5000);
}

```

```

solenoid(lockamp,2,0); //Shut Down Cooling
delay(3000);
solenoid(lockamp,1,0);
printf("\nCooling Shutdown\n");
delay(60000);
readtemp(&tmp);
if(tmp>rtemp){
    airdrop=airdrop+1;
    solenoid(lockamp,2,1);
    solenoid(lockamp,1,1);
    goto ret; // If non aircooled temp is still higher than rtemp
}
printf("Temperature Stabilized\n\n");
ibwrt(instrn,"C326,0",6); //Unlock limit arm
ibwrt(instrn,"C121,2,0,0",10); //Disarm min limit
ibwrt(instrn,"C3,2,0.0", 8); //unload specimen for measurement
delay(5000); //wait 5 seconds
printf("\r\a Specimen unloaded, position grips - hit any key
        when done\n");
getch();
ibwrt(instrn,smax,strlen(smax)); //establish peak load
printf("\a Peak Load Applied. Measure Crack Length - hit any key
        when done\n");
getch();
printf("Enter Crack Length (mm): ");
scanf("%f",&ilen);
ibwrt(instrn,"C3,2,0.0",8); //unload specimen
printf("Specimen unloaded, reposition grips - hit any key
        when done\n");
getch();
mean=zero*3.0*(100.0-ilen*2.0)/100.0;
peak=amp*3.0*(100.0-ilen*2.0)/100.0;
sprintf(szero, "C3,2,%f", mean);
sprintf(stamp, "C203,2,%f", peak-mean);
sprintf(smax, "C3,2,%f",peak);
ibwrt(instrn,stamp,strlen(stamp));
ibwrt(instrn,szero,strlen(szero));
printf("Setting Mean Load - hit a key to continue\n");
getch();
ibwrt(instrn,"C121,2,0,1",10); //arm min limit

```

```

ibwrt(instrn,"C326,1",6); //Lock Limits
clrscr();
i=0;
nprop++;
goto Temp;
end;
ibwrt(instrn, "C909,0", 6);
ibwrt(instrn, "C302", 4);
}

```

## **C.2 Program Listing for ‘aspect.f’**

The Fortran program ‘aspect.f’ uses the finite difference technique to numerically solve for the potential field of the film. Two output files are created: ‘vfield.dat’ and ‘output.dat’. The ‘vfield.dat’ file contains the potential at various coordinates throughout the film potential field at all crack length increments and aspect ratios. The file ‘output.dat’ contains the variation of potential difference with crack length at various aspect ratios.

Program execution calculates the important geometrical quantities of the problem using the subroutine ‘geometry’. With these variables the problem matrix for the entire problem can be formed using the subroutine ‘stiff’. After the formation of the problem matrix, the solution can be found by inverting this matrix using the ‘invert’ subroutine which applies the Gauss-Jordan elimination technique. This results in a potential field solution at discrete points or ‘nodes’ throughout the film area. By solving for the potential for various crack lengths, film aspect ratios, and locations of potential and current leads the effects of these variables on the potential field can be studied.

```

program field
  implicit real*8(a-h,o-z)

```

```

include 'pointers.cmn'
      common a(700000)
c -----
c Important Variables:
c -----
c curr : the value of current flow in amps RMS.
c ri   : the value of the conducting film resistivity.
c width: the overall width of the film (50 mm)
c height: the overall height of the film (25 mm)
c ndx  : the number of elements in the x-direction
c ndy  : the number of elements in the y-direction
c imax : the number of nodes in the x-direction
c jmax : the number of nodes in the y-direction
c aspect : the value of the film aspect ratio
c thk  : the film thickness in meters.
c nsize : the size of the solution vector
c
c Input Variables:
  iflag1=1
    curr=0.897
  curr=curr/1000.000000
    ri=2.7e-8
  width=50.0/1000.00000
  ndx=26
  ndy=14
  thk=2.3e-6
    imax=ndx+1
    jmax=ndy+1
  do iaspect=0,3
    aspect=0.25+dfloat(iaspect)
    height=aspect*width
  do icrack=25,ndx
    itmax=icrack
  nsize=itmax+(jmax-1)*imax
  ntotl=imax*jmax
  n1=1
  n2=n1+imax
  n3=n2+jmax
  n4=n3+nsize*nsize
  n5=n4+nsize

```

```

        n6=n5+nsize
        call geometry(height,width,imax,jmax,a(n1),a(n2))
open(unit=2,access='append',file='vfield.dat')
write(2,*)
write(2,*) 'Crack Length',1000.0*a(n1+icrack-1)
close(2)
if(iflag1.eq.1) then
    open(unit=1,access='append',file='output.dat')
    write(1,*) 'Current Level (mA): ',curr*1000.0
    write(1,*) 'Sense Position:',a(n1)*1000,a(n2+3)*1000
    write(1,*) 'Input Position:',a(n1)*1000,a(n2+6)*1000
    write(1,*) 'Base test temperature is 30 deg C'
    close(1)
endiflag1=0
endif
    call stiff(a(n1),a(n2),a(n3),a(n4),a(n5),nsize,itmax,ntotl,
    & imax,jmax,curr,ri,aspect,thk)
    end do
    end do
    end
c -----
c This subroutine assembles the problem matrix for inversion.
c -----
    subroutine stiff(xloc,yloc,s,f,v,nsize,itmax,ntotl,imax
    & ,jmax,curr,ri,aspect,thk)
    implicit real*8(a-h,o-z)
include 'pointers.cmn'
    dimension xloc(imax),yloc(jmax),s(nsize,nsize),
    & f(nsize),v(nsize)
c    Assemble matrix form of problem
c
    do k=1,nsize
        do l=1,nsize
            s(k,l)=0.0
            f(k)=0.0
            v(k)=0.0
        end do
    end do
    do j=1,jmax
        do i=1,imax

```

```

if(j.gt.1) npos=itmax+(j-2)*imax+i
if(j.eq.1) npos=i
if(j.eq.1) ndn=itmax+i
if(j.gt.1) ndn=npos+imax
if(j.eq.1.and.i.ge.itmax) npos=itmax
if(j.eq.2.and.i.le.itmax) nup=i
if(j.eq.2.and.i.gt.itmax) nup=itmax
if(j.gt.2) nup=npos-imax
if(i.lt.imax) dxp=xloc(i+1)-xloc(i)
if(i.gt.1) dxm=xloc(i)-xloc(i-1)
if(j.lt.jmax) dyp=yloc(j+1)-yloc(j)
if(j.gt.1) dym=yloc(j)-yloc(j-1)
if(j.eq.1) then
  dxa=(dxm+dxp)/2.0
  if(i.eq.1) then
    s(npos,npos)=-1.0*(dyp/(2.0*dxp)+dxp/(2.0*dyp))
s(npos,npos+1)=dyp/(2.0*dxp)
    s(npos,ndn)=dxp/(2.0*dyp)
  else if(i.gt.1.and.i.lt.itmax) then
    s(npos,npos)=-1.0*(dyp/(2.0*dxp)+dyp/(2.0*dxm)
      +dxa/dyp)
    s(npos,npos+1)=dyp/(2.0*dxp)
    s(npos,npos-1)=dyp/(2.0*dxm)
    s(npos,ndn)=dxa/dyp
  else if(i.eq.itmax) then
    s(i,i)=-1.0*(dxa/dyp+dyp/(2.0*dxm))
    s(i,i-1)=dyp/(2.0*dxm)
    s(i,ndn)=dxa/dyp
  else if(i.gt.itmax.and.i.lt.imax) then
    s(npos,npos)=s(npos,npos)-dxa/dyp
    s(npos,ndn)=dxa/dyp
  else if(i.eq.imax) then
    s(npos,npos)=s(npos,npos)-dxm/(2.0*dyp)
    s(npos,ndn)=dxm/(2.0*dyp)
  end if
else if(j.gt.1.and.j.lt.jmax) then
  dya=(dyp+dym)/2.0
  if(i.eq.1) then
    s(npos,npos)=-1.0*(dxp/(2.0*dyp)+dxp/(2.0*dym)
      +dya/dxp)

```

```

        s(npos,npos+1)=dya/dxp
        s(npos,nup)=dyp/(2.0*dym)
        s(npos,ndn)=dyp/(2.0*dym)
    else if(i.gt.1.and.i.lt.imax) then
        dxa=(dyp+dym)/2.0
        s(npos,npos)=-1.0*(dya/dxp+dya/dym+dxa/dyp+dxa/dym)
        s(npos,npos+1)=dya/dxp
        s(npos,npos-1)=dya/dym
        s(npos,nup)=dxa/dym
        s(npos,ndn)=dxa/dyp
    else if(i.eq.imax) then
        s(npos,npos)=-1.0*(dym/(2.0*dyp)+dym/(2.0*dyp)
            +dya/dym)
        s(npos,nup)=dym/(2.0*dyp)
        s(npos,ndn)=dym/(2.0*dyp)
        s(npos,npos-1)=dya/dym
    end if
else if(j.eq.jmax) then
    dxa=(dyp+dym)/2.0
    if(i.eq.1) then
        s(npos,npos)=-1.0*(dym/(2.0*dyp)+dyp/(2.0*dym))
        s(npos,npos+1)=dym/(2.0*dyp)
        s(npos,nup)=dyp/(2.0*dym)
    else if(i.gt.1.and.i.lt.imax) then
        s(npos,npos)=-1.0*(dym/(2.0*dyp)+dym/(2.0*dym)
            +dxa/dym)
        s(npos,npos+1)=dym/(2.0*dyp)
        s(npos,npos-1)=dym/(2.0*dym)
        s(npos,nup)=dxa/dym
    else if(i.eq.imax) then
        s(npos,npos)=-1.0*(dym/(2.0*dym)+dym/(2.0*dym))
        s(npos,npos)=s(npos,npos)*1.0e8
        s(npos,npos-1)=dym/(2.0*dym)
        s(npos,nup)=dym/(2.0*dym)
    end if
end if
end do
end do

call invert(s,nsize)
cond=1.0/ri

```

```

f(itmax)=curr/(cond*thk)
f(itmax+(7-2)*imax+1)=-1.0*curr/(cond*thk)
test=0.0
bound=0.0
do k=1,nsize
  test=test+s((itmax+2*imax+1),k)*f(k)
  bound=bound+s(itmax,k)*f(k)
end do
v(itmax)=bound
open(unit=1,access='append',file='output.dat')
open(unit=2,access='append',file='vfield.dat')
write(1,*) aspect,xloc(itmax),2000.0*(test-bound)
close(1)
do j=1,jmax
do i=1,imax
nflag=1
if(j.gt.1) npos=itmax+(j-2)*imax+i
if(j.eq.1.and.i.lt.itmax) npos=i
if(j.eq.1.and.i.ge.itmax) nflag=0
do k=1,nsize
  if(nflag.ne.0) v(npos)=v(npos)+s(npos,k)*f(k)
end do
if(nflag.eq.0) npos=itmax
write(2,*) 1000.*xloc(i),1000.*yloc(j),
& 1000.*(v(npos)-v(itmax))
if(i.eq.1.and.j.eq.4) write(*,*) test,bound,v(npos)
end do
end do
close(2)
return
end

```

```

c -----
c This subroutine calculates important geometrical
c constants based on the aspect ratio and size of the film.
c

```

```

subroutine geometry(height,width,imax,jmax,xloc,yloc)
implicit real*8(a-h,o-z)
include 'pointers.cmn'
dimension xloc(imax),yloc(jmax)
pap=6.0/1000.0

```

```

do i=1,imax
xloc(i)=width*(-1.0*cos((float(i-1)/float(imax-1))*
& (3.141592653/2.0))+1.0)
end do
yloc(1)=0.0
do j=2,7
yloc(j)=yloc(j-1)+(1.0/1000.0)
end do
do j=8,jmax
yloc(j)=pap+(height-pap)*(float(j-7)/float(jmax-7))**2.0
end do
return
end

```

```

C -----
subroutine invert(A,n)
implicit real*8(a-h,o-z)

```

```

C-----
C This subroutine inverts an n x n matrix on top
C of itself using Gauss-Jordan elimination technique
C-----
C

```

```

dimension A(n,n)
do 50 i=1,n
pivot=A(i,i)
b=1.0d0/pivot
do 10 ncol=1,n
10 A(i,ncol)=A(i,ncol)/pivot
do 40 k=1,n
if(k-i) 20,40,20
20 pivot=A(k,i)
do 30 ncol=1,n
30 A(k,ncol)=A(k,ncol)-A(i,ncol)*pivot
A(k,i)=-pivot*b
40 continue
50 A(i,i)=b
do i=1,n
end do
return
end

```

### C.3 Program Listing for 'creep.c'

The C++ program 'creep.c' is used to provide control and data acquisition for fully automated creep and fatigue testing of specimens. A flowchart of program execution is shown in Figure 6.1 of Chapter 6. Four test types may be selected from; constant temperature creep, in-phase temperature/load creep, out-of-phase temperature/load creep and constant temperature fatigue.

```
#pragma warn -pro
#include <time.h>
#include <decl.h>
#include <stdio.h>
#include <stdlib.h>
#include <dos.h>
#include "math.h"
#include "serial.h"
#include "instron.h"

void main(void){
    FILE *stream;
    short lockamp, instrn;
    long startt, currt, nstartt,ldur,rdur,trel,flag1;
    int n,ptemp,msens,tmp;
    char file[25], speak[15],srelax[15],sfreq[15],stamp[15]
        ,msen[20],llimit[16], ulimit[16],coffset[10];
    float load,pload,relax,freq,rload,ilen,peak,noffset,posi,iposi;
    double volt,mvsens,nvsens,voffset,ivolt,moffset;
    time_t t;
    s_open("COM1 12 n 8 2");
    find(&instrn, &lockamp);
    clrscr();
    printf("\nCreep/Fatigue Testing Program - Rev. 3 Jan 97\n\n");
    //Get user input for important test parameters//
    printf("Enter Data Storage Filename: ");
    scanf("%s", &file);
    printf("Input Peak Temperature (C): ");
    scanf("%d", &ptemp);
    printf("Input Peak Load (MPa):");
```

```

scanf("%f", &pload);
printf("Input Relaxation Load (MPa):");
scanf("%f", &rload);
pload=pload/1000.0;
rload=rload/1000.0;
printf("Input Loading Duration (min):");
scanf("%ld", &ldur);
printf("Input Relaxation Duration (min):");
scanf("%ld", &rdur);
printf("Input Load/Temp Relation ([1]constant,[2]in phase,
      [3]out of phase,[4]fatigue\n");
scanf("%ld",&trel);
if(trel==4){
printf("Input Fatigue Cycle Frequency (hz): ");
scanf("%f" &freq);
}
//Take Control of Instron//
ibwrt(instrn, "C909,0", 6);
ibwrt(instrn, "C909,1", 6);
printf("\npress the remote key for computer control\n");
printf("and then press any key to continue\n");
getch();
clrscr();
//Set Watchdog To off//
ibwrt(instrn, "C904,0", 6);
//Calibrate Zero On Instron//
printf("Calibrating Load Cell... Please Wait\n");
ibwrt(instrn, "C108,2,4", 8);
delay(20000);
//Set up Waveform//
printf("\n\nEnter Current Half Crack Length (mm): ");
scanf("%f", &ilen);
stream=fopen(file,"a+");
fprintf(stream,"Initial Crack Length: %f\n",ilen);
fclose(stream);
//Zero Actuator//
ibwrt(instrn, "C300,2", 6); //Transfer to Load Control//
peak=pload*3.0*(100.0-ilen*2.0)/100.0;
relax=rload*3.0*(100.0-ilen*2.0)/100.0;
sprintf(srelax, "C3,2,%f", relax);

```

```

    sprintf(speak, "C3,2,%f", peak);
    sprintf(stamp, "C203,2,%f", peak-relax);
    ibwrt(instrn, srelax, strlen(srelax));
    printf("Setting Relaxation Load: %f Kn, press a key to
    continue\n",relax*100);
    getch();
//Arm Safety Limits//
    sprintf(ulimit, "C122,2,1,%f", (peak+0.1*peak));
//Define Upper and Lower limits
    sprintf(llimit, "C122,2,0,%f", (0.2*relax));
    ibwrt(instrn, "C326,0", 6); //Disable & clear all safety limits
    ibwrt(instrn, "C121,2,0,0", 10); // Unlock minimum limit
    ibwrt(instrn, "C121,2,1,0", 10); // Unlock max limit
    ibwrt(instrn, llimit, strlen(llimit)); // Set minimum limit
    ibwrt(instrn, "C123,2,0,5", 10); // Unload on min limit
    ibwrt(instrn, "C121,2,0,1", 10); // Arm minimum limit
    ibwrt(instrn, ulimit, strlen(ulimit)); // Set maximum limit
    ibwrt(instrn, "C123,2,1,5", 10); // Unload on max limit
    ibwrt(instrn, "C121,2,1,1", 10); // Arm maximum limit
    ibwrt(instrn, "C326,1", 6); // Enable Safety limits
//Set up Lockin Amp//
    senlock(lockamp,"REMOTE 1"); //set remote control on
    senlock(lockamp,"FLT 3"); //Set Filter to Band Pass//
    senlock(lockamp,"OA 1999"); //Set Oscillator Amplitude to 2v//
    senlock(lockamp,"OF 9300,2"); //Set Oscillator Freq to 93 hz//
// Set Peak Temperature //
    if((trel == 1)|| (trel == 2)|| (trel==4)){
    printf("Setting Temp %d deg C\n",ptemp);
    writetemp(ptemp);
    readtemp(&tmp);
    while(tmp != ptemp){
    readtemp(&tmp);
    delay(2000);
    }}
    printf("3 Minute Temperature Stabilization Delay\n");
    delay(180000); //Stabilization Delay
// Initialize Lockin Amplifier and get Initial Settings.
    senlock(lockamp,"ASM"); //Automeasure
    delay(1000);
    ibwrt(lockamp,"AX0",3); // Perform Auto Offset

```

```

ibwrt(lockamp,"XOF",3); // Request offset value
ibrd(lockamp,coffset,10);
sprintf(coffset," %c%c%c%c  ",coffset[2],coffset[3]
        ,coffset[4],coffset[5]);
sscanf(coffset, "%f", &noffset);
ibwrt(lockamp,"SEN",3);
ibrd(lockamp,msen,10);
sscanf(msen,"%d",&msens);
sense(msens,&mvsens);
voffset=mvsens*noffset/1000.0;
printf("Test Offset: %f mV\n", voffset*1000);
senlock(lockamp,"XTC 4"); //set time constant for more averaging
senlock(lockamp,"EX 1"); //set expand function to "on"
readtemp(&tmp);
// Read Starting Time
printf("Reading Start Time\n");
t = time(NULL); //assigns time value to t in seconds (long)
startt=t;
flag1=1;
noffset=0.0;
begin;;
// Begin Collecting Data
if(trel==4) {
printf("Initializing Fatigue Loading, Hit a Key to Proceed\n");
ibwrt(instrn, "C201,2,3", 8); //Select Haversine Loading
ibwrt(instrn, stamp, strlen(stamp)); //Select Amplitude
sprintf(sfreq, "C202,2,%f", freq); //Select Frequency
ibwrt(instrn, sfreq, strlen(sfreq));
ibwrt(instrn, "C210,0", 6); //Set quarter cycle counter to zero
getch();
ibwrt(instrn, "C200,1", 6); //Begin Cycling
}
t = time(NULL);
nstartt=t;
currt=nstartt;
if(trel <= 3) {
printf("Setting Peak load to %f KN\n",peak*100);
ibwrt(instrn, speak, strlen(speak));
}
if((trel == 2)&&(flag1 != 1)){

```

```

solenoid(lockamp,1,0);
solenoid(lockamp,2,0);
printf("Setting Peak Temp\n");
writetemp(ptemp);
}
if((trel==3)&&(flag1 != 1)){
writetemp(0);
printf("Setting Cooling On\n");
solenoid(lockamp,1,1);
solenoid(lockamp,2,1);
}
delay(3000); //allow time for stabilization
if(flag1==1) {
feedbk(instrn,&posi,&load);
iposi=posi;
readlock(lockamp,voffset,mvsens,&volt,&nvsens,&moffset);
ivolt=volt*1000.0;
flag1=0;
}
n=100;
printf("currt %ld nstartt %ld currt-nstartt %ld ldur*60 %ld"
      ,currt,nstartt,(currt-nstartt),ldur*60);
while((currt-nstartt)<(ldur*60)){
t = time(NULL);
currt=t;
readlock(lockamp,voffset,mvsens,&volt,&nvsens,&moffset);
mvsens=nvsens;
voffset=moffset;
volt=volt*1000.0;
feedbk(instrn,&posi,&load);
readtemp(&tmp);
printf("TT %ld RT %ld min %f mV %f KN %f mm\n",
      (currt-startt)/60,(ldur*60-(currt-nstartt))/60,volt-ivolt
      ,load/1000.0,posi-iposi);
stream=fopen(file,"a+");
fprintf(stream,"%ld %ld %d %f %f %f\n",
      (currt-startt)/60,(ldur*60-(currt-nstartt))/60,tmp,volt
      ,load/1000.0,posi);
fclose(stream);
delay(n);

```

```

if(n>=180000) n=180000;
n=n+200;
}
// Shut down load
printf("Load Cycle Complete, unloading - Starting Relaxation\n");
delay(1000);
printf("Setting Relaxation load to %f KN\n",relax*100);
ibwrt(instrn,srelax,strien(srelax));
if(trel==2){
printf("Initiating Cooling\n");
writetemp(0);
solenoid(lockamp,1,1);
solenoid(lockamp,2,1);
}
if(trel==3){
solenoid(lockamp,1,0);
solenoid(lockamp,2,0);
printf("Initiating Heating\n");
writetemp(ptime);
}
t = time(NULL);
nstartt=t;
currt=nstartt;
// Begin Collecting Data
n=100;
while((currt-nstartt)<(rdur*60)){
t = time(NULL);
currt=t;
readtemp(&ttmp);
readlock(lockamp,voffset,mvsens,&volt,&nvsens,&moffset);
mvsens=nvsens;
voffset=moffset;
volt=volt*1000;
feedback(instrn,&posi,&load);
printf("TT %ld RT %ld min %f mV %f KN %f mm\n",
      (currt-startt)/60,(rdur*60-(currt-nstartt))/60,volt-ivolt
      ,load/1000.0,posi-iposi);
stream=fopen(file,"a+");
fprintf(stream,"%ld %ld %d %f %f %f\n",
      (currt-startt)/60,(rdur*60-(currt-nstartt))/60,tmp,volt

```

```
        ,load/1000.0,psi);  
fclose(stream);  
delay(n);  
if(n>=180000) n=180000;  
n=n+200;  
}  
// End Relaxation Period  
goto begin;  
}
```